EFFECTS OF ATMOSPHERIC TURBULENCE ON MICROWAVE AND MILLIMETER WAVE SATELLITE COMMUNICATIONS SYSTEMS

D.M.J. Devasirvatham
and
D.B. Hodge

The Ohio State University

The Ohio State University

ElectroScience Laboratory

Department of Electrical Engineering
Columbus, Ohio 43212

Technical Report 712759-6
Contract NASW-3393
May 1981

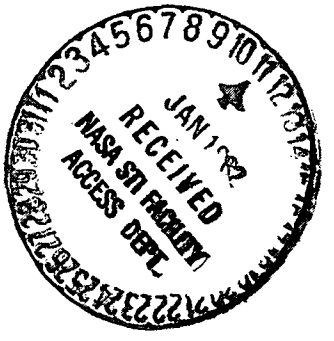

NASA Headquarters
HQ Contracts and Grants Division
Washington, D.C. 20546

NOTICES

When Government drawings, specifications, or other data are used for any purpose other than in connection with a definitely related Government procurement operation, the United States Government thereby incurs no responsibility nor any obligation whatsoever, and the fact that the Government may have formulated, furnished, or in any way supplied the said drawings, specifications, or other data, is not to be regarded by implication or otherwise as in any manner licensing the holder or any other person or corporation, or conveying any rights or permission to manufacture, use, or sell any patented invention that may in any way be related thereto.

Unclassified

SECURITY CLASSIFICATION OF THIS PAGE *(When Data Entered)*

REPORT DOCUMENTATION PAGE		READ INSTRUCTIONS BEFORE COMPLETING FORM
1. REPORT NUMBER	2. GOVT ACCESSION NO.	3. RECIPIENT'S CATALOG NUMBER
4. TITLE *(and Subtitle)* EFFECTS OF ATMOSPHERIC TURBULENCE ON MICROWAVE AND MILLIMETER WAVE SATELLITE COMMUNICATIONS SYSTEMS		5. TYPE OF REPORT & PERIOD COVERED Technical Report 6. PERFORMING ORG. REPORT NUMBER ESL 712759-6
7. AUTHOR(s) D.M.J. Devasirvatham and D.B. Hodge		8. CONTRACT OR GRANT NUMBER(s) Contract NASW-3393
9. PERFORMING ORGANIZATION NAME AND ADDRESS The Ohio State University ElectroScience Laboratory, Department of Electrical Engineering Columbus, Ohio 43212		10. PROGRAM ELEMENT, PROJECT, TASK AREA & WORK UNIT NUMBERS
11. CONTROLLING OFFICE NAME AND ADDRESS NASA Headquarters HQ Contracts and Grants Division Washington, D.C. 20546		12. REPORT DATE May 1981 13. NUMBER OF PAGES 210
14. MONITORING AGENCY NAME & ADDRESS*(if different from Controlling Office)*		15. SECURITY CLASS. *(of this report)* Unclassified 15a. DECLASSIFICATION/DOWNGRADING SCHEDULE
16. DISTRIBUTION STATEMENT *(of this Report)*		
17. DISTRIBUTION STATEMENT *(of the abstract entered in Block 20, if different from Report)*		
18. SUPPLEMENTARY NOTES		
19. KEY WORDS *(Continue on reverse side if necessary and identify by block number)*		

20. ABSTRACT *(Continue on reverse side if necessary and identify by block number)*

This study presents a model of the microwave and millimeter wave link in the presence of atmospheric turbulence, with emphasis on satellite communications systems. The analysis is based on standard methods of statistical theory. The results are directly usable by the design engineer.

DD FORM 1 JAN 73 1473 EDITION OF 1 NOV 65 IS OBSOLETE

Unclassified

SECURITY CLASSIFICATION OF THIS PAGE *(When Data Entered)*

Effects of turbulence on the received wave are studied using the Kolmogorov, Von Karman, and Gaussian models, and compared. The Gaussian model is simply related to the other two for purposes of comparison and is found to be a useful engineering approximation. An equivalent structure constant is also defined for the latter.

A generalized theory of the aperture antenna in turbulence is formulated. The uniform and tapered circular aperture antennas are specifically evaluated for any arbitrary angle of arrival of the wave in the main beam, and related to each other.

The receiver, which has hitherto been neglected, is shown to play a fundamental role in the interpretation of signals which have passed through turbulence. Receivers are classed as synchronous and asynchronous. The signal measured by each class is described. Properties of the turbulence may be directly related to the output of the synchronous receiver defined in this study.

Using experimental results, an equivalent atmosphere, homogeneously turbulent over the propagation path, with appropriate parameters, is shown to be suitable for prediction of long term average behavior. It is described by a height 6 km over an earth of 4/3 the physical radius, or 8479 km. The long term average refractive index variance is 0.4×10^{-12}. The average correlation length is 46 m. The average equivalent structure constant is 5.3×10^{-14}. Extreme conditions are also estimated. The model predicted the experimental results over a range of frequencies of 15 to 1.

The variance and the mean signal level degradation as measured by the two receivers, the fluctuating power, antenna gain, and gain degradation, are studied as functions of frequency from 3 to 90 GHz, aperture size, and elevation angle or equivalent path length. While the numerical results should be used with caution, the effects of turbulence are seen to be significant to the systems designer at the higher frequencies, lower elevation angles, or larger antenna apertures.

Asynchronous receivers may be preferable for communications links. However, properties of turbulence are better measured by links employing synchronous receivers.

ACKNOWLEDGMENTS

A venture of this nature depends on a large number of people, both professional and personal, for its fruition. They are too numerous to fully acknowledge individually.

I thank, first, my adviser Professor D.B. Hodge for his guidance and support during this study. His advice helped to transform the basic research into a finished work and to negotiate the many pitfalls on the way. His supervision created an atmosphere conducive to research and learning.

I also thank the other members of the reading committee: Professors J.H. Richmond and L. Peters, Jr. Their expertise served to iron out several questions and details pertaining to the research.

Mr. R.C. Taylor and his colleagues, Messers R.W. Evans and D.E. Henry, have taught me much about satellite communications engineering. They helped to ground me on the practical aspects of this science and craft.

I thank The Ohio State University ElectroScience Laboratory for financial support, and the Director, Professor C.H. Walter, for his active assistance. The research was funded by the National Aeronautics and Space Administration, NASA Headquarters, Washington, D.C., under Contract No. NASW-3393. I also wish to thank the Fulbright Scholarship program, the United States Educational Foundation in Sri Lanka, and the U.S. State Department, for this opportunity to study in the United States.

The typescript was prepared by Ms. K. Holle, who has produced a very readable copy of the difficult material. She was assisted by Ms. S. Owens. The drafting was done by Messers R.L. Davis and J.M. Gibson.

Finally, this work owes much to my personal friends. They supported me through times of difficulty and offered me warmth and affection, to make my stay in the United States a memorable one. To them I give my grateful and heartfelt thanks.

The material in this report has been used in partial fulfillment of the degree Doctor of Philosophy in Electrical Engineering at The Ohio State University.

TABLE OF CONTENTS

LIST OF TABLES

LIST OF FIGURES

NOTATION

$\bar{A}_0$	=	Vector Amplitude of a Plane Wave
$\tilde{\bar{A}}(\bar{r})$	=	Random Incident Wave
A_{phys}	=	Physical Aperture Area
A_e	=	Effective Aperture Area
A_{e0}	=	Maximum Effective Aperture Area
a	=	Circular Aperture Antenna Radius
B	=	Correlation Function
b	=	Correlation Coefficient
C	=	Relative Correlation Length ℓ_n/a
C_m	=	$C/\sqrt{m}$ m=0,1,...
C_n^2	=	Structure Constant of the Turbulence
C_{ng}^2	=	Equivalent Structure Constant of Gaussian Spectrum
D	=	Antenna Diameter

$D(...)$	=	Structure Function
$\bar{E}_r$	=	Received Electric Field
$\bar{E}_t$	=	Transmitted Field in the Far Zone
F	=	Frequency (GHz)
$\bar{f}$	=	Antenna Feed Illumination Function
f_χ	=	Log Amplitude Spectral Filter Function
f_ψ	=	Phase Spectral Filter Function
f_a	=	Focal Length of Antenna
$G_{0\ max}$	=	Directive Gain of Antenna on Axis
$G_0(...)$	=	Directive Gain Function of Antenna
G_d	=	Degraded Directive Gain
ΔG	=	Gain Degradation
g	=	Unnormalized Voltage Gain Pattern Function
g_V	=	Normalized Voltage Gain Pattern Function
g_0	=	Normalized Power Gain Pattern Function
g_d	=	Gain Degradation Factor
$g(...)$	=	Characteristic Function of a Multidimensional Random Variable

h	=	Height of Equivalent Homogeneous Atmosphere
I_r	=	Received Current at Antenna Terminal
I_t	=	Transmitting Current at Antenna Terminal
I_C	=	Correlation Integral for Uniform Illumination
I_γ	=	Correlation Integral for Gaussian Illumination
$I(...)$	=	An Integral
$\overline{J}_t$	=	Equivalent Transmitting Surface Current Density Distribution
J_0	=	Maximum Transmitting Surface Current Density in the Aperture
$J_\nu(.)$	=	Cylindrical Bessel Function
j	=	$\sqrt{-1}$
K_V	=	Voltage Constant
K_P	=	Power Constant
k	=	Wave Propagation Constant
$\overline{k}$	=	(k_x,k_y,k_z) = Wave Propagation Vector
$\overline{k}_s$	=	(k_x,k_y) = Projection of $\overline{k}$ on the Aperture Plane
L	=	Path Length Through the Atmosphere

l	=	Length or Index of Summation
ℓ	=	Size of Turbulence Eddies
ℓ_n	=	Correlation Length of Refractive Index Fluctuations
m	=	Index of Summation
n	=	Refractive Index of the Atmosphere
P_{dca}	=	Received DC Power Measured by an Asynchronous Receiver
P_{dcs}	=	Received DC Power Measured by a Synchronous Receiver
ΔP_{dca}	=	DC Power Degradation Measured by an Asynchronous Receiver
ΔP_{dcs}	=	DC Power Degradation Measured by a Synchronous Receiver
P_{fl}	=	Fluctuating Component of Received Power
P_R	=	Total Received Power
P_{RO}	=	Power Received with Plane Wave Incidence
$\bar{P}$	=	Point or Position Vector in Antenna Aperture Plane
$\bar{P}'$	=	Point or Position Vector in Antenna Focal Plane
$\hat{p}$	=	Polarization Vector of a Wave
$\hat{p}_f$	=	Polarization Vector of the Aperture Feed Function
p	=	Index of Summation

q	=	Index of Summation
$\bar{r}$	=	Position Vector in Space
r	=	Length of $\bar{r}$
$\bar{R}$	=	Normalized Position Vector in Antenna Aperture Plane
R	=	Length of $\bar{R} = \rho/a$
R_a	=	Real Part of Antenna Impedance
R_e	=	Physical Radius of the Earth
S	=	Physical Aperture Plane of Antenna
$S_{\mu,\nu}(.)$	=	Lommel Function
S_{inc}	=	Magnitude of Incident Power Density
s^2_{syn}	=	Variance of Received Signal Measured by Synchronous Receiver
s^2_{asyn}	=	Variance of Received Signal Measured by Asynchronous Receiver
T_p	=	Power Taper of Feed Illumination
$\tilde{\bar{U}}(\bar{P})$	=	Random Received Field in the Aperture Plane
$\tilde{\bar{U}}'(\bar{P}')$	=	Random Received Field in the Focal Plane
$\bar{U}_0$	=	Average Received Field in the Aperture Plane

V_r	=	Received Voltage at Antenna Terminal
V_{d0}	=	Received Voltage with Wave Incident on Antenna Axis
V_{syn}	=	Received Antenna Voltage Measured by a Synchronous Receiver
V_{asyn}	=	Received Antenna Voltage Measured by an Asynchronous Receiver
V_t	=	Transmitting Voltage at Antenna Terminal
x,y	=	Coordinates in the Aperture Plane
x',y'	=	Coordinates in the Focal Plane
Z_a	=	Impedance of Antenna
Z_l	=	Impedance Terminating Receiving Antenna
$\Gamma(z)$	=	Gamma Function
$\Gamma(a,z)$	=	Imcomplete Gamma Function (See Reference [30] #8.350.2)
$\gamma(a,z)$	=	Incomplete Gamma Function (Reference [30] #8.350.1)
$\Phi(a,b,z)$	=	Degenerate Hypergeometric Function (Reference [30] #9.210.1)
$\Psi(a,b,z)$	=	Degenerate Hypergeometric Function (Reference [30] #9.210.2)
r,θ,ϕ	=	Spherical Coordinates

ρ,ξ	=	Cylindrical Coordinates in Aperture Plane
θ	=	Normalized Angle of Arrival of Wave
$\tilde{\chi}$	=	Log Amplitude of Wave
χ_0	=	Mean Log Amplitude = $< \tilde{\chi} >$
$\tilde{\psi}$	=	Phase
λ	=	Wavelength
η_0	=	Characteristic Impedance of Free Space
σ_n^2	=	Variance of Refractive Index Fluctuations
σ_χ^2	=	Log Amplitude Variance
σ_ψ^2	=	Phase Variance
σ_w^2	=	Wave Variance
$\Phi_n(\kappa)$	=	Spectrum of Turbulence
κ	=	Turbulence Wave Number
κ_0	=	$1/L_0$
κ_m	=	$5.92/\ell_0$
ε	=	Elevation Angle to Spacecraft
τ	=	Gaussian Illumination Taper Constant

$\langle\ \rangle$	=	Statistical Expectation
$\underline{\cdot}$	=	Vector Quantity
$\tilde{\cdot}$	=	Random Quantity
$\cdot^{*}$	=	Complex Conjugate
$\sim$	=	Varies As
$\approx$	=	Approximately Equals

CHAPTER I

INTRODUCTION

1.1 Overview

The allocation and use of ever higher frequencies in the microwave and millimeter wave regions of the electromagnetic spectrum has been spurred by the information explosion that followed the dawn of the space age. The attendant satellite communications technology, which had its modest beginnings in the ECHO satellite of 1960, generated its own demand. Taking over a large share of intercontinental telephone communications, it also opened the way for wholly new services such as computer links, data nets, and intercontinental television links as well as direct television broadcasting by satellite.

The resulting congestion has mandated the use of higher frequencies in hitherto unexplored regions of the electromagnetic spectrum. The new bands have been primarily determined by the characteristics of the terrestrial atmosphere. They are usually situated in 'electromagnetic windows', i.e., regions of relatively low attenuation away from resonance regions of its constituents, except in special cases such as secure short hop links. The fundamental constraint imposed by the windows on the choice of frequencies for general purpose usage precluded incremental changes in frequencies used and a gradual evolution of the technology. The new bands usually require quantum jumps in frequency along with a wholly new range of generating and receiving equipment.

The initially low powers and sensitivities, coupled with the usually greater interaction with the atmosphere pose many problems to the systems designer. The effects of scintillation caused by atmospheric turbulence and bulk effects such as layers and fronts may all take their toll and need to be quantified. Attenuation statistics in clear air and rain are needed to ensure reliable links and to optimize parameters.

One 'easy' solution to the problem of ensuring adequate system margins has been the use of large antennas, where permissible, to increase the directive gain. This increases the effective sensitivity of the receiver. However, it is now realized that perturbations of the received wave front across a large antenna by turbulence will, in effect, decrease its gain. This may also be thought of as an aperture to medium coupling loss. Indeed, at some point, an array of smaller antennas feeding coherently summing receivers begins to provide superior performance at lower cost over a single receiver fed by a large antenna.

The effects of the atmosphere on receiving systems had been encountered much earlier by optical astronomers. The familiar twinkling of the stars due to atmospheric turbulence, while celebrated in fiction, results in the degradation of the image at the focal plane of a telescope. The image spot may move randomly in the viewing field, causing a blurring of the image. In some cases, the image may even break up into several spots. These phenomena limit the resolution of the instrument. Further, the time available with good viewing conditions is also curtailed.

Another related problem is the study of the surface tolerance of large antennas. Deviations from the optimum geometry of the surface due to tolerances in construction, thermal expansion, and the distortion caused by gravity result in a reduction in the gain of the antenna. The distortion of the incident wavefront by these deviations, when viewed by the feed system, is an exact analog of turbulence induced distortion and may indeed be indistinguishable from it.

Unfortunately, much of the study that has ensued is not in a form that is directly usable by the microwave engineer. The links between the parameters used by the optical astronomer, the microwave engineer, the antenna engineer, and the specialist in propagation have rarely been made explicit. Arduous measurements made by each group have usually remained within their own domains. The system designer has consequently relied on rules of thumb, empirical factors, overdesign, or has ignored the problem altogether.

1.2 Outline of the Study

References [11, 36, 44] have examined some aspects of the problems discussed above. The book by Shifrin [11] has been particularly useful. It provides a detailed analysis of linear and rectangular aperture antennas in the presence of turbulence. Unfortunately, there is very little material on the physical properties of the turbulence itself and the emphasis appears to be on the troposcatter problem. Theobold and Hodge [36] proposed a phenomenological model of the communications link. The wave incident on the antenna is decomposed into an amplitude varying component which is fixed in direction and a component which is fixed in amplitude, but varying in direction. Knepp [44] discussed a Gaussian tapered antenna. However, the results do not appear to be readily usable by the engineer. The last two works discuss on-axis incidence of the incoming wave only. None of the studies recognize the effect of the receiver on the measurement of the received signal statistics.

Much of the literature referred to in this work are of use in a particular section only. Therefore, they are reviewed in the beginning of the relevant chapter and will not be presented at this point.

It was felt, in light of the preceding discussion, that a coherent solution to the problem of a receiving system in the earth's turbulent atmosphere would be useful. Elements of propagation theory, of use to

the designer, have been selected from the wealth of information available. A statistical analysis of an antenna in a turbulent medium is presented. The effects of the receiver on the signal gathered by the antenna, which appears to have been ignored hitherto, were analyzed with surprising and far reaching implications. The results are brought together to form a complete picture of the behavior of the communications link in turbulence.

This study attempts, first, to formulate the basics of the problem of the receiving aperture in a homogeneous turbulent medium. The medium is described using a simple statistical model. The concepts of elementary antenna theory are used. The effects of the feed system are included as an integral part of the analysis.

The propagation medium is then analyzed and several models of atmospheric turbulence are compared. The statistics of the wave received at the antenna after propagating through the atmosphere are formulated. An analytically convenient model is then chosen and shown to be a reasonable engineering approximation to more commonly accepted models.

The role of the receiver in the perceived signal statistics is studied next. The type of demodulator circuit used is shown to play a vital part in measuring the fluctuations of the received signal. Thus, two general classes of receivers, called synchronous and asynchronous receivers, are defined. The statistics of the signal as measured by these receivers are formulated.

The particular case of the circular aperture is then examined in greater detail. Uniform and Gaussian shaped feed illumination are considered. The former also serves to link the results to the optical telescope in the particular case of focusing systems. The general behavior of the gain of the circular antenna in turbulence is shown.

Next, experimental results are used to ascribe numerical values to the parameters of the propagation model. This describes the long term

average behavior of the atmospheric link. Estimates of the extreme conditions of turbulence are also made.

Using these estimates of the average and extremes of atmospheric turbulence, the behavior of the variance and the average non-fluctuating power of the signal measured by asynchronous and synchronous receivers is studied. The degradation of the gain of the receiving antenna is also examined to obtain a deeper understanding of the effects of turbulence on microwave and millimeter wave satellite communications systems. Finally, some useful design curves based on these results are given, with extensions to some frequencies of future interest.

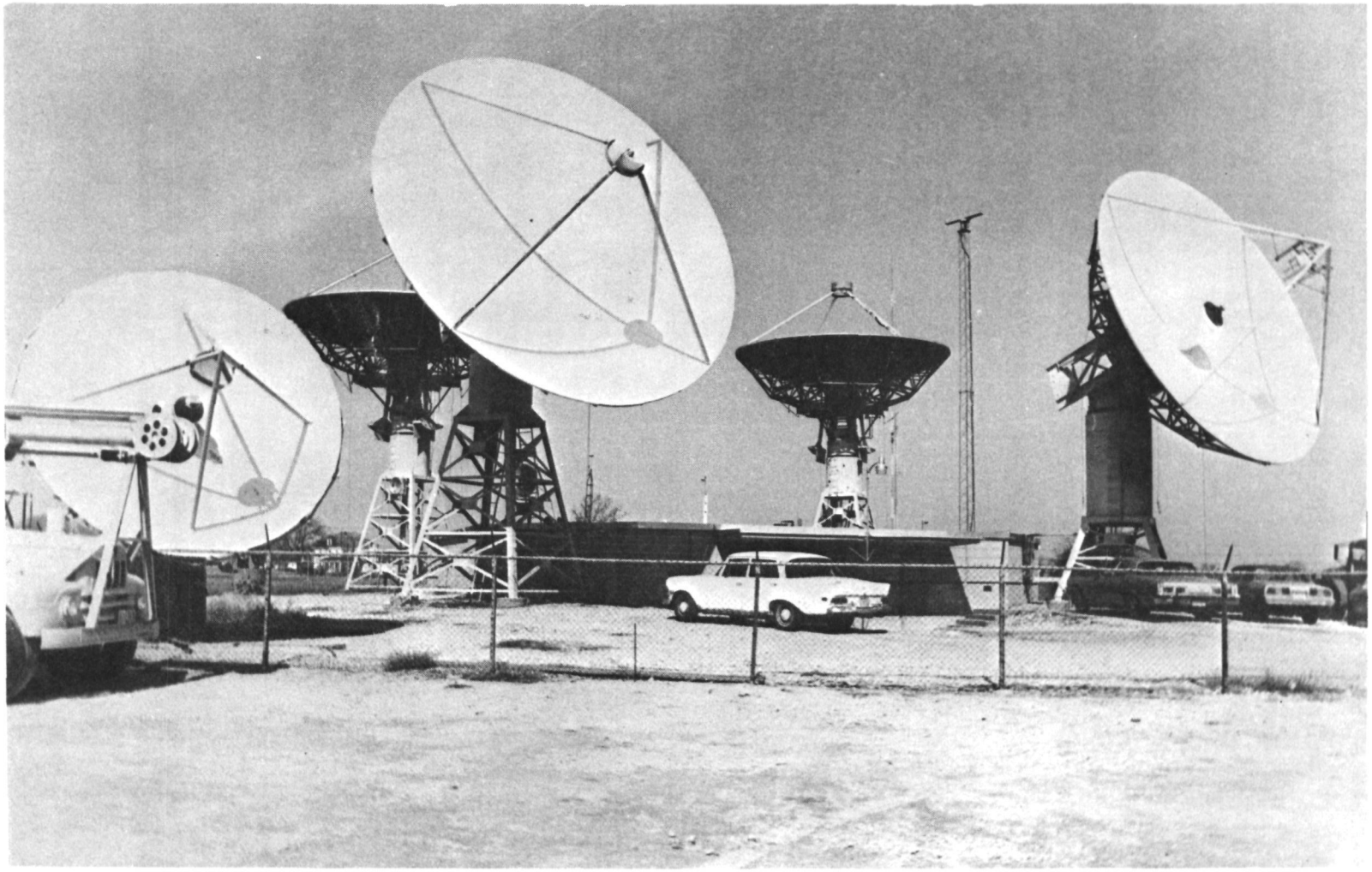

Figure 1.1. Satellite Communications Facility at The Ohio State University ElectroScience Laboratory.

CHAPTER II

THE ANTENNA

This chapter examines the basic theory of the aperture antenna as a transmitter or receiver in the presence of statistically fluctuating media. The effect of the feed pattern is included.

The far field pattern of an antenna acting as a transmitter is discussed briefly. The terminal voltage of a receiving antenna is then evaluated, first for plane wave incidence, to relate it to the case of the transmitter. The theory is then extended by considering the incident wave to be perturbed arbitrarily in amplitude and phase in space.

Finally, the perturbations are allowed to vary randomly in time and space to represent the effects of turbulence. The results are also related to the field in the focal plane of a focusing antenna. This links the antenna and the optical telescope.

The aperture of the antenna is assumed to lie in the x-y plane and is denoted by S, as shown in Figure 2.1. $\overline{P} = (x,y)$ or $P(\overline{R})$, where $\overline{R}$ is a vector on the surface x-y, represents any point on the aperture. $\hat{n}$ is a unit vector normal to S. $Q(\overline{r})$ is any point in the forward half-space at which the transmitted field $\overline{E}_t$ or the received field $\overline{E}_r$ is measured. The $e^{j\omega t}$ time convention is used in describing phasors.

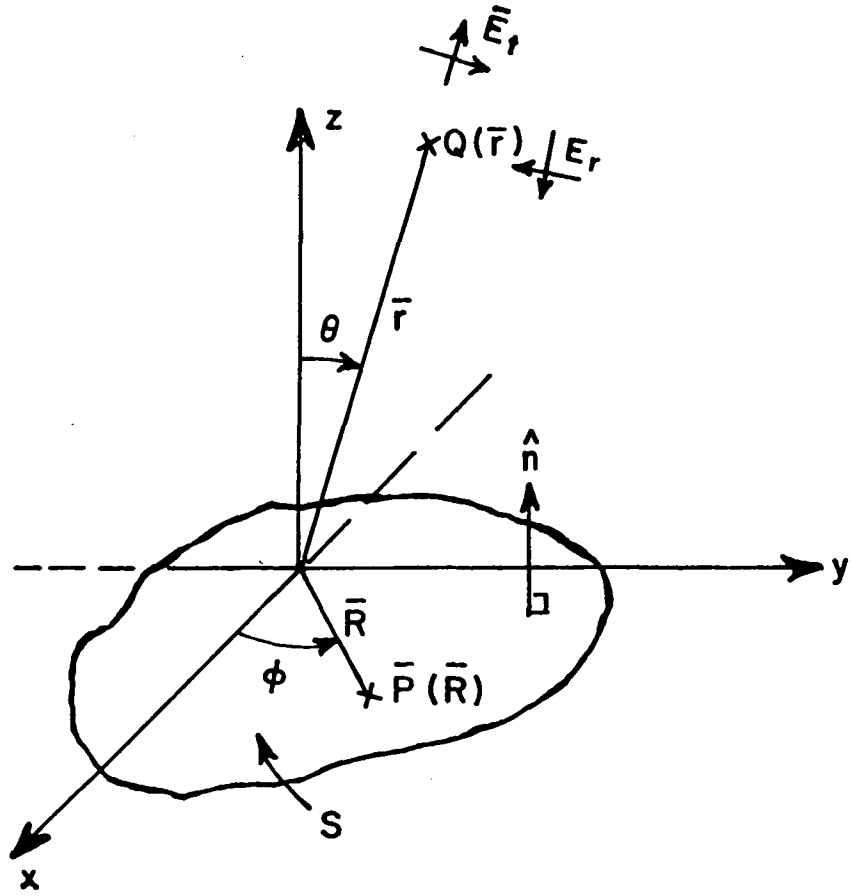

Figure 2.1. Antenna aperture geometry.

2.1 The Antenna as a Transmitter

In this section, expressions are derived for the far field pattern of an aperture antenna acting as a transmitter for comparison later with the receiving antenna.

Let the antenna produce a field distribution on the infinite x-y plane. Using the surface equivalence principle the aperture fields could be replaced by electric and magnetic equivalent current density distributions $\bar{J}_e(x,y)$ and $\bar{M}_e(x,y)$, where

$$\bar{J}_e = \hat{n} \times \bar{H}$$

$$\bar{M}_e = \bar{E} \times \hat{n} \quad .$$

$\bar{E}$ and $\bar{H}$ are the electric and magnetic fields in the aperture plane. Alternatively, an equivalent electric current density $\bar{J}_t(x,y)$ alone may be assumed such that

$$\bar{J}_t = 2\, \hat{n} \times \bar{H} \, .$$

The above formulations are valid only in the half-space faced by the antenna.

Further, let

$$\bar{J}_t(x,y) = J_0\, \bar{f}(x,y) = J_0\, f(x,y)\, \hat{p}_f \qquad (2.1.1)$$

where J_0 is a complex constant and $f(x,y)$ is the dimensionless normalized aperture illumination function or feed function, such that

$$|f(x,y)|_{max} = 1 \qquad (2.1.2)$$

and $\hat{p}_f$ is the unit polarization vector of the aperture illumination.

Then, the radiated electric field pattern in the forward direction in the far (Fraunhofer) zone is given by [1],

$$\bar{E}_t(\theta,\phi) = \frac{j\eta_0 e^{-jkr}}{2\lambda r} \int_{\infty} \bar{J}_t(x,y)\, e^{jk\sin\theta(x\cos\phi + y\sin\phi)}\, dxdy \qquad (2.1.3)$$

where r,θ,ϕ are the spherical coordinates of the observation point. η_0 is the characteristic impedance of free space. λ is the wavelength, and

k, the propagation constant, is given in magnitude by

$$k = \frac{2\pi}{\lambda} \quad .$$

The signed constant, k, is also the magnitude of $\bar{k}$ where

$$k_x = k \sin\theta \cos\phi$$

$$k_y = k \sin\theta \sin\phi$$

$$k_z = k \cos\theta \quad .$$

Then the component of $\bar{k}$ lying in the aperture plane is

$$\bar{k}_s = (k_x, k_y) \tag{2.1.4}$$

and

$$\bar{E}_t(k_x,k_y) = \frac{jn_o e^{-jkr}}{2\lambda r} J_0 \int_{\infty} \bar{f}(x,y)\, e^{j(k_x x + k_y y)}\, dxdy. \tag{2.1.5}$$

Let

$$\bar{g}(k_x,k_y) = \int_{\infty} \bar{f}(x,y)\, e^{j(k_x x + k_y y)}\, dxdy. \tag{2.1.6}$$

We recognize that $\bar{g}(k_x,k_y)$ is the Fourier transform of the aperture current distribution function. It is called the (unnormalized) electric field pattern function of the antenna in free space. Therefore,

$$\bar{E}_t(k_x,k_y) = \frac{jn_o e^{-jkr}}{2\lambda r} J_0\, \bar{g}(k_x,k_y) \quad . \tag{2.1.7}$$

The magnitude of the field in any direction of polarization, $\hat{p}$, in the far zone is given by

$$E_{tp}(k_x, k_y) = \frac{j\eta_0 e^{-jkr}}{2\lambda r} J_0 \hat{p} \cdot \bar{g}(k_x, k_y) \quad . \tag{2.1.8}$$

Most of the transmitted energy is contained in the main beam of the antenna and the side lobe levels are assumed to be low. Consequently, the fields in the x-y plane and the equivalent surface density, $\bar{J}_t$, may be considered to be small except over the physical aperture, S, itself. Therefore, the integration may be carried out over S alone with small error to give

$$\bar{E}_t(k_x, k_y) = \frac{j\eta_0 e^{-jkr}}{2\lambda r} J_0 \int_S \bar{f}(x,y)\, e^{j(k_x x + k_y y)}\, dxdy \quad . \tag{2.1.9}$$

Finally, a more compact representation, using vector notation for (2.1.9) is,

$$\bar{E}_t(\bar{k}_s) = \frac{j\eta_0 e^{-jkr}}{2\lambda r} J_0 \int_S \bar{f}(\bar{P})\, e^{j\bar{k}_s \cdot \bar{P}}\, dS \quad . \tag{2.1.10}$$

All the other equations could also be written in a similar form. This notation will be used in the following sections.

2.2 The Antenna as a Receiver

A general expression for the voltage at the terminal of an aperture antenna acting as a receiver is derived in this section. The antenna is represented by the physical aperture, S. The feed system is assumed to be accessible at some point so that voltage and current can be measured. We further stipulate that the wave guide or transmission line will support only one propagating mode. Higher order modes are usually excited by reflection at the end of the feed section; but we assume that these are strongly attenuated before the point of measurement.

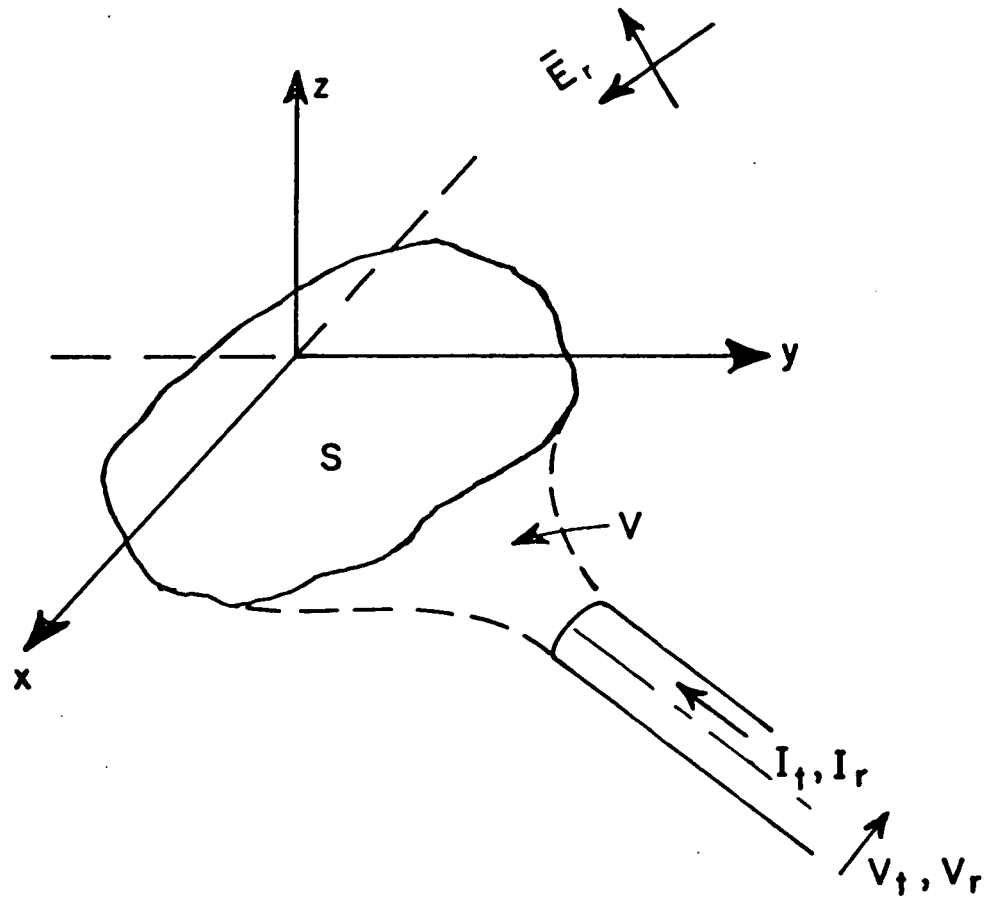

Figure 2.2. The antenna feed system.

V_t and I_t are the voltage and current, respectively, measured when the antenna is used as a transmitter. V_r and I_r are similarly measured during reception. Directions of these quantities are defined in Figure 2.2.

Let an incident electric field be denoted by $\bar{E}_r$. Its angle of arrival with respect to the antenna is measured in spherical coordinates as (θ,ϕ). The vector notation indicates the direction of polarization.

The Rayleigh-Carson Reaction Integral theorem of mixed form [2,3] states that,

$$V_t I_r - V_r I_t = \int_{\infty} (\bar{J}_e \cdot \bar{E}_r - \bar{M}_e \cdot \bar{H}_r)\, dS \qquad (2.2.1)$$

and if

Z_a = Antenna Impedance

Z_l = Load Impedance

$V_t = I_t Z_a$

$V_r = -I_r Z_l$.

Replacing $(\bar{J}_e, \bar{M}_e)$ by the equivalent current density $(\bar{J}_t, \bar{0})$,

$$V_r = \frac{-1}{\left[1 + \frac{Z_a}{Z_l}\right] I_t} \int_{\infty} \bar{J}_t \cdot \bar{E}_r \, dS. \qquad (2.2.2)$$

Thus, the effect of the current distribution due to the antenna feed is to weight the incoming field and is included in (2.2.2). The actual implementation of the feed system, be it a horn at the focus of a parabolic antenna or a system of wave guides connected to various points of the radiating surface, is immaterial to Equation (2.2.2). Hence, all classes of aperture antennas are included.

2.3 Case 1: Plane Wave Incidence

The general expression for the antenna terminal voltage derived in Section 2.2 is applied to the plane wave incidence case. The identity of the transmitting far field and the receiving patterns are established.

Consider a plane wave travelling toward the origin. Its angle of arrival is measured as shown in Figure 2.1. It may then be represented as

$$\overline{E}_r = \overline{A}_0 \, e^{-j(k_x x + k_y y + k_z z)} \tag{2.3.1a}$$

$$= \overline{A}_0 \, e^{-j\overline{k}\cdot\overline{r}} \tag{2.3.1b}$$

$$= \hat{p} \, A_0 \, e^{-j\overline{k}\cdot\overline{r}} \tag{2.3.1c}$$

where $\hat{p}$ is the unit polarization vector of the plane wave. A_0 is the constant amplitude of the wave.

Now $\overline{J}_t(\overline{P})$ was defined to lie only in the x-y plane. Therefore, from (2.2.2)

$$V_r = \frac{-1}{\left[1 + \frac{Z_a}{Z_1}\right] I_t} \int_{\infty} \overline{J}_t(\overline{P}) \cdot \overline{E}_r(\overline{P}) \; dS. \tag{2.3.2}$$

where

$$\overline{E}_r(\overline{P}) = \overline{E}_r(\overline{r})\Big|_{z=0} \tag{2.3.3}$$

$$= \overline{A}_0 \, e^{-j(k_x x + k_y y)} \tag{2.3.4}$$

$$= \overline{A}_0 \, e^{-j\overline{k}_s\cdot\overline{P}} \tag{2.3.5}$$

is the field distribution of the incident wave over the aperture plane. Further, using (2.1.1) and (2.3.2)

$$V_r = \frac{-1}{\left[1 + \frac{Z_a}{Z_1}\right]} \frac{J_0}{I_t} \int_{\infty} \bar{f}(\bar{P}) \cdot \bar{E}_r(\bar{P}) \; dS \quad .$$

Let the constant

$$K_V = \frac{-1}{\left[1 + \frac{Z_a}{Z_1}\right]} \frac{J_0}{I_t} \quad . \tag{2.3.6}$$

Then,

$$V_r = K_V \int_{\infty} \bar{f}(\bar{P}) \cdot \bar{E}_r(\bar{P}) \; dS \tag{2.3.7}$$

or

$$V_r(\bar{k}_s) = K_V \bar{A}_0 \cdot \int_{\infty} \bar{f}(\bar{P}) \, e^{-j\bar{k}_s \cdot \bar{P}} \; dS \quad , \tag{2.3.8}$$

i.e., from (2.1.6)

$$V_r(\bar{k}_s) = K_V A_0 \hat{p} \cdot \bar{g}(-\bar{k}_s) \quad . \tag{2.3.9}$$

Note that the sign of k in $\bar{k}_s$ is negative for a wave travelling toward the origin of coordinates. Equations (2.3.9) and (2.1.8) are seen to have the same form. Therefore, the receiving pattern for plane wave incidence is identical to the far field transmitting pattern.

Finally, using the approximations discussed in Section 2.1, the integral in Equation (2.3.8) may be carried out over the physical aperture only, so that

$$V_r(\bar{k}_s) = K_V \bar{A}_0 \cdot \int_S \bar{f}(\bar{P})\, e^{-j\bar{k}_s \cdot \bar{P}}\, dS \ . \qquad (2.3.10)$$

$V_r(\bar{k}_s)$ gives the voltage at the antenna terminals due to a plane wave incident in a direction such that the projection of the propagation vector on the antenna aperture plane is $\bar{k}_s$.

2.4 Case 2: Perturbed Wave Incidence

The incident wave is now perturbed deterministically in amplitude and phase; and the antenna terminal voltage is derived. This is an intermediate step toward the randomly varying incidence case.

Consider a wave of the form

$$\bar{E}_r = \bar{A}(\bar{r})\, e^{-j\bar{k}\cdot\bar{r}} \qquad (2.4.1)$$

incident on the aperture antenna. $\bar{A}(\bar{r})$ is the complex amplitude which is not constant over a plane transverse to the direction of propagation. This could be visualized as the result of an initially plane wave, with constant amplitude and phase in a plane transverse to its direction of propagation, which has undergone perturbations along its front. An example is the field near a small fixed scatterer. Using (2.3.3) - (2.4.1),

$$\bar{E}(\bar{r})\Big|_{z=0} = \bar{A}(\bar{P})\, e^{-j\bar{k}_s \cdot \bar{P}} \qquad (2.4.2)$$

$$V_r(\bar{k}_s) = K_V \int_S \bar{f}(\bar{P}) \cdot \bar{A}(\bar{P})\, e^{-j\bar{k}_s \cdot \bar{P}}\, dS \ . \qquad (2.4.3)$$

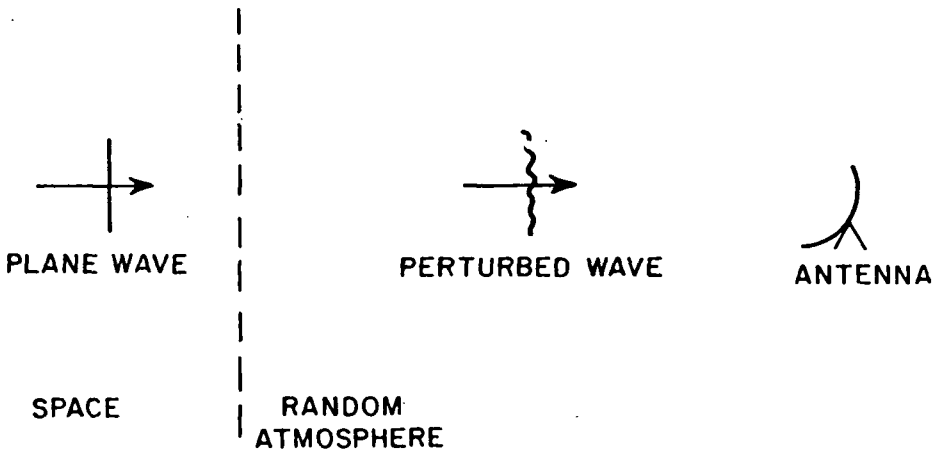

Figure 2.3. Perturbation of a propagating wave by the turbulent atmosphere.

2.5 Case 3: Randomly Varying Perturbed Wave Incidence

The expression for the antenna terminal voltage will now be extended to the case of a randomly varying incident wave. A plane wave, travelling from a spacecraft and incident on the earth's atmosphere, encounters inhomogeneities in pressure, temperature, and humidity (Figure 2.3). Their influence is strongest in the lower troposphere due to changes in the refractive index. The effect of bulk refraction is to bend the propagating ray as a whole. This is a relatively slow phenomenon and could be considered to be quasi-static over times on the order of several cycles of carrier frequency. It will not be considered in the following analysis.

Inhomogeneities of smaller scale sizes are also present in the atmosphere. The wave, moving in a direction $\bar{k}$ with respect to the antenna's frame of reference is increasingly perturbed as it propagates through these inhomogeneities. Further, as these fluctuations are random in space and time varying, the perturbation of the wavefront will also be random in space and time. However, it is reasonable to assume that the average direction of propagation of the wave as a whole is essentially unchanged. It is, therefore, convenient to separate out the basic propagating direction and the random fluctuations.

Let

$$\tilde{\bar{E}}_r = \tilde{\bar{A}}(\bar{r},t)\ e^{-j\bar{k}\cdot\bar{r}} ,$$

where

$$\tilde{\bar{A}}(\bar{r},t) = \bar{A}_0\ e^{\tilde{\chi}(\bar{r},t) + j\tilde{\psi}(\bar{r},t)} .$$

The tilde denotes random quantities. $\tilde{\bar{A}}$ is a function of position and time. $\bar{A}_0$ is the amplitude of the wave that would be present if there were no perturbations. χ is the log amplitude of the wave and the phase fluctuations are given by ψ.

The statistics of $\tilde{\chi}$ and $\tilde{\psi}$ are directly related to the statistics of the medium. This will be considered in detail in Chapter Three. The processes are assumed to be stationary and, hence, ergodicity may be invoked. Therefore, we may restate the above equations as functions of space only as

$$\tilde{\bar{E}}_r = \tilde{\bar{A}}(\bar{r})\ e^{-j\bar{k}\cdot\bar{r}} \qquad (2.5.1)$$

$$\tilde{\bar{A}}(\bar{r}) = \bar{A}_0\ e^{\tilde{\chi}(\bar{r}) + j\tilde{\psi}(\bar{r})} . \qquad (2.5.2)$$

Let the value of $\tilde{\bar{E}}_r$ on the x-y plane be

$$\tilde{\bar{E}}_r(\bar{P}) = \tilde{\bar{E}}_r(\bar{r})\Big|_{z=0}$$

$$= \tilde{\bar{U}}(\bar{P})\ e^{-j\bar{k}_s\cdot\bar{P}} \qquad (2.5.3)$$

where

$$\tilde{\bar{U}}(\bar{P}) = \bar{A}_0\ e^{\tilde{\chi}(x,y,0) + j\tilde{\psi}(x,y,0)}$$

$$\tilde{U}(\bar{P}) = \bar{A}_0 \, e^{\tilde{\chi}(\bar{P}) + j\tilde{\psi}(\bar{P})} \quad . \tag{2.5.4}$$

$\bar{P}$ is the surface vector (x,y) as before. Evaluation at z=0 is understood and will be dropped from the notation in the following.

The voltage at the antenna terminal when receiving such a wave would be

$$\tilde{V}_r(\bar{k}_s) = K_V \int_{\infty} \bar{f}(\bar{P}) \cdot \tilde{\bar{E}}_r(\bar{P}) \; dS \quad . \tag{2.5.5}$$

Once again, using the engineering approximations discussed in Section 2.1,

$$\tilde{V}_r(\bar{k}_s) = K_V \int_{S} \bar{f}(\bar{P}) \cdot \tilde{\bar{U}}(\bar{P}) \, e^{-j\bar{k}_s \cdot \bar{P}} \; dS \quad . \tag{2.5.6}$$

Equations (2.5.5) and (2.5.6) are the statistical extensions of (2.3.7) and (2.3.10).

2.6 Fields in the Focal Plane of a Focusing System

In the particular case of a focusing system, when the incident field is paraxial, the field in the focal plane of the antenna may be obtained fairly easily ([11], pp. 231-236). The results can also be directly applied to the optical telescope, which can be considered to be a focusing antenna with a uniform polarization insensitive aperture illumination function. Let

f_a	=	focal length of the antenna
$\bar{P}$	=	(x,y) be a point on the antenna aperture
$\bar{P}'$	=	(x',y') be a point on the focal plane
$\tilde{U}(x,y)$	=	the magnitude of the incident field on the aperture plane

$\tilde{U}'(x',y')$ = the magnitude of the field in the focal plane.

Then, neglecting polarization,

$$\tilde{U}'(x',y') = \frac{j\, e^{-jkf_a}}{\lambda f_a} \int_S \tilde{U}(x,y)\, e^{j\frac{k}{f_a}(xx' + yy')}\, dS. \qquad (2.6.1)$$

Equation (2.6.1) is seen to be similar in form to the expression for the terminal voltage of a receiving antenna. Therefore, it serves to link the results obtained for an antenna to the optical telescope.

Comparing (2.6.1) and (2.5.6), it is seen that if the following substitutions,

$k\, x'/f_a$ for $k \sin\theta \cos\phi$

$k\, y'/f_a$ for $k \sin\theta \sin\phi$

$\tilde{U}(x',y')$ for $\tilde{V}_r$

are made, the results derived for the received voltage may be also applied to the focal field.

Clearly, the description of the received voltage, $\tilde{V}_r$, or the field in the focal plane, $\tilde{U}'$, in terms of statistical averages, requires knowledge of the statistics of $\tilde{U}(\bar{P})$. This is considered in Chapter Three.

In summary, the theory of the receiving aperture antenna was considered. The basic formulation was extended to describe the behavior of the antenna when a randomly varying perturbed wave is incident upon it. Finally, the field in the focal plane of the antenna was shown to be useful in relating the results obtained in this study to the optical telescope.

CHAPTER III

PROPAGATION IN TURBULENCE

3.1 Introduction

The propagation of electromagnetic waves through the turbulent atmosphere has been the subject of intensive investigation over several decades. A vast literature exists, detailing several approaches to the problem. Some basic references [4-22], and works referred to in their bibliography, may be consulted for comprehensive study.

Chernov [4] and V.I. Tatarski [5,6] brought together much of the earlier work and also provided a broad theoretical basis for plane wave propagation through the turbulent atmosphere. This was extended by Schmeltzer [7], considering laser beams, to include spherical wave, finite aperture cases. The Rytov method of evaluating the wave equation is used in these works. The range of applicability of the Rytov method, which requires, inter alia, that the magnitude of the fluctuations of the wave be 'small', sparked considerable debate [19]. Various mathematical approaches, such as the mutual coherence theory [20], have been used to study the strong fluctuation case.

In 1941, A.N. Kolmogorov proposed a theory of turbulence which is applicable to the earth's atmosphere [21]. This is now a generally

accepted description. Lee and Harp [22], used a more heuristic model of the atmosphere, i.e., a set of phase gratings, to obtain solutions to a wide range of problems. Ishimaru, in his books [8,9], provides a useful collection of these ideas, as well as some of his own, in a readable text.

This chapter considers some aspects of the propagation of a plane wave in a turbulent atmosphere. A review of basic concepts is followed by comments on the Gaussian and Kolmogorov models for clear air propagation. The simpler Gaussian model is also considered because it is more tractable, mathematically. The two models are then compared to obtain an understanding of the uses and possible errors associated with the Gaussian approximation. Some new expressions are also derived for log amplitude and phase, variance and correlation functions.

3.2 Preliminaries

The propagation of electromagnetic waves along terrestrial or earth-space paths in the microwave through optical portions of the spectrum is most influenced by that portion of the earth's atmosphere called the troposphere. This denotes that part of the atmosphere extending from the earth's surface up as high as 17 km. The refractive index, n, of the atmosphere is approximately one and is given by

$$n = 1 + \Delta n \tag{3.2.1}$$

and the refractivity, N, is given by

$$N = (n-1)\times 10^6 = \frac{77.6}{T}\left(P + \frac{4810\ e}{T}\right) \tag{3.2.2}$$

in the microwave region and

$$N = (n-1)x10^6 = \frac{77.6\ P}{T} \qquad (3.2.3)$$

in the optical region. Here, N is on the order of 300 and

P = Barometric pressure in millibars (1 mm. Hg = 1.3332 millibars)
e = Partial pressure of water vapor in millibars
T = Absolute temperature, degrees Kelvin.

The typical decrease of n with increasing height causes any propagating ray to bend downwards. This can be eliminated in calculations, under conditions of standard refraction, by considering the earth to be a sphere of radius equal to 4/3 the physical radius, or, approximately 8479 km. This approximate correction will be used throughout this work.

The pressure, temperature, and humidity also vary randomly from place to place and with time at any place due to atmospheric turbulence. The resulting random variation in the refractive index perturbs the propagating electromagnetic wave causing amplitude scintillation and phase fluctuation. Other atmospheric effects such as absorption and depolarization have been extensively treated in the literature and will not be considered here.

The correlation function, $B_f(\bar{r}_1,\bar{r}_2)$, of a multi-dimensional random field, $f(\bar{r})$, is defined [6] as

$$B_f(\bar{r}_1,\bar{r}_2) = \langle [f(\bar{r}_1) - \langle f(\bar{r}_1)\rangle] [f(\bar{r}_2)^* - \langle f(\bar{r}_2)^*\rangle]\rangle \ . \qquad (3.2.4)$$

The random process is said to be homogeneous if it has a constant mean and its correlation function is unaffected by simultaneous translation of $\bar{r}_1$ and $\bar{r}_2$ by the same amount in the same direction. It is the generalized concept of a stationary process. The correlation function

of a homogeneous random field depends only on the difference $\bar{r} = \bar{r}_1 - \bar{r}_2$, so that

$$B_f(\bar{r}_1,\bar{r}_2) = B_f(\bar{r}_1-\bar{r}_2) = B_f(\bar{r}) \quad . \tag{3.2.5}$$

A homogeneous random field is said to be isotropic if $B_f(\bar{r})$ depends only on $r = |\bar{r}|$, i.e., only on the distance between the observation points.

$$B_f(\bar{r}_1,\bar{r}_2) = B_f(r) \quad . \tag{3.2.6}$$

Many meterological phenomena are not properly described by homogeneous, isotropic, random processes. However, in many cases a new process $f(\bar{r}_1) - f(\bar{r}_2)$ can be formed which is well behaved (homogeneous). $f(\bar{r})$ is then called a locally homogeneous process. Its correlation function is no longer a function of $\bar{r}_1-\bar{r}_2$ alone; but also depends on $\bar{r}_1$ and $\bar{r}_2$, individually. Therefore, the structure function

$$D_f(\bar{r}) = \langle |f(\bar{r}_1+\bar{r}) - f(\bar{r}_1)|^2 \rangle \tag{3.2.7}$$

is a more useful parameter of such a field. It is a function of $\bar{r}_1-\bar{r}_2$ only. Furthermore, if $D_f(\bar{r})$ is a function of r only, the process is called a locally homogeneous isotropic random field.

It should be noted that the structure function exists for homogeneous as well as locally homogeneous random processes. A unique correlation function, on the other hand, exists for homogeneous processes only.

The three-dimensional correlation function, $B_f(\bar{r})$, and its spectrum $\Phi_f(\bar{\kappa})$ are related by the Fourier transform [23],

$$\Phi_f(\bar{\kappa}) = \frac{1}{(2\pi)^3} \int_{\infty} B_f(\bar{r})\, e^{-j\bar{\kappa}\cdot\bar{r}}\, d\bar{r} \tag{3.2.8}$$

$$B_f(\bar{r}) = \int_{\infty} \Phi_f(\bar{\kappa})\, e^{j\bar{\kappa}\cdot\bar{r}}\, d\bar{\kappa} \quad . \tag{3.2.9}$$

Also, the structure function, $D_f(\bar{r})$, is related to the spectrum by [24],

$$D_f(\bar{r}) = 2 \int_{\infty} (1 - \cos\bar{\kappa}\cdot\bar{r})\Phi_f(\bar{\kappa})\, d\bar{\kappa} \quad . \tag{3.2.10}$$

If the turbulence is both homogeneous and isotropic, these reduce to [23,24],

$$\Phi_f(\kappa) = \frac{1}{2\pi^2\kappa} \int_0^{\infty} B_f(r)\sin(\kappa r) r\, dr \tag{3.2.11}$$

$$B_f(r) = \frac{4\pi}{r} \int_0^{\infty} \Phi_f(\kappa)\sin(\kappa r)\kappa\, d\kappa \tag{3.2.12}$$

$$D_f(r) = 8\pi \int_0^{\infty} \Phi_f(\kappa) \left(1 - \frac{\sin \kappa r}{\kappa r}\right) \kappa^2\, d\kappa \tag{3.2.13}$$

$$\kappa = \frac{2\pi}{\ell} \text{ (cycles/meter)},$$

is called the spatial frequency, or the turbulence wave number. ℓ is the size of turbulence eddies.

Also, for homogeneous isotropic turbulence,

$$D_f(r) = 2\left[B_f(0) - B_f(r)\right] \quad . \tag{3.2.14}$$

Since $B_f(0) = \sigma_f^2$, if $b_f(r)$ is the correlation coefficient,

$$D_f(r) = 2\sigma_f^2(1 - b_f(r)) \quad . \tag{3.2.15}$$

Finally, for the correlation function to exist in general, the spectrum, $\Phi_f(\kappa)$, must be regular. However, the structure function can exist even if the spectrum has a singularity at the origin. This is a particularly useful property of the structure function.

3.3 The Gaussian Model of Atmospheric Turbulence

In this model, the turbulence is assumed to be homogeneous and isotropic. Consequently, the correlation function of the refractive index fluctuation exists and is a function of spatial separation, r, only. It is defined by

$$B_{ng}(r) = \sigma_n^2 \, e^{-\frac{r^2}{\ell_n^2}} \quad , \tag{3.3.1}$$

where

σ_n^2 = variance of n

ℓ_n = correlation length .

The correlation coefficient is then

$$b_{ng}(r) = e^{-\frac{r^2}{\ell_n^2}} \quad . \tag{3.3.2}$$

Thus, ℓ_n is the separation at which the correlation coefficient falls to $\frac{1}{e}$. Hence, for the Gaussian Model, from (3.2.11) through (3.2.13),

$$\Phi_{ng}(\kappa) = \frac{\sigma_n^2 \ell_n^3}{8\pi\sqrt{\pi}} \, e^{-\frac{\kappa^2 \ell_n^2}{4}} \tag{3.3.3}$$

$$D_{ng}(r) = 2\sigma_n^2\left(1 - e^{-\frac{r^2}{\ell_n^2}}\right) \tag{3.3.4}$$

$$= 2\sigma_n^2(1 - b_{ng}(r)) \quad . \tag{3.3.5}$$

Note that (3.3.3) may also be written as

$$\Phi_{ng}(\kappa) = \frac{\sigma_n^2 \ell_n^3}{8\pi\sqrt{\pi}} e^{-\frac{\kappa^2}{\kappa_g^2}} \quad , \tag{3.3.6}$$

where

$$\kappa_g = \frac{2}{\ell_n} \quad . \tag{3.3.7}$$

This representation is useful when comparing the Gaussian spectrum with the Kolmogorov and Von Karman spectra.

3.4 Modified Kolmogorov Models

The turbulence spectrum of the Kolmogorov model is divided into three regions by two scale sizes: the outer scale of turbulence, L_0, and the inner scale (or microscale) of turbulence, ℓ_0 [25,26]. Let ℓ be the size of turbulence eddies.

1. Input range $\qquad L_0 < \ell, \qquad \kappa < \frac{2\pi}{L_0}$

Large scale atmospheric characteristics such as wind form turbulence eddies of this dimension. Thus, energy is input to the turbulence system from the thermal and kinetic energy of the atmosphere. The process is,

in general, anisotropic and varying, depending on climatic conditions. Consequently, it has not yet been described successfully in closed form. The spectrum is, therefore, undefined in this region.

The value of L_0 may vary widely. Close to the ground, it is usually taken to be equal to the height from the ground. In the free atmosphere it may be in the range of 10-100 m or more, differing significantly in different regions of space and depending on the turbulence inducing mechanism.

2. Inertial range $\quad \ell_0 < \ell < L_0 \qquad \frac{2\pi}{L_0} < \kappa < \frac{2\pi}{\ell_0}$

The eddies formed in the input range are unstable and fragment into smaller ones. These break up as well, continuing in this manner and causing energy to be distributed from the small to large turbulence wave numbers. There is very little energy loss in this process. Kolmogorov has shown that the spectrum in this region follows the law,

$$\Phi_{nk}(\kappa) \sim \kappa^{-\frac{11}{3}} \qquad (3.4.1)$$

and may be considered to be isotropic. Most cases of microwave propagation are affected predominantly by this region of the wave number spectrum.

3. Dissipation range $\quad \ell < \ell_0, \qquad \frac{2\pi}{\ell_0} < \kappa$

The energy in the turbulence, which was transferred through the inertial subrange, is dissipated through viscous friction by very small eddies. An accurate characterization of the spectrum is not known. It tends to zero rapidly and is frequently assumed to be of the form,

$$\Phi_{nk}(\kappa) \sim e^{-\frac{\kappa^2}{\kappa_m^2}}, \qquad (3.4.2a)$$

with

$$\kappa_m = \frac{5.92}{\ell_0} . \qquad (3.4.2b)$$

ℓ_0 is variously assumed to lie in the range of 1-10 mm. The composite spectrum, in the region other than the input range has been expressed by Tatarski as [6]

$$\Phi_{nk}(\kappa) = 0.033 C_n^2 \kappa^{-\frac{11}{3}} e^{-\frac{\kappa^2}{\kappa_m^2}} , \qquad (3.4.3)$$

where C_n^2 is the structure constant which will be considered in greater detail below.

The spectrum of the atmospheric turbulence is locally homogeneous. Hence, (see Section 3.2), a correlation function does not exist. However, the structure function exists and is related to $\Phi_n(\kappa)$ by the relationship (3.2.8).

In the inertial subrange, which is approximately isotropic, if we approximate the full spectrum by (3.4.1), we can write the structure function of the Kolmogorov spectrum, using (3.2.13), as

$$D_{nk}(r) = C_n^2 r^{\frac{2}{3}} \qquad L_0 >> r >> \ell_0 . \qquad (3.4.4)$$

This defines the structure constant in this case.

Von Karman Model

In order to obtain a full range solution using the Kolmogorov spectrum, the input region needs to be defined. One approximation which eliminates the singularity at the origin in (3.4.3) and gives a homogeneous isotropic spectrum is [27,28].

$$\Phi_{nv} = K_{\phi}(\kappa_L^2 + \kappa^2)^{-\frac{11}{6}} e^{-\frac{\kappa^2}{\kappa_m^2}}, \tag{3.4.5}$$

where

$$K_{\phi} \approx \frac{\Gamma\left(\frac{11}{6}\right)}{\pi\sqrt{\pi}\,\Gamma\left(\frac{1}{3}\right)} L_0^{-\frac{2}{3}} \sigma_n^2 . \tag{3.4.6}$$

$$\kappa_L = \frac{1}{L_0} . \tag{3.4.7}$$

Also, since ℓ_0 is of the order of a few millimeters, κ_m is very large. Assuming that $\kappa_m \to \infty$, the corresponding structure function is, [28],

$$D_{nv}(r) = 2\sigma_n^2 \left[1 - \frac{2^{\frac{2}{3}}}{\Gamma\left(\frac{1}{3}\right)} \left(\frac{r}{L_0}\right)^{\frac{1}{3}} K_{\frac{1}{3}}\left(\frac{r}{L_0}\right)\right] \tag{3.4.8}$$

where $K_{\frac{1}{3}}(x)$ is the modified cylindrical Bessel function. (3.4.8) should correspond to (3.4.4) for small r. Hence,

$$C_n^2 \approx 1.91\, L_0^{-\frac{2}{3}}\, \sigma_n^2 \qquad \left(m^{-\frac{2}{3}}\right) \quad . \tag{3.4.9}$$

Comparing (3.2.15) and (3.4.8), we obtain the correlation function

$$B_{nv}(r) = \sigma_n^2\, \frac{2^{\frac{2}{3}}}{\Gamma\left(\frac{1}{3}\right)} \left(\frac{r}{L_0}\right)^{\frac{1}{3}} K_{\frac{1}{3}}\left(\frac{r}{L_0}\right) \quad . \tag{3.4.10}$$

Therefore, when $\kappa_m \to \infty$, so that (3.4.9) is applicable,

$$B_{nv}(r) = 0.3100 C_n^2\, L_0^{\frac{2}{3}} \left(\frac{r}{L_0}\right)^{\frac{1}{3}} K_{\frac{1}{3}}\left(\frac{r}{L_0}\right) \tag{3.4.11}$$

and

$$\Phi_{nv}(\kappa) = 0.033 C_n^2 (\kappa_L^2 + \kappa^2)^{-\frac{11}{6}} e^{-\frac{\kappa^2}{\kappa_m^2}} \quad . \tag{3.4.12}$$

3.5 Averages of the Components of the Received Field

The random field in the aperture plane of a receiving antenna was described in (2.5.4) as,

$$\tilde{U}(\bar{P}) = \bar{A}_0\, e^{\tilde{\chi}(\bar{P}) + j\tilde{\psi}(\bar{P})} \quad . \tag{3.5.1}$$

In this section we obtain expressions for the variances, σ_χ^2 and σ_ψ^2, of the log amplitude and phase $\tilde{\chi}$ and $\tilde{\psi}$, respectively.

Let,

L = the path length travelled by the wave in the atmosphere,

ρ = the distance between two points in a plane transverse to the direction of propagation.

Then [29], assuming a homogeneous isotropic medium, it can be shown that for any quantity, x, the transverse correlation function is

$$B_x(\rho) = 2\pi^2 k^2 L \int_0^\infty f_x(\kappa)\Phi_n(\kappa)J_0(\kappa\rho)\kappa \, d\kappa \, , \qquad (3.5.2)$$

where

$f_x(\kappa)$ = the spectral filter function of x.

This is so named since it, together with the zeroth order cylindrical Bessel function, filters the spectrum, $\Phi_n(\kappa)$, to give the correlation function B_x. It is obtained from (3.5.1) using Rytov's first approximation. Then, for a plane wave, the log amplitude and phase filter functions are [29],

$$f_\chi(\kappa) = 1 - \frac{\sin\left(\frac{\kappa^2 L}{k}\right)}{\frac{\kappa^2 L}{k}} \qquad (3.5.3)$$

$$f_\psi(\kappa) = 1 + \frac{\sin\left(\frac{\kappa^2 L}{k}\right)}{\frac{\kappa^2 L}{k}} \, . \qquad (3.5.4)$$

The transverse correlation functions may be defined as,

$B_\chi(\rho) = \sigma_\chi^2 b_\chi(\rho)$ = the log amplitude correlation function,

$B_\psi(\rho) = \sigma_\psi^2 b_\psi(\rho)$ = the phase correlation function.

σ^2 and b denote the variance and correlation coefficients in the transverse plane, respectively. The following results are derived in Appendix A2 and simply stated below.

Gaussian Spectrum

From Appendix (A2.1),

$$\left.\begin{matrix} B_\chi(\rho) \\ B_\psi(\rho) \end{matrix}\right\} = \frac{\sqrt{\pi}}{2}\sigma_n^2 \ell_n k^2 L \left[e^{-\frac{\rho^2}{\ell_n^2}} \mp \frac{1}{W_g} \sum_{m=0}^{\infty} \frac{1}{m!} \left[\frac{-\rho^2}{\ell_n^2 \sqrt{1+W_g^2}} \right]^m \right.$$

$$\left. \frac{\sin\left[m \tan^{-1} W_g \right]}{m} \right] \quad , \qquad (3.5.5)$$
$$(3.5.6)$$

where the Gaussian wave parameter is

$$W_g = \frac{4L}{k\ell_n^2} \quad . \qquad (3.5.7)$$

Also, if we define the wave correlation function as

$$B_w(\rho) = B_\chi(\rho) + B_\psi(\rho) \quad , \qquad (3.5.8)$$

then

$$B_w(\rho) = \sqrt{\pi}\,\sigma_n^2 \ell_n k^2 L\, e^{-\frac{\rho^2}{\ell_n^2}} \qquad (3.5.9)$$

$$\sigma_x^2 = \frac{\sqrt{\pi}}{2}\,\sigma_n^2 \ell_n k^2 L \left[1 - \frac{\tan^{-1} W_g}{W_g}\right] \tag{3.5.10}$$

$$\sigma_\psi^2 = \frac{\sqrt{\pi}}{2}\,\sigma_n^2 \ell_n k_n^2 L \left[1 + \frac{\tan^{-1} W_g}{W_g}\right], \tag{3.5.11}$$

and

$$\sigma_w^2 = \sqrt{\pi}\;\sigma_n^2 \ell_n k^2 L \,. \tag{3.5.12}$$

Note that

$$\sigma_x^2 b_x(\rho) + \sigma_\psi^2 b_\psi(\rho) = \sigma_w^2 b_n(\rho) \tag{3.5.13a}$$

$$\sigma_x^2 + \sigma_\psi^2 = \sigma_w^2 \tag{3.5.13b}$$

$$\sigma_x^2(1 - b_x(\rho)) + \sigma_\psi^2(1 - b_\psi(\rho)) = \sigma_w^2(1 - b_n(\rho)) \,. \tag{3.5.13c}$$

From (3.2.15) we recognize each set of terms in (3.5.13c) to be one-half the corresponding structure function. Hence,

$$D_x(\rho) + D_\psi(\rho) = D_w(\rho) \,. \tag{3.5.13c*}$$

Von Karman Spectrum

From Appendix A2.2,

$$\left.\begin{matrix} B_\chi(\rho) \\ B_\psi(\rho) \end{matrix}\right\} = 0.033\pi^2 L_0^{\frac{5}{3}} C_n^2 k^2 L \cdot \sum_{p=0}^{\infty} \frac{(-1)^p}{(p!)^2}\left(\frac{\rho}{2L}\right)^{2p} \cdot \left\{ \Gamma(p+1)\Psi(p+1, p+\tfrac{1}{6}, Z_0) \right.$$

$$\left. \mp \frac{1}{W_0} Im\left[\Gamma(p) Z^{\frac{11}{6}-p} \Psi\left(\frac{11}{6}, \frac{17}{6}-p, Z\right)\right]\right\} \qquad (3.5.14)$$
$$(3.5.15)$$

where

$$Z = Z_0 - jW_0$$

$$Z_0 = \frac{1}{\kappa_m^2 L_0^2}$$

$$W_0 = \frac{L}{kL_0^2} \qquad (3.5.16a)$$

$$W_m = \frac{W_0}{Z_0} = \frac{\kappa_m^2 L}{k} \qquad (3.5.16b)$$

W_0 and W_m may be called wave parameters for the Von Karman model. Next,

$$B_w(\rho) = 0.033\pi^2\, 2L_o^{\frac{5}{3}} C_n^2 k^2 L \cdot \sum_{p=0}^{\infty} \frac{(-1)^p}{(p!)^2}\left(\frac{\rho}{2L}\right)^{2p} \Gamma(p+1)\Psi(p+1, p+\tfrac{1}{6}, Z_0) \qquad (3.5.17)$$

$$\left.\begin{matrix}\sigma_\chi^2 \\ \sigma_\psi^2\end{matrix}\right\} = 0.033\pi^2\,\frac{6}{5}\,L_0^{\frac{5}{3}}C_n^2k^2L\cdot\left\{1 \mp \Gamma\left(\frac{1}{6}\right)\frac{1}{W_0}\,Im\left[(-1)^{-\frac{11}{6}}\gamma\left(\frac{11}{6},-Z_0+jW_0\right)\right]\right\} \tag{3.5.18}$$

(3.5.19)

$$\sigma_w^2 = 0.033\pi^2\,\frac{12}{5}\,L_0^{\frac{5}{3}}C_n^2k^2L \quad . \tag{3.5.20}$$

Kolmogorov Spectrum

This spectrum is not homogeneous and isotropic. Therefore, the correlation functions are not defined. The singularity at the origin of the extended spectrum (3.4.3) results in $f_\psi(\kappa)\Phi_{nk}(\kappa)$ being singular. However, $f_\chi(\kappa)\Phi_{nk}(\kappa)$ is finite for all κ. Thus, only σ_χ^2 may be calculated. This is obtained in Appendix (A2.3),

$$\sigma_\chi^2 = 0.033\pi^2\,\frac{6}{5}\,\Gamma\left(\frac{1}{6}\right)\kappa_m^{-\frac{5}{3}}C_n^2k^2L\cdot\left[\frac{6}{11}(1+W_m^2)^{\frac{11}{12}}\,\frac{\sin\left(\frac{11}{6}\tan^{-1}W_m\right)}{W_m} - 1\right] . \tag{3.5.21}$$

Note that if $W_m >> 1$, this reduces to the common $k^{\frac{7}{6}}L^{\frac{11}{6}}$ form.

3.6 Some Properties of Propagation in Turbulence

Some general properties of propagation in homogeneous turbulence are discussed in this section using the concept of filter functions. A detailed treatment may be found in [9] and is not attempted here.

Consider a medium having a Gaussian spectrum as an example. Figure 3.1 shows such a spectrum together with examples of the amplitude and phase filter functions, $f_\chi(\kappa)$ and $f_\psi(\kappa)$.

Equation (3.5.2) shows that the integrand of the expressions for amplitude and phase variance include the product of the turbulence spectrum and the corresponding spectral filter function. Thus, it will be seen from Figure 3.1 that the phase fluctuations are affected by all eddy sizes and especially by those in the input region. On the other hand, for the log amplitude fluctuations, setting

$$f_\chi(\kappa) = 1$$

to determine the cut-off point yields

$$\sin\left(\frac{\kappa^2 L}{k}\right) \quad 0$$

so that the smallest κ for which $f_\chi(\kappa) = 1$ is

$$\kappa = \frac{\sqrt{2\pi}}{\sqrt{\lambda L}} \quad .$$

For smaller wave numbers, the amplitude filter function tends rapidly to zero, while for larger wave numbers, i.e., smaller eddies, the value of the spectrum is smaller. Hence, the major contribution to log amplitude fluctuations comes from eddies having sizes of about $\sqrt{2}\sqrt{\lambda L}$, i.e., comparable to the size of the Fresnel zone.

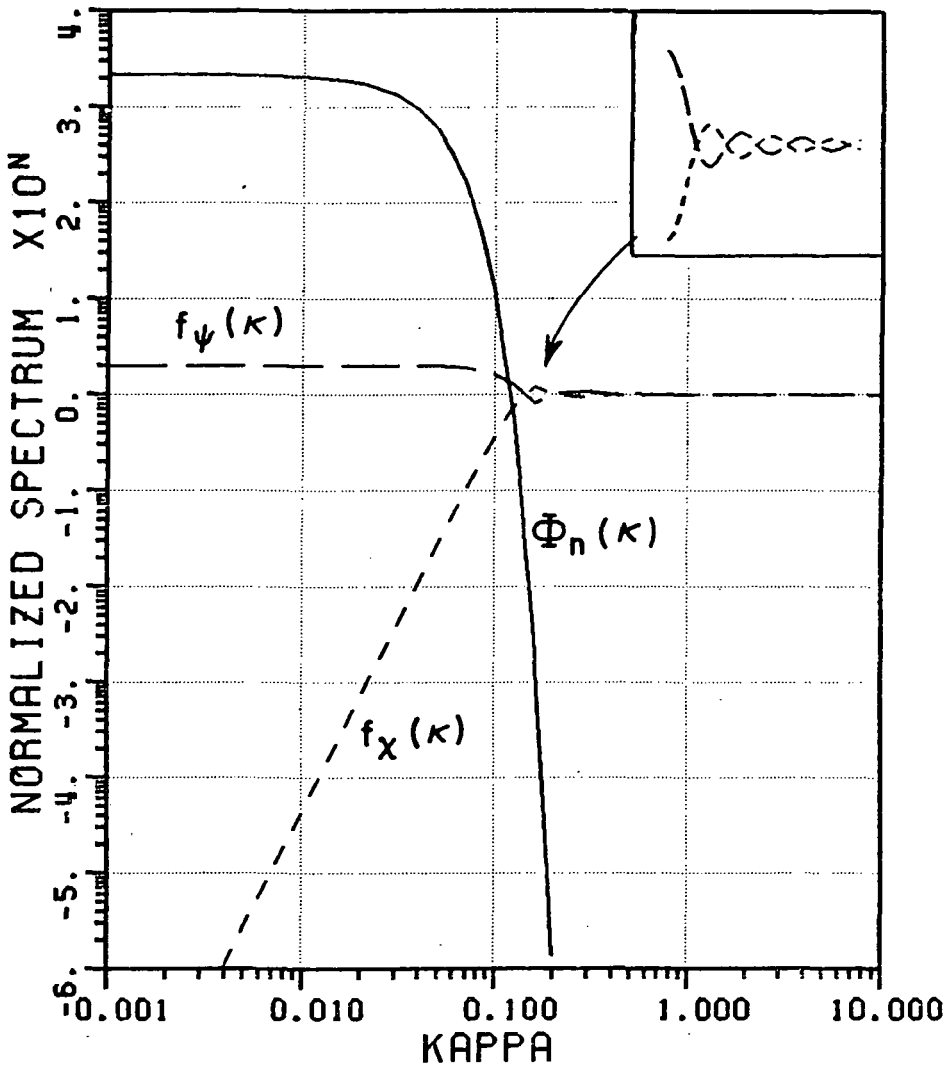

Figure 3.1. Atmospheric spectrum and filter functions. ℓ_n = 46 m, F = 30 GHz, L = 100 km.

Case 1: Geometrical Optics Region ($W_g << 1$)

$$W_g = \frac{4L}{k\ell_n^2}$$

Then

$$L << \frac{\ell_n^2}{\lambda} .$$

This case is illustrated in Figure 3.2.

From (3.5.10) and (3.5,11), using

$$\tan^{-1} W_g \approx W_g - \frac{W_g^3}{3}$$

$$\left.\begin{matrix}\sigma_\chi^2 \\ \sigma_\psi^2\end{matrix}\right\} = \frac{\sqrt{\pi}}{2}\sigma_n^2 \ell_n k^2 L \left[1 \mp \left(1 - \frac{4^2 L^2}{3k^2\ell_n^4}\right)\right] ,$$

so

$$\sigma_\chi^2 = \frac{8\sqrt{\pi}}{3}\sigma_n^2 \frac{L^3}{\ell_n^3} \qquad (3.6.1)$$

$$\sigma_\psi^2 = \sqrt{\pi}\,\sigma_n^2 \ell_n k^2 L . \qquad (3.6.2)$$

Thus, σ_χ^2 is independent of frequency and is proportional to L^3. However, σ_ψ^2 is proportional to k^2 and L.

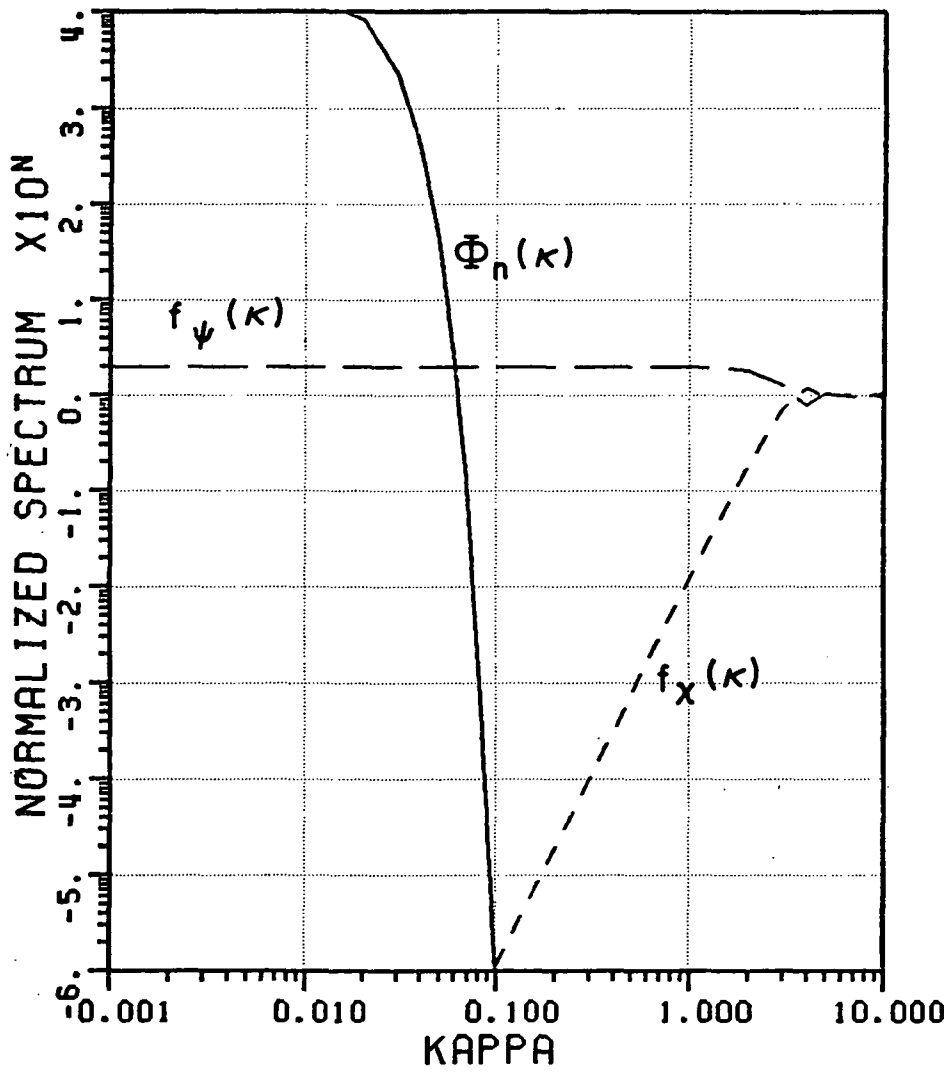

Figure 3.2. Spectral filter functions for the geometrical optics region. ℓ_n = 100 m, F = 90 GHz, L = 0.5 km.

Case 2: Long Path Region ($W_g >> 1$)

In this case

$$\frac{\ell_n^2}{\lambda} << L \ .$$

This is illustrated in Figure 3.3. Again, from (3.5.10) and (3.5.11) and using

$$\frac{\tan^{-1} W_g}{W_g} << 1 \ ,$$

$$\sigma_\chi^2 = \sigma_\psi^2 = \frac{\sqrt{\pi}}{2} \sigma_n^2 \ell_n k^2 L \quad . \tag{3.6.3}$$

Now both σ_χ^2 and σ_ψ^2 are approximately equal and are proportional to k^2 and L.

σ_w^2 remains proportional to k^2L in both the geometrical optics and long path regions.

Though the Gaussian spectrum was used here as an example, it is important to note that the same behavior is true for any homogeneous isotropic spectrum.

In a medium having a Von Karman spectrum,

$$W_m << 1$$

denotes the geometrical optics region, with

$$\sigma_\chi^2 \sim L^3 \text{ and } \sigma_\psi^2 \sim k^2 L$$

and

$$1 << W_0$$

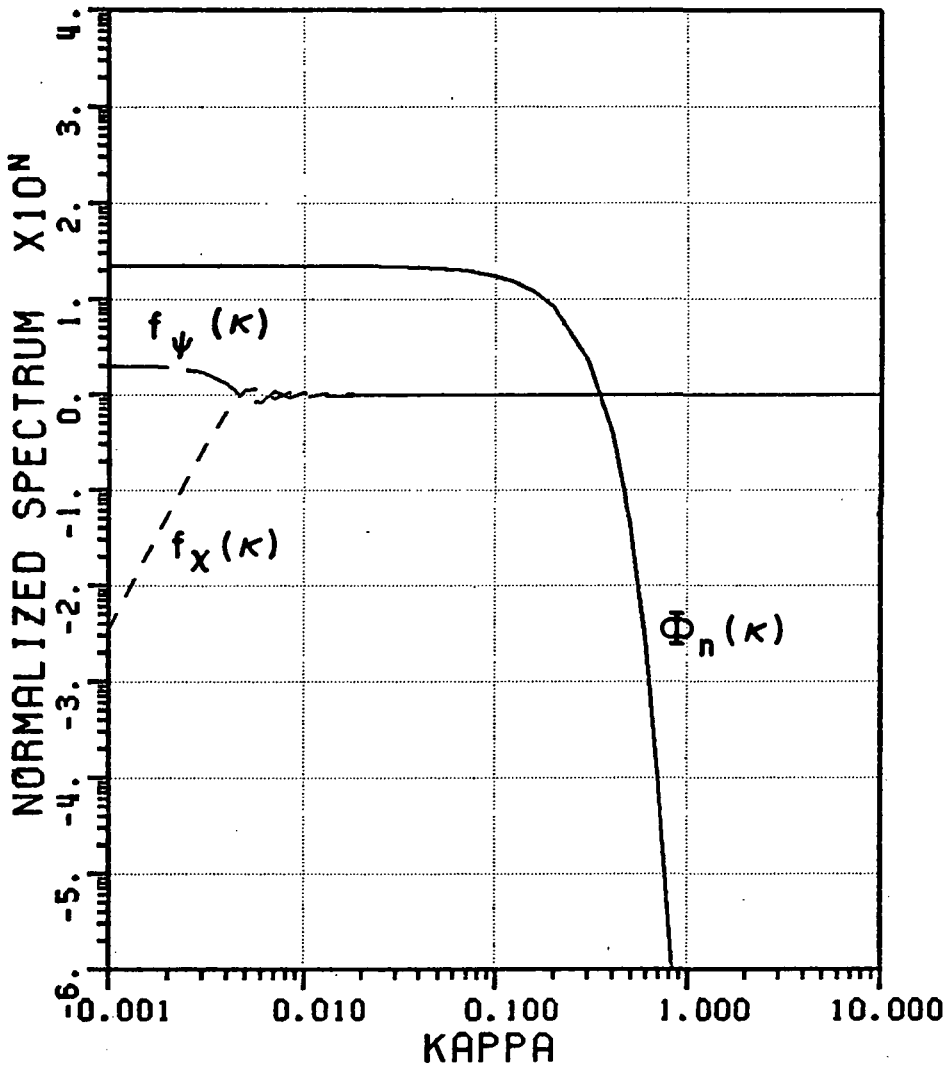

Figure 3.3. Spectral filter functions for the long path region. ℓ_n = 10 m, F = 0.1 GHz. L = 300 km.

represents the long path region, where

$$\sigma_x^2 = \sigma_\psi^2 \sim k^2 L \quad .$$

Also,

$$W_0 < 1 < W_m$$

represents the intermediate region in which the propagation characteristics are dominated by the inertial subrange. Here

$$\sigma_x^2 \sim k^{\frac{7}{6}} L^{\frac{11}{6}} \quad . \qquad \sigma_\psi^2 \sim k^2 L \quad .$$

If the medium is represented by the extended Kolmogorov spectrum alone, there will be no long path region. Then, the wave parameter, W_m, will divide the spectrum into the inertial subrange and the geometrical optics region only. The remarks on these regions, made above, would still apply.

3.7 Comparison of Spectra

Some main features of the Gaussian and Von Karman spectra are compared in this section and are related to each other.

Figure 3.4 shows typical correlation functions for both the Gaussian and Von Karman spectra, (3.3.1) and (3.4.11), respectively. The main parameters in this plot are

$$\ell_n = 40 \text{ m}$$

$$L_0 = 52 \text{ m}$$

$$\ell_0 = 10 \text{ mm}.$$

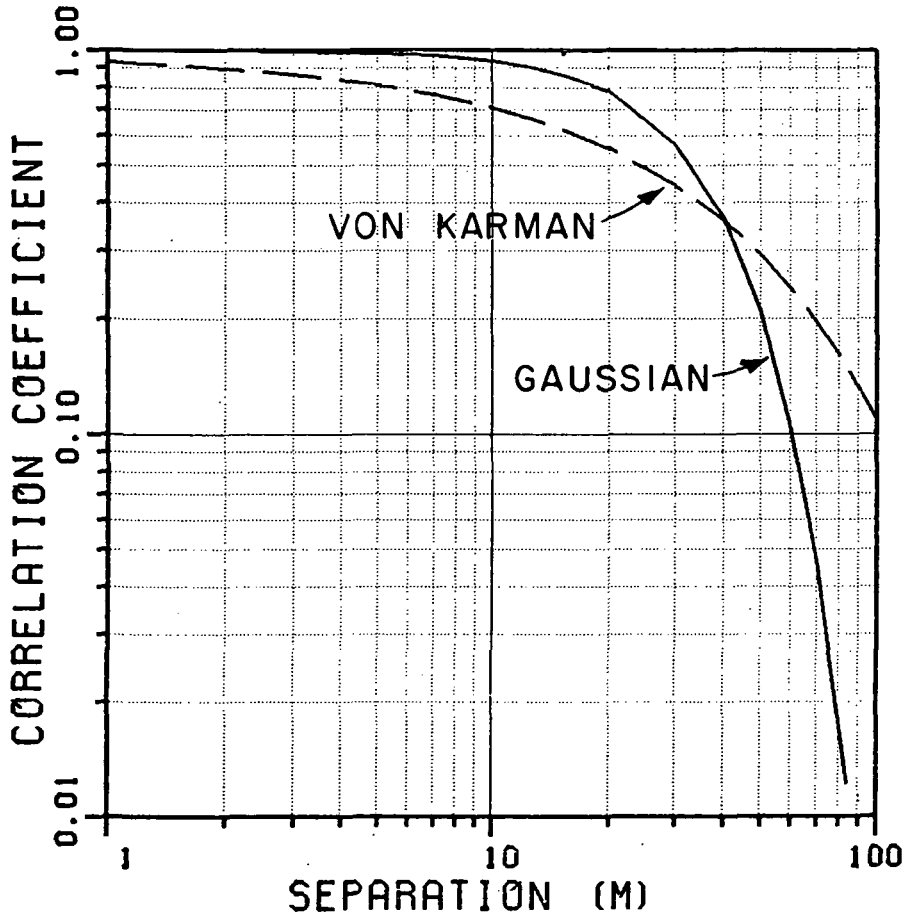

Figure 3.4. A comparison of correlation coefficients of the Gaussian and Von Karman models.
ℓ_n = 40 m, L_0 = 52 m, ℓ_0 = 10 mm.

In an attempt to find a meaningful comparison, the parameters of the Von Karman spectrum were chosen so that both spectra showed the same correlation length, defined as that length at which the correlation coefficient drops to 1/e. The correlation length of the Gaussian spectrum is, of course, ℓ_n. It was found, somewhat surprisingly, that over a fairly wide range of values of ℓ_n, the simple relationship

$$\frac{L_0}{\ell_n} = 1.2 \text{ to } 1.4 \tag{3.7.1}$$

appears to hold if the correlation lengths are forced to be equal. Under these conditions, the Gaussian correlation function shows a higher value than the Von Karman spectrum over small separations. However, for fairly wide separations, the Gaussian function cuts off sharply while the Von Karman spectrum exhibits a higher, although insignificant, correlation.

Figure 3.5 shows the corresponding spectra, given by (3.3.3) and (3.4.12), respectively. The most clearly defined difference is the much higher value of the Von Karman spectrum throughout the input region. There is a short region where the spectra cross over. The slopes are fairly close in a portion of this region. For high values of κ, the Von Karman spectrum, once again, is higher. In light of the preceding discussions on amplitude and phase filter functions, these characteristics imply that the variance of a propagating wave will be higher in the long path and the geometrical optics regions of the Von Karman spectrum.

Another comparison was also made. The expressions for the wave variances of the two spectra are given by (3.5.12) and (3.5.20). Since both quantities show a k^2L dependence, the condition under which they are identical is easily found. If

$$\sigma^2_{wg} = \sigma^2_{wv}$$

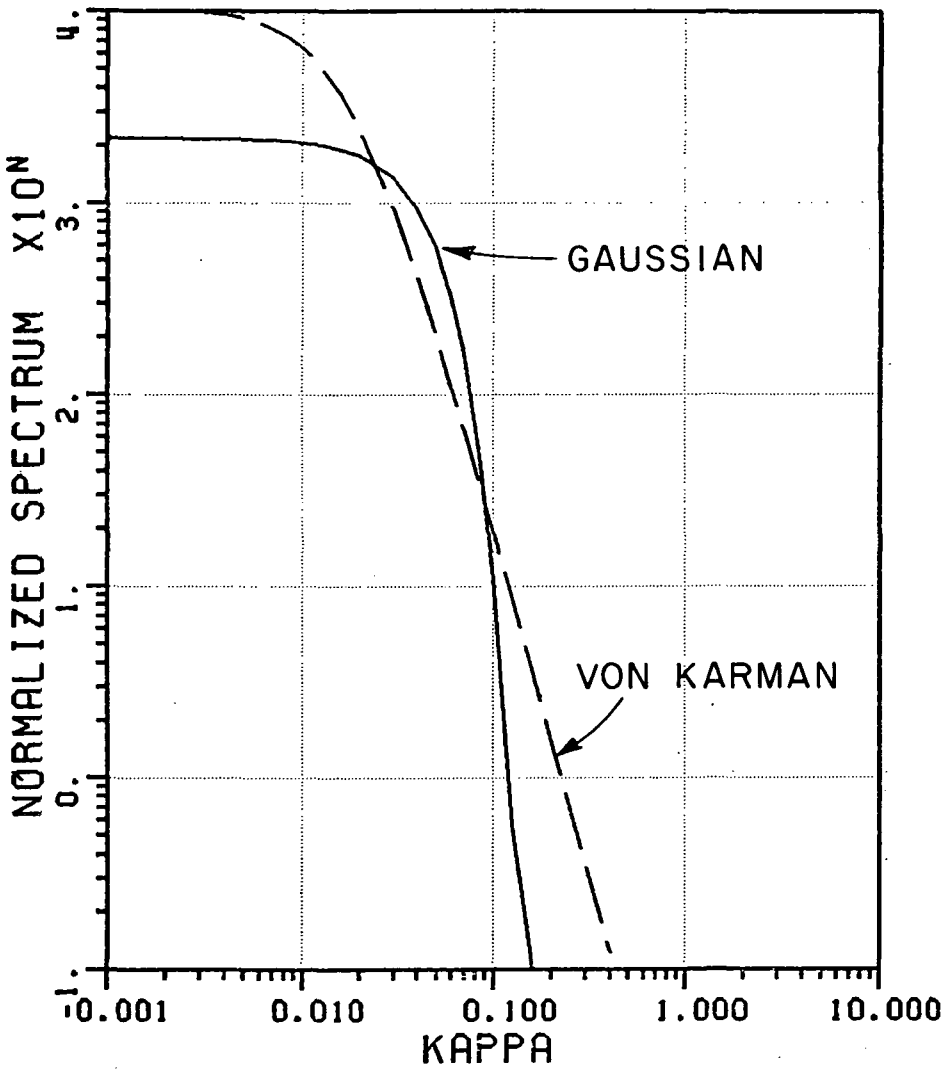

Figure 3.5. A comparison of spectra of the Gaussian and Von Karman models.
ℓ_n = 40 m, L_0 = 52 m, ℓ_0 = 10 mm.

$$\sqrt{\pi}\,\sigma_n^2 \ell_n k^2 L = 0.033\pi^2 C_n^2 \left(\frac{12}{5}\right) L_0^{\frac{5}{3}} k^2 L \quad .$$

Then, using (3.4.9) we obtain

$$L_0 = 1.2\,\ell_n \quad . \tag{3.7.2}$$

Comparing (3.7.1) and (3.7.2), it is clear that (3.7.2) is a reasonable basis for matching the Gaussian and the Von Karman spectra.

The discussion so far has not included the variance of the refractive index fluctuations. This may be accomplished by using (3.7.2) together with (3.4.9) to define an equivalent structure constant, C_{ng}^2, for the Gaussian spectrum.

$$C_{ng}^2 = 1.91\,(1.2\,\ell_n)^{-\frac{2}{3}}\sigma_n^2 \tag{3.7.3}$$

This quantity, by itself, is meaningless. It does serve a useful purpose, however, as an aid for comparing the two spectra. This is especially useful as most experimental and theoretical works describe C_n^2 and not σ_n^2.

For the purposes of engineering calculations, the Gaussian spectrum provides a reasonably good approximation to the Von Karman spectrum. Its advantages for analytical purposes are many. Its major sources of possible error, if borne in mind when interpreting the results, are tolerable. Consequently, the analysis that follows will assume a homogeneous, isotropic Gaussian spectrum, given by (3.3.1) and (3.3.3).

3.8 Moments of the Aperture Field

The moments of the aperture field of an antenna in a turbulent medium are given in this section. The following assumptions are made:

1) The turbulence spectrum is assumed to be homogeneous, isotropic, and Gaussian. Its correlation function is, therefore, also Gaussian.
2) The average direction of propagation of the wave, as a whole, is unchanged. Also, there is no depolarization of the wave.
3) The antenna is relatively large in terms of wavelength. Hence, the beamwidth is fairly small, i.e., on the order of a few degrees at most. The side lobe levels are also assumed to be low.

The third approximation above implies that if the analysis is confined to the main lobe, even down to the first null, the aperture plane is nearly transverse to the direction of propagation. Thus, correlation functions and variances in the aperture plane are substantially the same as those derived for the transverse plane. This is referred to as the paraxial approximation.

Under these assumptions, if $\tilde{\bar{U}}(\bar{P})$ is the random field in the aperture plane, then from Appendix A3, letting

$$U_0 = A_0 \, e^{\chi_0 + \sigma_\chi^2 + j\sigma_\chi\sigma_\psi b_{\chi\psi}(0)} , \tag{3.8.1}$$

we find that

$$< \tilde{\bar{U}}(\bar{P}) > = \bar{U}_0 \, e^{-\frac{1}{2}\sigma_w^2} \tag{3.8.2}$$

and

$$< \tilde{U}(\overline{P}_1)\ \tilde{U}(\overline{P}_2)^* > = |U_0|^2\ e^{-\sigma_w^2}\ e^{\sigma_w^2 b_n(\rho)} \qquad (3.8.3)$$

where

$$\rho = |\overline{P}_1 - \overline{P}_2|$$

and

$$\overline{U}_0 = \hat{p} U_0 \ . \qquad (3.8.4)$$

$\hat{p}$ is the polarization vector as before.

It is interesting, as pointed out by Shifrin [11], that under the assumptions made for this analysis, $<\tilde{U}(\overline{P}_1)\ \tilde{U}(\overline{P}_2)^*>$ remains the same whether the amplitude and phase perturbations are mutually dependent or not. Therefore, the mean power pattern and other parameters associated with the power pattern are also independent of the nature of the interaction between the random amplitude and phase, if any.

3.9 Incident Power Density

The expected value of the time average power density of the incident field in the antenna aperture is

$$< S_{inc} > = \frac{1}{2}\ Re < \tilde{E}_r(\overline{P}) \times \tilde{H}_r(\overline{P})^* > \qquad (3.9.1)$$

where $\tilde{H}_r(\overline{P})$ is the random incident magnetic field in the aperture plane. If the perturbations are such that the incident wave can be considered to be locally plane, then taking η_0 as the characteristic impedance of free space.

$$< S_{inc} > = \frac{< \tilde{\overline{E}}_r(\overline{P}) \cdot \tilde{\overline{E}}_r(\overline{P})^* >}{2\eta_0} \quad . \tag{3.9.2}$$

Therefore, from (3.8.3),

$$< S_{inc} > = \frac{|U_0|^2}{2\eta_0} \quad . \tag{3.9.3}$$

Fried [34] has shown from energy considerations that, for a plane wave propagating through the turbulent atmosphere, assuming no out of path scattering,

$$\chi_0 = -\sigma_\chi^2 \quad . \tag{3.9.4}$$

This implies that the power density, $< S_{inc} >$, is constant. These assumptions will not, however, be made in this work. U_0 will be left in its full form.

Summarizing, the main thrust of this chapter was to find moments of the field in the aperture plane of the antenna. To obtain these, the general characteristics of some models of atmospheric refractive index fluctuations were studied. The averages of the components of the received field were also obtained for these models. The Gaussian model for homogeneous turbulence was related to the Von Karman model and was found to be a reasonable approximation for engineering calculations.

CHAPTER IV

THE RECEIVING SYSTEM

4.1 General Comments

The results derived so far concern the effect of the atmosphere and the antenna only. In this chapter we examine some effects of the receiver on the reception of the scintillating signal.

The receiver will be defined as that section of the receiving system which follows the antenna. Its role is to extract information from the incoming signal. To do this it may use, in some manner, the amplitude, phase, frequency, or a combination of these parameters, of the antenna output. The type of processing has a profound influence, not only on the statistics of the final output of the receiver, but also on the perceived statistics of the incoming signal as measured through the receiving system.

In this study, the final output of the receiver will be called the output signal, while the incoming signal as measured through the receiver will be termed the measured signal. It is important to realize that in general the output signal, the measured signal, and the incoming signal, as defined above, will not be the same. The measured signal is

deduced from the output signal using the inverse of the receiver characteristics. However, due to the processing done by the receiver, some of the attributes of the incoming signal may be irretrievably lost. Therefore, the measured signal may be only a partial description of the incoming signal. An obvious example is that of the frequency modulation (FM) receiver, which eliminates amplitude information from the incoming signal through the use of limiters.

This study will concentrate on receivers which do not destroy amplitude information. Expressions are derived for the received signal voltage level, non-fluctuating power or dc power, total power, normalized variance, and the degradation of the dc power, as measured by the receiver. For this purpose, the antenna will be assumed to be conjugate matched to the receiver in the rest of this study.

Further, the average effective aperture, gain, and gain degradation of the antenna are also obtained. These parameters of the antenna do not depend on the receiver used.

The receiver will be divided into one of two broad classes as follows:

a) Synchronous receivers.

b) Asynchronous receivers.

Synchronous Receivers

A receiver using phase locked loops in its demodulating chain falls in the first category, as does any receiver using the phase information contained in the signal. It should be noted that an amplitude modulation (AM) receiver using a synchronous detector belongs to this group as well. Such a synchronous receiver's output amplitude, V_{os}, is affected by the amplitude scintillation and phase fluctuations of the incoming wave. Therefore, letting the tilde denote random quantities as

before, we may write

$$\tilde{V}_{os} = \text{function of } (\tilde{V}_r) \ .$$

A receiver that employs limiters on the signal amplitude and uses the phase information only, is affected by phase fluctuations. If ϕ_{os} is the measured phase at the output,

$$(\tilde{\phi}_{os}) = \text{function of } (\text{Arg } (\tilde{V}_r)) \ .$$

Consider a synchronous amplitude modulation receiver. Let V_{syn} be the received signal voltage as measured by this receiver. Then, since no amplitude or phase information is destroyed by the processing circuitry,

$$\tilde{V}_{syn} = RX_s^{-1}(\tilde{V}_{os}) = \tilde{V}_r \ . \qquad (4.1.1)$$

RX_s^{-1} is the inverse of the synchronous receiver transfer function and represents the receiver calibration curve.

Next, consider the average value of $\tilde{V}_{syn}$

$$< \tilde{V}_{syn} > = < \tilde{V}_r > \ . \qquad (4.1.2)$$

From (2.5.6), the mean received voltage is

$$< \tilde{V}_{syn} > = < \tilde{V}_r > = K_V \int_S < \tilde{\bar{U}}(\bar{P}) > \cdot \bar{f}(\bar{P}) \, e^{-j\bar{k}_s \cdot \bar{P}} \, dS$$

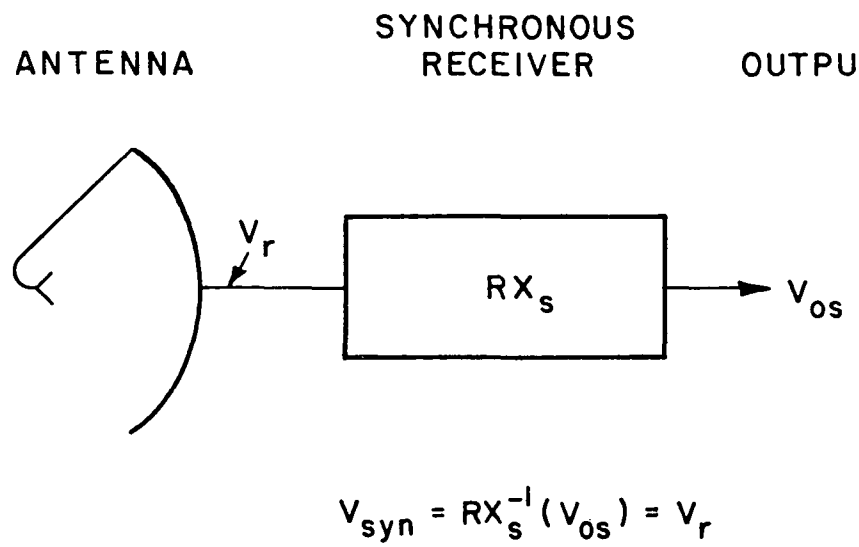

Figure 4.1. The received signal measured by a synchronous receiver.

$$< \tilde{V}_{syn} > = < \tilde{V}_r > = K_V \int_S (\hat{p}\cdot\hat{p}_f) < \tilde{U}(\bar{P}) > f(\bar{P})\, e^{-j\bar{k}_s\cdot\bar{P}}\, dS \ . \tag{4.1.3}$$

The mean squared received voltage is

$$< |\tilde{V}_{syn}|^2 > = < |\tilde{V}_r|^2 > = |K_V|^2 \iint_S \iint_S |\hat{p}\cdot\hat{p}_f|^2 < \tilde{U}(\bar{P}_1)\tilde{U}(\bar{P}_2)^* >$$

$$f(\bar{P}_1)f(\bar{P}_2)^*\, e^{-j\bar{k}_s\cdot(\bar{P}_1-\bar{P}_2)}\, dS_1 dS_2 \ . \tag{4.1.4}$$

We define the normalized variance as

$$\varepsilon^2_{syn} = \frac{< |\tilde{V}_r|^2 > - |< \tilde{V}_r >|^2}{|< \tilde{V}_r >|^2} \quad . \tag{4.1.5}$$

Asynchronous Receivers

A receiver using a square-law detector to process amplitude information belongs to this category. This type of receiver does not use the phase of the incoming signal. Hence, it is sensitive to amplitude scintillation of the antenna voltage only. Any fluctuation of the overall phase front of the incoming wave will not be detected by the receiver, except in the sense that it affects the amplitude of the antenna output. If V_{oa} is the receiver output voltage, we may write

$$\tilde{V}_{oa} = \text{function of } (|\tilde{V}_r|) \ .$$

In the particular case of a receiver using square-law detection,

$$V_{oa} \sim |V_r|^2 \ .$$

Consequently, fluctuations of $\tilde{V}_r$, as measured by this receiver will be less than that measured by a synchronous receiver. This is an important difference.

Let V_{asyn} be the received signal as measured by an asynchronous amplitude modulation receiver. Then,

$$\tilde{V}_{asyn} = RX_a^{-1}(V_{oa}) = |\tilde{V}_r| \tag{4.1.6}$$

where RX_a^{-1} represents the calibration curve of the asynchronous receiver.

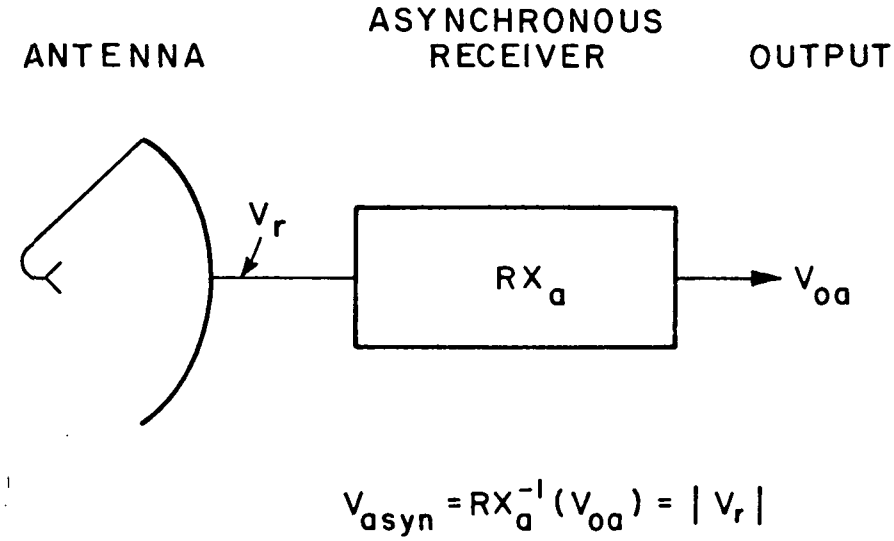

Figure 4.2. The received signal measured by an asynchronous receiver.

Considering average levels,

$$\langle \tilde{V}^2_{asyn} \rangle = \langle |\tilde{V}_r|^2 \rangle = |K_V|^2 \iint_S \iint_S \langle \tilde{U}(\bar{P}_1)\tilde{U}(\bar{P}_2)^* \rangle \, |\hat{p}\cdot\hat{p}_f|^2$$

$$f(\bar{P}_1)f(\bar{P}_2)^* \, e^{-j\bar{k}_s\cdot(\bar{P}_1-\bar{P}_2)} \, dS_1 dS_2$$

as before.

It is not possible to obtain $\langle \tilde{V}_r \rangle$, since there is no phase information in the output. However, $\langle |\tilde{V}_r| \rangle$ may be obtained as follows:

$$\langle \tilde{V}_{asyn} \rangle = \langle |\tilde{V}_r| \rangle = \langle \sqrt{|\tilde{V}_r|^2} \rangle \quad . \tag{4.1.7}$$

The normalized variance of the signal, as measured by an asynchronous detector, is

$$\sigma^2_{asyn} = \frac{< |\tilde{V}_r|^2 > - < |\tilde{V}_r| >^2}{< |\tilde{V}_r| >^2} \quad . \tag{4.1.8}$$

4.2 Average Received Voltage (synchronous receiver)

From (4.1.2)

$$< \tilde{V}_{syn} > = < \tilde{V}_r(\bar{k}_s) > \tag{4.2.1}$$

and from (3.8.2) and (4.1.3)

$$< \tilde{V}_{syn} > = \bar{U}_0 \, e^{-\frac{1}{2}\sigma_w^2} K_V \cdot \int_S \bar{f}(\bar{P}) \, e^{-j\bar{k}_s \cdot \bar{P}} \, dS \quad . \tag{4.2.2}$$

Let

$$I_V(\bar{k}_s) = \int_S f(\bar{P}) \, e^{-j\bar{k}_s \cdot \bar{P}} \, dS \tag{4.2.3}$$

and

$$I_{V\,max} = \left| I_V(\bar{k}_s) \right|_{max} \tag{4.2.4}$$

over all $\bar{k}_s$.

Define

$$g_V(\bar{k}_s) = \frac{I_V(k_s)}{I_{V\ max}} \leq 1 \qquad (4.2.5)$$

and

$$V_{d0} = U_0 K_V I_{V\ max} \quad . \qquad (4.2.6)$$

Then,

$$< \tilde{V}_{syn} > = V_{d0}\, e^{-\frac{1}{2}\sigma_w^2}\, g_V(\bar{k}_s)\, \hat{p}\cdot\hat{p}_f \quad . \qquad (4.2.7)$$

V_{d0} is the measured signal voltage when the wave is incident along the main beam axis, with no polarization mismatch. $g_V(\bar{k}_s)$ is the normalized plane wave voltage (or electric field) pattern function. Therefore, Equation (4.2.7) shows that though there is a reduction in the received signal voltage, there is no change in the field pattern function when the measurements are made using a synchronous AM receiver.

4.3 Total Received Power

The total received power, assuming a matched load is

$$P_R = \frac{< |\tilde{V}_r(\bar{k}_s)|^2 >}{2|Z_1|^2} R_1 \quad . \qquad (4.3.1)$$

R_1 is the load resistance, being the real part of $Z_1 = Z_a^*$.

From (3.8.3) and (4.1.4),

$$< |\tilde{V}_r(k_s)|^2 > = |p \cdot p_f|^2 \; |U_0|^2 \; e^{-\sigma_w^2} \; |K_V|^2 \; I_p(\bar{k}_s) \; , \qquad (4.3.2)$$

where

$$I_p(\bar{k}_s) = \iint_S \; e^{\sigma_w^2 b_n(\bar{P}_1, \bar{P}_2)} \; f(\bar{P}_1) f(\bar{P}_2)^* \; e^{-j\bar{k}_s \cdot (\bar{P}_1 - \bar{P}_2)} \; dS_1 dS_2 \; . \qquad (4.3.3)$$

Consider the unperturbed plane wave incidence case, i.e., $\sigma_w^2 = 0$. The integral becomes

$$I_{PO} = \iint_S f(\bar{P}_1) f(\bar{P}_2)^* \; e^{-j\bar{k}_s \cdot (\bar{P}_1 - \bar{P}_2)} \; dS_1 dS_2$$

$$= \int_S f(\bar{P}_1) \; e^{-j\bar{k}_s \cdot \bar{P}_1} \; dS_1 \cdot \left\{ \int_S f(\bar{P}_2) \; e^{-j\bar{k}_s \cdot \bar{P}_2} \; dS_2 \right\}^*$$

$$= \left| \int_S f(\bar{P}) \; e^{-j\bar{k}_s \cdot \bar{P}} \; dS \right|^2$$

$$= \left| I_V(\bar{k}_s) \right|^2 \; ,$$

from (4.2.3). This is the plane wave power pattern. Further, let

$$I_{PO\,max} = \left| I_V(\bar{k}_s) \right|^2_{max} \qquad (4.3.4)$$

and

$$g_0(\bar{k}_s) = \frac{I_{P0}(\bar{k}_s)}{I_{P0\ max}} = \left|g_V(\bar{k}_s)\right|^2 \quad . \tag{4.3.5}$$

$g_0(\bar{k}_s)$ is the normalized power pattern function of the antenna when receiving an unperturbed plane wave. Then, (4.3.2) becomes

$$<|\tilde{V}_r(\bar{k}_s)|^2> = |\hat{p}\cdot\hat{p}_f|^2\ |U_0|^2\ |K_V|^2\ |I_{V\ max}|^2\ g_0(\bar{k}_s)\ e^{-\sigma_w^2 \frac{I_p(\bar{k}_s)}{I_{P0}(\bar{k}_s)}} .$$

Now define

$$g_d = e^{-\sigma_w^2 \frac{I_p(\bar{k}_s)}{I_{P0}(\bar{k}_s)}} \quad . \tag{4.3.6}$$

Using (4.2.6) we obtain

$$<|\tilde{V}_r(\bar{k}_s)|^2> = |V_{d0}|^2\ g_0(\bar{k}_s) g_d\ |\hat{p}\cdot\hat{p}_f|^2 \quad . \tag{4.3.7}$$

Therefore, the received total power

$$P_R = P_{R0} g_0(\bar{k}_s) g_d\ |\hat{p}\cdot\hat{p}_f|^2 \quad , \tag{4.3.8}$$

where

$$P_{R0} = \frac{|V_{d0}|^2}{2|Z_1|^2} R_1 \quad . \tag{4.3.9}$$

P_{RO} is the maximum received power for plane wave incidence with no polarization mismatch. g_d is called the gain degradation factor. It accounts for the reduction of the measured total power (and gain) when the incident wave is perturbed by turbulence.

A method of evaluating (4.3.6), which also helps to bring out its physical properties is by using the relationship

$$e^{\sigma_w^2 b_n} = 1 + \sum_{m=1}^{\infty} \frac{(\sigma_w^2 b_n)^m}{m!} \tag{4.3.10}$$

in Equation (4.3.3). Then,

$$I_p(\bar{k}_s) = I_{P0}(\bar{k}_s) + \sum_{m=1}^{\infty} \frac{\sigma_w^{2m}}{m!} I_{Pm}(\bar{k}_s) \ , \tag{4.3.11}$$

where

$$I_{Pm}(\bar{k}_s) = \iint_{S\ S} b_n(\bar{P}_1,\bar{P}_2)^m \ f(\bar{P}_1) f(\bar{P}_2)^* \ e^{-j\bar{k}_s \cdot (\bar{P}_1 - \bar{P}_2)} \ dS_1 dS_2 \ . \tag{4.3.12}$$

Let

$$I_{Cm}(\bar{k}_s) = \frac{I_{Pm}(\bar{k}_s)}{I_{P0}(\bar{k}_s)} \ , \tag{4.3.13}$$

where I_{Cm} will be called the correlation integral. It will be shown later that this is a function of the degree of correlation of the wave over the antenna aperture.

Thus, we may write (4.3.8) as

$$P_R = P_{RO} g_0(\bar{k}_s)\, e^{-\sigma_w^2} \left\{ 1 + \sum_{m=1}^{\infty} \frac{\sigma_w^{2m}}{m!} I_{Cm}(\bar{k}_s) \right\} |\hat{p}\cdot\hat{p}_f|^2 . \qquad (4.3.14)$$

Now it is seen that

$$g_d = e^{-\sigma_w^2} \sum_{m=0}^{\infty} \frac{\sigma_w^{2m}}{m!} I_{Cm}(\bar{k}_s) \quad . \qquad (4.3.15)$$

$$I_{C0}(\bar{k}_s) = 1 \quad . \qquad (4.3.16)$$

Finally, we let

$$P_{RO} g_0(\bar{k}_s)\, e^{-\sigma_w^2} = \frac{< \tilde{V}_{syn} >^2}{2|Z_1|^2} R_1 = P_{dcs} \qquad (4.3.17)$$

which we identify as the measured dc power, P_{dcs}, using the synchronous receiver. It corresponds to the coherent power in the wave, as defined by Ishimaru. The second term in (4.3.14) must, therefore, represent the fluctuating power. Hence,

$$P_R = P_{dcs} + P_{f1} \qquad (4.3.18)$$

where

$$P_{f1} = P_{RO} g_0(\bar{k}_s)\, e^{-\sigma_w^2} \sum_{m=1}^{\infty} \frac{\sigma_w^{2m}}{m!} I_{Cm}(\bar{k}_s) \quad . \qquad (4.3.19)$$

The fluctuating power, P_{f1}, corresponds to the incoherent power in the wave as defined by Ishimaru.

4.4 Signal Variance (synchronous receiver)

The normalized variance of the measured signal, from (4.1.5) and (4.3) is

$$s^2_{syn}(\bar{k}_s) = \frac{P_R - \frac{|<\tilde{V}_{syn}>|^2}{2|Z_1|^2} R_1}{\frac{|<\tilde{V}_{syn}>|^2}{2|Z_1|^2} R_1} \qquad (4.4.1)$$

$$= \frac{g_0(\bar{k}_s) g_d - e^{-\sigma_w^2 |g_V(\bar{k}_s)|^2}}{e^{-\sigma_w^2 |g_V(\bar{k}_s)|^2}} \quad .$$

Therefore,

$$s^2_{syn}(\bar{k}_s) = e^{\sigma_w^2} g_d - 1 \quad . \qquad (4.4.2)$$

If (4.3.15) is used, we have

$$s^2_{syn}(\bar{k}_s) = \sum_{m=1}^{\infty} \frac{\sigma_w^{2m}}{m!} I_{Cm}(\bar{k}_s) \quad . \qquad (4.4.3)$$

Finally,

$$s^2_{syn}\ (dB) = 10 \log_{10} s^2_{syn} \quad . \qquad (4.4.4)$$

4.5 Average Signal Level Degradation (synchronous receiver)

The average signal level degradation may be defined as the reduction in the measured dc power compared to that in the absence of turbulence.

$$\Delta P_{dcs} = -10 \log_{10} \frac{P_{dcs}}{P_{dcs}\Big|_{\text{No fluctuations}}} \quad \text{(dB)} \qquad (4.5.1)$$

For the synchronous receiver, from (4.3.17)

$$P_{dcs} = P_{R0} g_0(\bar{k}_s)\, e^{-\sigma_w^2}$$

$$\Delta P_{dcs} = -10 \log_{10} e^{-\sigma_w^2} \quad \text{(dB)} \qquad (4.5.2)$$

$$\Delta P_{dcs} = 4.343\, \sigma_w^2 \quad \text{(dB)} \quad . \qquad (4.5.3)$$

It should be noted that ΔP_{dcs} is independent of the antenna parameters. This is because it is a measure of the reduction in the true coherent power in the incoming wave. This is clearly a function of the turbulence only.

4.6 Average Received Voltage (asynchronous receiver)

$$\langle \tilde{V}_{asyn} \rangle = \langle |\tilde{V}_r(\bar{k}_s)| \rangle = \langle \sqrt{|\tilde{V}_r(\bar{k}_s)|^2} \rangle \qquad (4.6.1)$$

From Appendix A4, for small fluctuations,

$$\langle \tilde{V}_{asyn} \rangle \approx |V_{d0}|\, |g_V(\bar{k}_s)| \left\{ \frac{1}{2}\left[1 + g_d\right] - \frac{1}{8}\left[1 - 2g_d + e^{4\sigma_x^2}\right] \right\} |\hat{p}\cdot\hat{p}_f| \,. \qquad (4.6.2)$$

The steady state or dc power of the measured signal is then

$$P_{dca} = \frac{\langle \tilde{V}_{asyn} \rangle^2}{2|Z_1|^2} R_1 \,.$$

Therefore,

$$P_{dca} \approx P_{R0} g_0(\bar{k}_s) \left\{ \frac{1}{2}\left[1 + g_d\right] - \frac{1}{8}\left[1 - 2g_d + e^{4\sigma_x^2}\right] \right\}^2 |\hat{p}\cdot\hat{p}_f|^2 \,. \qquad (4.6.3)$$

This should be compared with the dc power for the synchronous receiver (4.3.8). Note that whereas the latter measures the true coherent power in the wave, the asynchronous receiver measures the dc power in the envelope of the antenna output. It is insensitive to fluctuations in the phase of the incoming signal.

4.7 Signal Variance (asynchronous receiver)

$$s^2_{asyn}(\bar{k}_s) = \frac{\langle |\tilde{V}_r|^2 \rangle - \langle |\tilde{V}_r| \rangle^2}{\langle |\tilde{V}_r| \rangle^2} \qquad (4.7.1)$$

$$s^2_{asyn}(\bar{k}_s) = \frac{g_d}{\left\{\frac{1}{2}\left[1 + g_d\right] - \frac{1}{8}\left[1 - 2g_d + e^{4\sigma^2_x}\right]\right\}^2} - 1 \quad . \qquad (4.7.2)$$

Also,

$$s^2_{asyn}\ (dB) = 10\ \log_{10}\ s^2_{asyn} \quad . \qquad (4.7.3)$$

Equation (4.7.2) should be compared with (4.4.2) for the synchronous receiver. s^2_{asyn} is a measure of the fluctuating power in the envelope of the antenna output signal.

4.8 Average Signal Level Degradation (asynchronous receiver)

Using (4.6.3) and noting once more that

$$P_{dca}\Big|_{\text{No fluctuations}} = P_{R0}g_0(\bar{k}_s)$$

$$\Delta P_{dca} = -10\ \log_{10}\ \frac{P_{dca}}{P_{dca}\Big|_{\text{No fluctuations}}} \quad . \qquad (4.8.1)$$

The measured signal level degradation is

$$\Delta P_{dca} \approx -10\ \log_{10}\left\{\frac{1}{2}\left[1 + g_d\right] - \frac{1}{8}\left[1 - 2g_d + e^{4\sigma^2_x}\right]\right\}^2 \quad (dB) \quad . \qquad (4.8.2)$$

ΔP_{dca} reflects the phenomenon that as the turbulence increases, a portion of the average power in the antenna output is converted to modulation side bands.

4.9 Average Effective Aperture

The average effective aperture, A_e, of the receiving antenna is defined as

$$A_e = \frac{< \text{Total Received Power} >}{< \text{Incident Power Density} >} \quad . \tag{4.9.1}$$

From (3.9.3) and (4.3.8), with matched polarization, and load,

$$A_e = \frac{\left\{ \frac{|V_{d0}|^2}{2|Z_1|^2} R_1 \right\} g_0(\bar{k}_s) g_d}{\frac{|U_0|^2}{2\eta_0}} \quad .$$

Therefore,

$$A_e = A_{e0} g_0(\bar{k}_s) g_d \tag{4.9.2}$$

where

$$A_{e0} = |K_p|^2 \, I_{P0\,max} \tag{4.9.3}$$

$$K_p = K_V \frac{\sqrt{\eta_0 R_1}}{|Z_1|} \quad . \tag{4.9.4}$$

A_{e0} is the maximum effective aperture of the antenna, when receiving an unperturbed plane wave.

4.10 Average Directive Gain

Define the average (degraded) gain as

$$G_d = \frac{4\pi}{\lambda^2} \cdot \text{Average Effective Aperture} \quad . \tag{4.10.1}$$

From (4.9.2), we may write

$$G_d(\bar{k}_s) = G_{0\ max}\, g_0(\bar{k}_s) g_d \ , \tag{4.10.2}$$

where

$$G_{0\ max} = \frac{4\pi A_{e0}}{\lambda^2}$$

$$= \frac{4\pi}{\lambda^2} |K_p|^2 I_{P0\ max} \quad . \tag{4.10.3}$$

Further, if we expand g_d, as in (4.3.15),

$$G_d(\bar{k}_s) = G_{0\ max}\, g_0(\bar{k}_s)\, e^{-\sigma_w^2} \sum_{m=0}^{\infty} \frac{\sigma_w^{2m}}{m!} I_{Cm}(\bar{k}_s) \quad . \tag{4.10.4}$$

From (4.10.4), we may define

$$G_0(\bar{k}_s) = G_{0\ max}\, g_0(\bar{k}_s) \quad . \tag{4.10.5}$$

$G_{0\ max}$ is the maximum directive gain for unperturbed plane wave incidence. $G_0(\bar{k}_s)$ is the plane wave incidence, power gain function. Hence,

$$G_d(\bar{k}_s) = G_0(\bar{k}_s) g_d \quad . \tag{4.10.6}$$

4.11 Gain Degradation

The gain degradation of the antenna in a direction $\bar{k}_s$ is defined as

$$\Delta G(\bar{k}_s) = G_0(\bar{k}_s)_{dB} - G_d(\bar{k}_s)_{dB}, \tag{4.11.1}$$

where

$$G_{dB} = 10 \log_{10} G \quad . \tag{4.11.2}$$

Then, from 4.10.6,

$$\Delta G(k_s) = -10 \log_{10} g_d \quad . \tag{4.11.3}$$

It is seen, from 4.9, 4.10, and 4.11, that the antenna parameters such as effective aperture area, gain, and gain degradation are defined using the total received power and not the dc power. Therefore, gain degradation is not the same as the measured dc power degradation. The gain includes both fluctuating and non-fluctuating components of the incoming wave. Therefore, under conditions of heavy turbulence, it does not represent the usable power in the wave.

It follows from the above discussion that gain degradation must represent the fluctuating power that is scattered out of the antenna beam. This will be discussed with examples in Chapter Seven.

The two classes of receivers have now been delineated. A quick survey of the literature indicates that the distinction between the results for the two classes of receivers in the presence of turbulence has not been appreciated. Indeed, it appears that measurements of turbulence have been generally performed using asynchronous AM receivers, employing square law detectors. This clearly does not present a complete

picture of the turbulence as the phase information is lost. However, the more serious problem is that the statistics of the experimental results appear to be then calculated using the principles of the synchronous AM receiver!

To summarize this chapter, two general classes of receivers, called synchronous and asynchronous receivers, respectively, have been defined. An important distinction has been drawn between the incoming signal, the output signal, and the measured signal or the incoming signal as perceived by these receivers. Though the measured signal will be the same for both synchronous and asynchronous AM receivers in the absence of turbulence, fundamental differences occur when scintillation is present. Thus, care must be taken to ensure that the proper receiver is used for the intended application, and that the appropriate results are used when calculating signal characteristics in turbulence.

CHAPTER V

THE CIRCULAR APERTURE

5.1 General Relationships

The generalized relationships for the problem of the aperture antenna in a turbulent atmosphere have been obtained in the preceding chapters. These results will be applied to the specific case of the circular aperture antenna in this chapter. Fundamental expressions will be evaluated for any arbitrary angle of incidence of the incoming wave which does not deviate significantly from the main beam. The particular case of on-axis incidence will be then considered. The analysis will be carried out for a circular aperture with no feed taper, as well as for the Gaussian tapered aperture antenna.

The circular aperture is of general interest. As shown in Chapter Two, the results of the formulation are independent of the mechanics of the feed system. Thus, the circular parabolic antenna can be studied, for example. Furthermore, with the proper choice of parameters, the results can be applied to the field in the focal plane of a focusing system.

The geometry of the problem is shown in Figure 5.1. Any point on the plane aperture, diameter 'D', is specified by the cylindrical polar

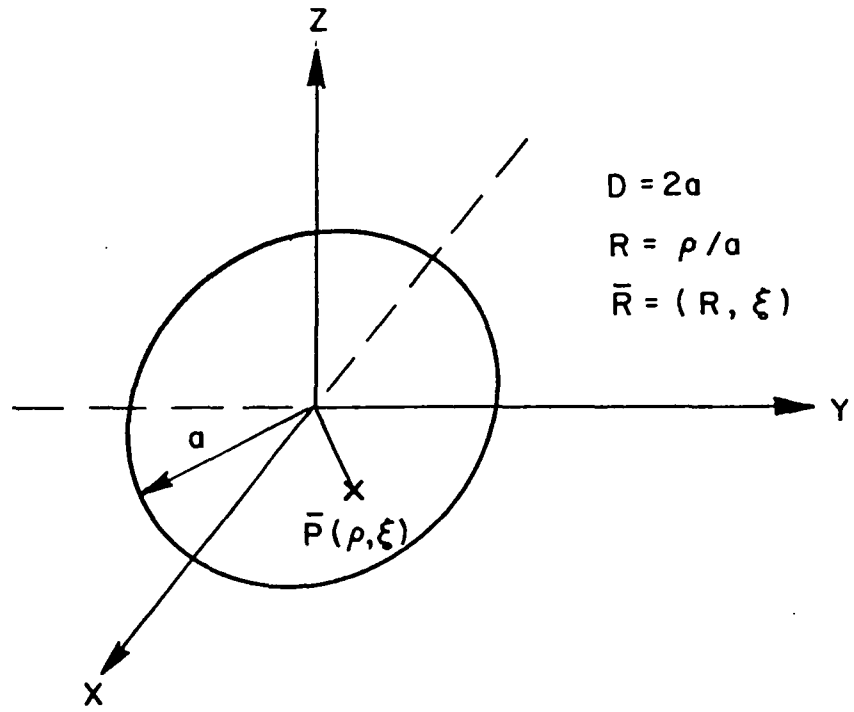

Figure 5.1. Geometry of the circular aperture antenna.

coordinates (ρ,ξ). The radius 'a' is chosen to be the characteristic dimension. We define a normalized set of cylindrical coordinates, (R, ξ) or $\bar{R}$, where

$$R = \frac{\rho}{a} \quad . \tag{5.1.1}$$

Then,

$$x = a\, R \cos\xi$$

$$y = a\, R \sin\xi \quad .$$

The Jacobian of the transformation is a^2R.

The relative correlation length or correlation ratio is

$$C = \frac{\ell_n}{a} = \frac{2\ell_n}{D} \quad . \tag{5.1.2}$$

The distance between any two points $\bar{R}_1$ and $\bar{R}_2$ is $\frac{1}{a}$ such that

$$1^2 = a^2(R_1^2 + R_2^2 - 2R_1R_2\cos(\xi_1 - \xi_2)),$$

so that the correlation coefficient for a Gaussian model atmosphere is

$$b_n = e^{\frac{-(R_1^2 + R_2^2 - 2R_1R_2\cos(\xi_1 - \xi_2))}{C^2}}$$

$$= e^{\frac{-|\bar{R}_1 - \bar{R}_2|^2}{C^2}} \quad . \tag{5.1.3}$$

Also, let the generalized angle of arrival be

$$\Theta = -ka\sin\theta = -\pi\left(\frac{D}{\lambda}\right)\sin\theta \quad . \tag{5.1.4}$$

The vector (k_x,k_y), defined by (2.1.4), which indicates the angle of arrival, (θ,ϕ), transforms to the corresponding generalized angle of arrival vector (Θ,ϕ).

The following are basic integrals which pertain to the circular aperture. From (4.2.3)

$$I_V(\Theta,\phi) = a^2 \int_0^1 \int_0^{2\pi} f(\bar{R})\, e^{j\Theta R\cos(\xi-\phi)}\, R\,d\xi\,dR \qquad (5.1.5a)$$

$$I_{V\,max} = I_V(\Theta,\phi)_{max} \qquad (5.1.5b)$$

$$g_V(\Theta,\phi) = \frac{I_V(\Theta,\phi)}{I_{V\,max}} \qquad (5.1.6)$$

From (4.3.3)

$$I_p(\Theta,\phi) = a^4 \int_0^1 \int_0^{2\pi} \int_0^1 \int_0^{2\pi} e^{\sigma_w^2 b_n(\bar{R}_1,\bar{R}_2)}\, f(\bar{R}_1) f(\bar{R}_2)^*$$

$$e^{j\Theta R_1\cos(\xi_1-\phi) - j\Theta R_2\cos(\xi_2-\phi)}\, R_1 R_2\, d\xi_1\, dR_1\, d\xi_2\, dR_2 \qquad (5.1.7)$$

$$I_{PO}(\Theta,\phi) = |I_V(\Theta,\phi)|^2 \qquad (5.1.8a)$$

$$I_{PO\,max} = |I_{V\,max}|^2 \qquad (5.1.8b)$$

$$g_d = e^{-\sigma_w^2 \frac{I_p(\Theta,\phi)}{I_{PO}(\Theta,\phi)}} \qquad (5.1.9)$$

If this is evaluated by the power series method in (4.3.12), then

$$I_{Pm}(\Theta,\phi) = a^4 \int_0^1 \int_0^{2\pi} \int_0^1 \int_0^{2\pi} b_n(\bar{R}_1,\bar{R}_2)^m \, f(\bar{R}_1) f(\bar{R}_2)^* \, e^{j\Theta R_1 \cos(\xi_1-\phi)} \, e^{-j\Theta R_2 \cos(\xi_2-\phi)} \, R_1 R_2 \, d\xi_1 \, dR_1 \, d\xi_2 \, dR \, . \tag{5.1.10}$$

For the Gaussian correlation coefficient,

$$b_n^m = e^{\frac{-|\bar{R}_1-\bar{R}_2|^2}{C_m^2}} \, , \tag{5.1.11}$$

where

$$C_m = \frac{C}{\sqrt{m}} \, . \tag{5.1.12}$$

If the magnitude of $f(\bar{R})$ is a function of $|R|$ only and the direction of the polarization vector of the feed illumination, $\hat{p}_f$, is independent of position on the aperture, then all results will be independent of ϕ and will be functions of the generalized angle of arrival, Θ, only.

From (5.1.10), (5.1.11), (4.3.12), and (4.3.13), it is seen that the only parameter that changes with m in $I_{Cm}(\bar{k}_s)$ is C_m. Therefore, we define

$$I_C(C_m,\bar{k}_s) = I_{Cm}(\bar{k}_s) \quad . \tag{5.1.13}$$

$I_C(C_m,\bar{k}_s)$ will be called the correlation integral for the circular aperture.

5.2 Uniform Illumination

This section studies the uniformly illuminated circular aperture. The results are applicable to linear or circularly polarized focusing or non-focusing radio aperture antennas. A focusing antenna is one which, by using reflecting or refracting elements, directs the incoming rays to a focal point. The optical telescope, which may be considered to be a polarization insensitive circular focusing aperture, is another example of a uniform aperture.

A uniformly illuminated aperture is represented by the aperture function

$$\bar{f}(\bar{R}) = 1 \cdot \hat{p}_f \quad . \tag{5.2.1}$$

Then, from Appendix A5, the magnitude of the voltage gain pattern is

$$g_V(\theta) = \frac{2J_1(\theta)}{\theta} \quad . \tag{5.2.2}$$

Also,

$$I_{V\ max} = \pi a^2 = A_{phys} \tag{5.2.3}$$

$$I_{PO\ max} = (\pi a^2)^2 = A_{phys}^2 \quad . \tag{5.2.4}$$

The plane wave power gain pattern function is

$$g_0(\Theta) = \left\{ \frac{2J_1(\Theta)}{\Theta} \right\}^2 \quad . \tag{5.2.5}$$

If

$$\delta_C = \frac{C\Theta}{2} \quad , \tag{5.2.6}$$

the correlation integral is

$$I_C(C,\Theta) = \frac{C^4}{g_0(\Theta)} \sum_{p=0}^{\infty} \sum_{q=0}^{p} \binom{p}{q} \frac{Q_C(C,\Theta)^2}{p!} \tag{5.2.7}$$

$$Q_C(C,\Theta) = \sum_{t=0}^{\infty} \frac{(-1)^t}{t!} \frac{1}{\delta_C^{\mu+1}} \left[\frac{(\nu+\mu-1)}{2^\mu} \Theta J_\nu(\Theta) S_{\mu-1,\nu-1}(\Theta) \right.$$

$$\left. - \frac{1}{2^\mu} \Theta J_{\nu-1}(\Theta) S_{\mu,\nu}(\Theta) + \frac{\Gamma\left(\frac{\nu+\mu+1}{2}\right)}{\Gamma\left(\frac{\nu-\mu+1}{2}\right)} \right] \quad , \tag{5.2.8}$$

where

$\nu = p - 2q$

$\mu = 2t + p + 1$

$J_\nu(\theta)$ = the cylindrical Bessel function

$S_{\mu,\nu}(\theta)$ = the Lommel function.

5.3 On-Axis Incidence (uniform illumination)

For on-axis incidence, $\theta = 0$. Hence,

$\Theta = 0$

$$g_V(0) = 1 \tag{5.3.1}$$

$$g_0(0) = 1 \tag{5.3.2}$$

$$I_C(C,0) = \sum_{p=0}^{\infty} \left\{ C^2 \frac{\gamma\left(p+1, \frac{1}{C^2}\right)}{p!} \right\}^2 \tag{5.3.3}$$

$$g_d(C,\sigma_w^2,0) = e^{-\sigma_w^2} \sum_{m=0}^{\infty} \frac{(\sigma_w^2)^m}{m!} I_C(C_m,0) \quad . \tag{5.3.4}$$

It can be shown easily, by considering the individual terms, that

$I_C(C,0) \longrightarrow 1$ as $C \longrightarrow \infty$

$I_C(C,0) \longrightarrow C^2$ as $C \longrightarrow 0$.

Figure 5.2 shows the axial incidence correlation integral, $I_C(C,0)$, as a function of the correlation ratio, C. The figure also shows an empirical approximation to $I_C(C,0)$ given by

$$I_C(C,0) \approx \tfrac{1}{2}(1 - e^{-\frac{1}{C^2}}) + \tfrac{1}{2}(1 - e^{-\frac{1}{C}})^2 \ . \qquad (5.3.5)$$

This expression was arrived at by inspection of the first few terms of (5.3.3) and by trial and error. It is a simpler expression to evaluate. However, the rigorous expression, (5.3.3), will be used in this study.

It is seen that I_C acts like a high pass filter with a cut off point, C_{crit}, at which its value falls to $\frac{1}{2}$ being given by

$$C_{crit} \approx 1 \ . \qquad (5.3.6)$$

C_{crit} will be called the critical relative correlation length. Thus, when the correlation ratio is very high, $g_d(C,\sigma_w^2,0) \rightarrow 1$. From (4.3.8), $P_R \rightarrow P_{RO}$.

When the correlation length, ℓ_n, is comparable to the antenna size, ($C \sim 1$), the gain degradation factor becomes progressively smaller. When the correlation length is much less than the antenna size, ($C << 1$). Then, $g_d(C,\sigma_w^2,0) \rightarrow e^{-\sigma_w^2}$ and $P_R \rightarrow P_{RO}\, e^{-\sigma_w^2}$.

Thus, the range of the received power is

$$P_{RO}\, e^{-\sigma_w^2} \leq P_R \leq P_{RO} \ . \qquad (5.3.7)$$

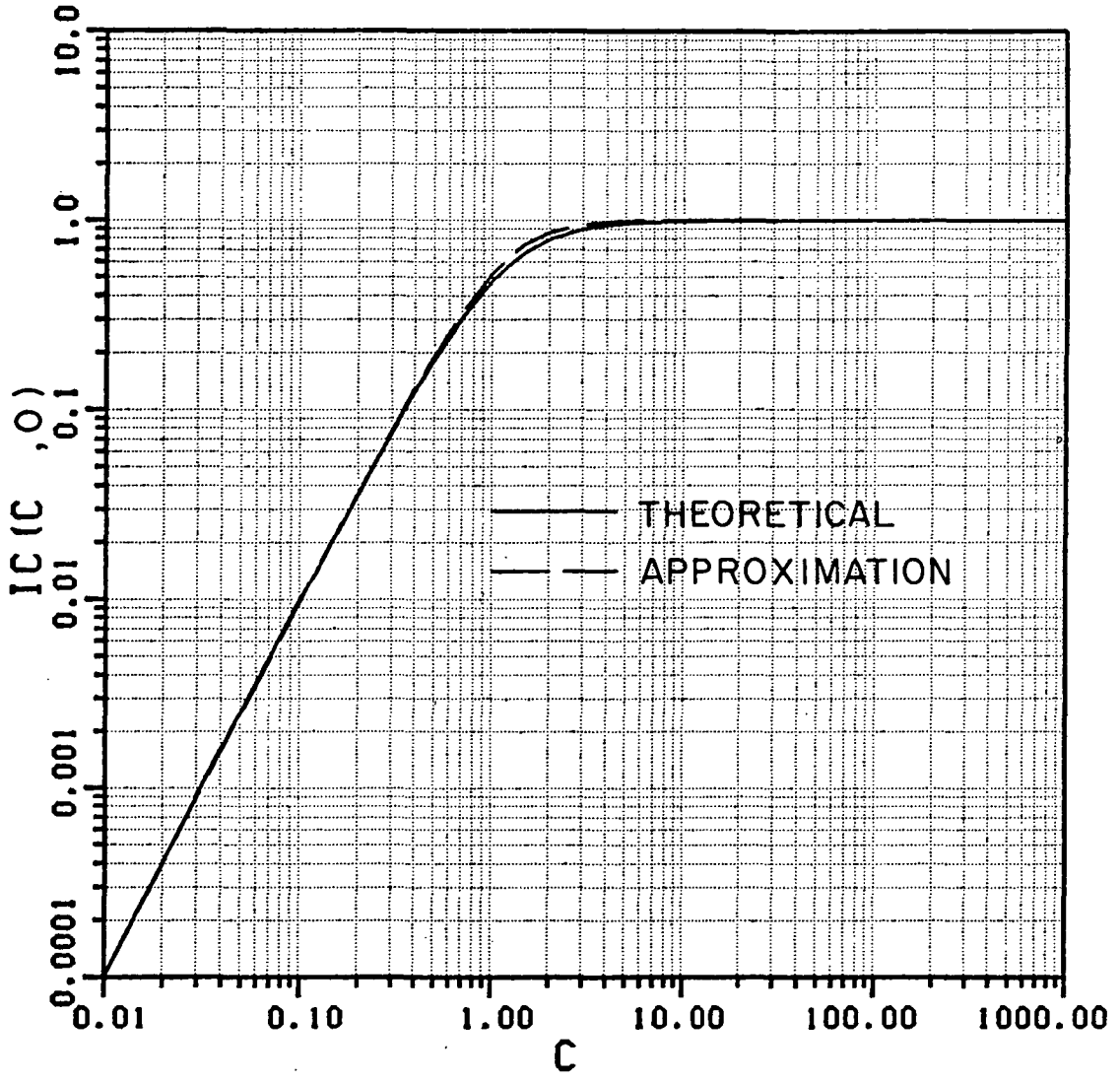

Figure 5.2. Correlation integral $I_C(C,0)$ for a uniformly illuminated circular receiving aperture antenna for on-axis incidence.

Figures 5.3 and 5.4 are used to illustrate these effects. Figure 5.3 shows the behavior of on-axis gain, $G_d(0)$ (4.10.6), at 30 GHz, as the antenna size is increased from 10 cm to 100 m. A correlation length, ℓ_n, of 10 m was assumed and the family of curves represents values of σ_w^2 of 0, 1, 3, and 5, respectively. These numbers, while not unreasonable, are an example of a very turbulent atmosphere and, hence, have been chosen for illustrative purposes only.

Figure 5.4 shows the gain degradation, $\Delta G(0)$ (4.11.3), for the same set of conditions. It is, in fact, the behavior of the degradation integral, $g_d(C,\sigma_w^2,0)$.

5.4 Gaussian Tapered Illumination

The aperture distribution of the feed illumination is often tapered to obtain some desired property of the antenna. For example, where a low side lobe level is desired, the energy incident on the rim of the aperture, when considered as a transmitter, may be reduced to minimize edge diffraction effects.

One distribution which is an example of this class of problems and which also lends itself to analytical studies is the Gaussian taper. The Gaussian taper circular aperture illumination function is represented by

$$\overline{F}(\overline{R}) = e^{-\frac{R^2}{\tau^2 \hat{p}_f}}. \qquad (5.4.1)$$

Then, from Appendix A6,

$$g_V(\Theta) \approx e^{-\frac{\tau^2 \Theta^2}{4}} \qquad (5.4.2)$$

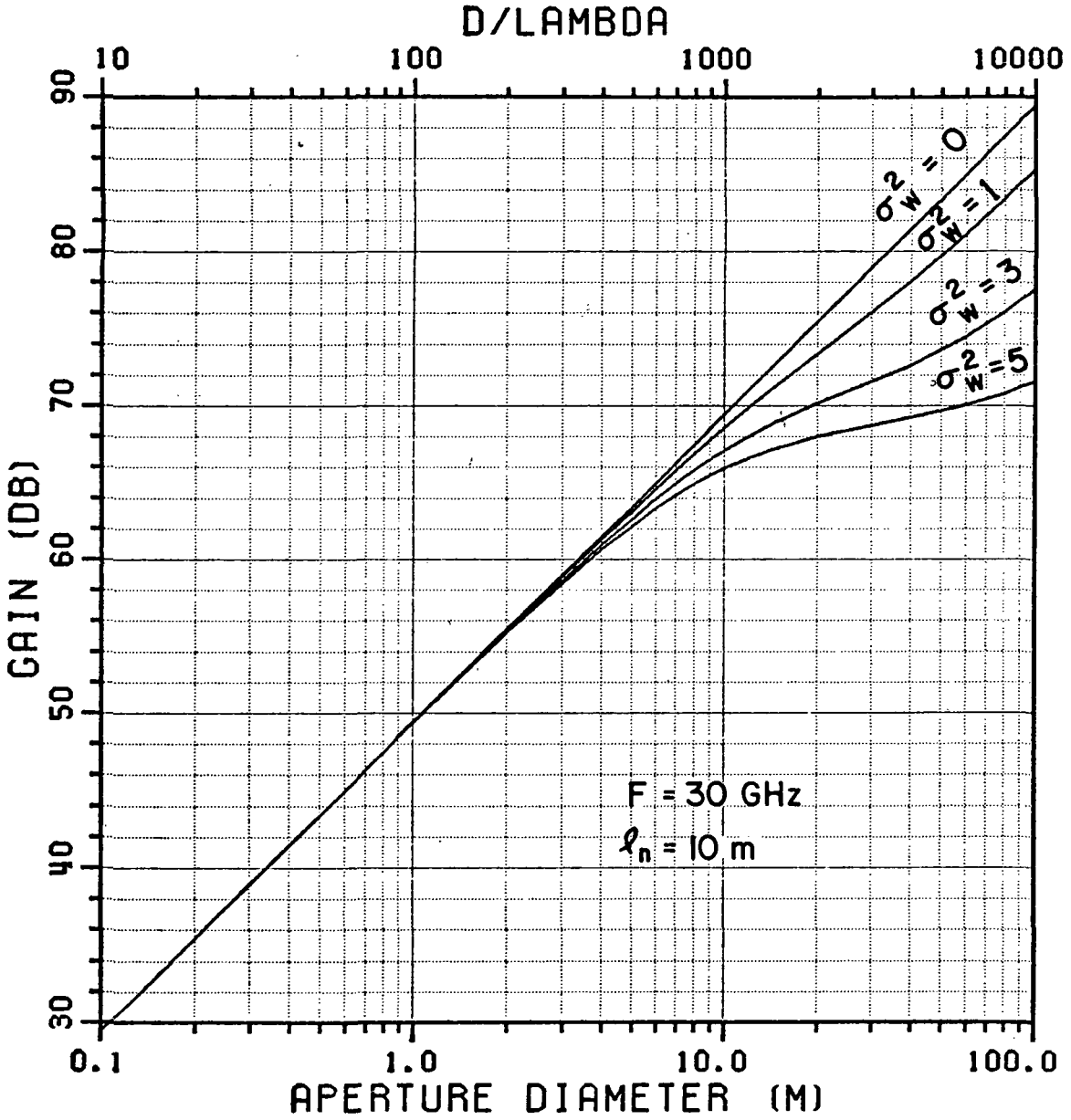

Figure 5.3. Gain of uniformly illuminated circular receiving aperture antennas in turbulence.

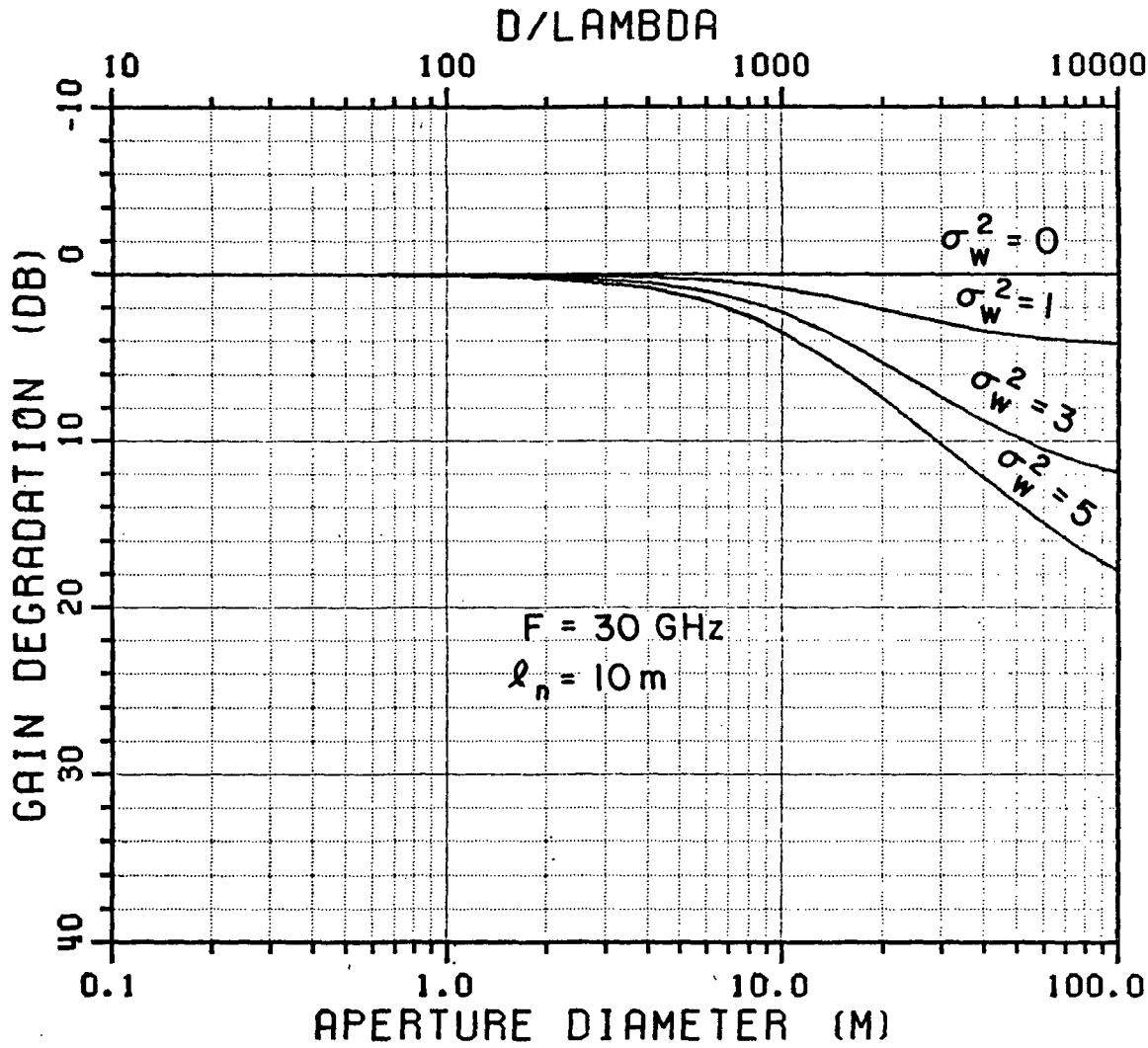

Figure 5.4. Gain degradation of uniformly illuminated circular receiving aperture antennas in turbulence.

$$I_{V\ max} = A_{phys}\,\tau^2\left(1 - e^{-\frac{1}{\tau^2}}\right) \tag{5.4.3}$$

$$I_{PO\ max} = \left\{ A_{phys}\,\tau^2\left(1 - e^{-\frac{1}{\tau^2}}\right)\right\}^2 \tag{5.4.4}$$

$$g_0(\theta) = e^{-\frac{\tau^2\theta^2}{2}} \quad . \tag{5.4.5}$$

If

$$\frac{1}{\gamma^2} = \frac{1}{C^2} + \frac{1}{\tau^2} \tag{5.4.6a}$$

and

$$\frac{1}{\gamma_m^2} = \frac{1}{C_m^2} + \frac{1}{\tau^2} \quad , \tag{5.4.6b}$$

the correlation integral for Gaussian illumination is

$$I_\gamma(C,\theta) = \frac{\left(\frac{\gamma}{\tau}\right)^4}{g_0(\theta)\left[1 - e^{\frac{-1}{\tau^2}}\right]^2} \sum_{p=0}^{\infty}\left(\frac{\gamma^2}{C^2}\right)^p \sum_{q=0}^{p}\binom{p}{q}\frac{Q_C(\gamma,\theta)^2}{p!} \quad . \tag{5.4.7}$$

$Q_C(\gamma,\theta)$ is defined in (5.2.8) with δ_γ substituted for δ_C.

5.5 On-Axis Incidence (Gaussian illumination)

$$\theta = 0$$

$$g_V(0) = 1 \tag{5.5.1}$$

$$g_0(0) = 1 \tag{5.5.2}$$

$$I_\gamma(C,0) = \frac{1}{\left[1 - e^{\frac{-1}{\tau^2}}\right]^2} \sum_{p=0}^{\infty} \left(\frac{\gamma^2}{C^2}\right)^{2p} \left\{\frac{\gamma^2}{\tau^{2p}!} \; \gamma\left(p+1, \frac{1}{\gamma^2}\right)\right\}^2 \tag{5.5.3}$$

$$g_d(C,\sigma_w^2,0) = e^{-\sigma_w^2} \sum_{m=0}^{\infty} \frac{\left(\sigma_w^2\right)^m}{m!} I_\gamma(C_m,0) \; . \tag{5.5.4}$$

Figure 5.5 shows the correlation integral for Gaussian illumination, $I_\gamma(C,0)$, as a function of the correlation ratio, C, for values of the taper, τ, from 1.0 to 0.1. When τ is large, the results tend to the uniform illumination case, as would be expected. Narrowing the aperture illumination function by reducing τ slides the curve to the left, allowing the relative correlation, C, to be smaller before any degradation effects are noticeable. It will be seen from (5.4.2) that reducing τ also widens the beamwidth.

Reducing τ, in essence, reduces the effective aperture of the antenna. The antenna appears to be smaller than its physical size alone would indicate. Therefore, for a given correlation ratio, C, the effective correlation ratio, C_{eff}, is larger than ℓ_n/a, thus reducing degradation effects.

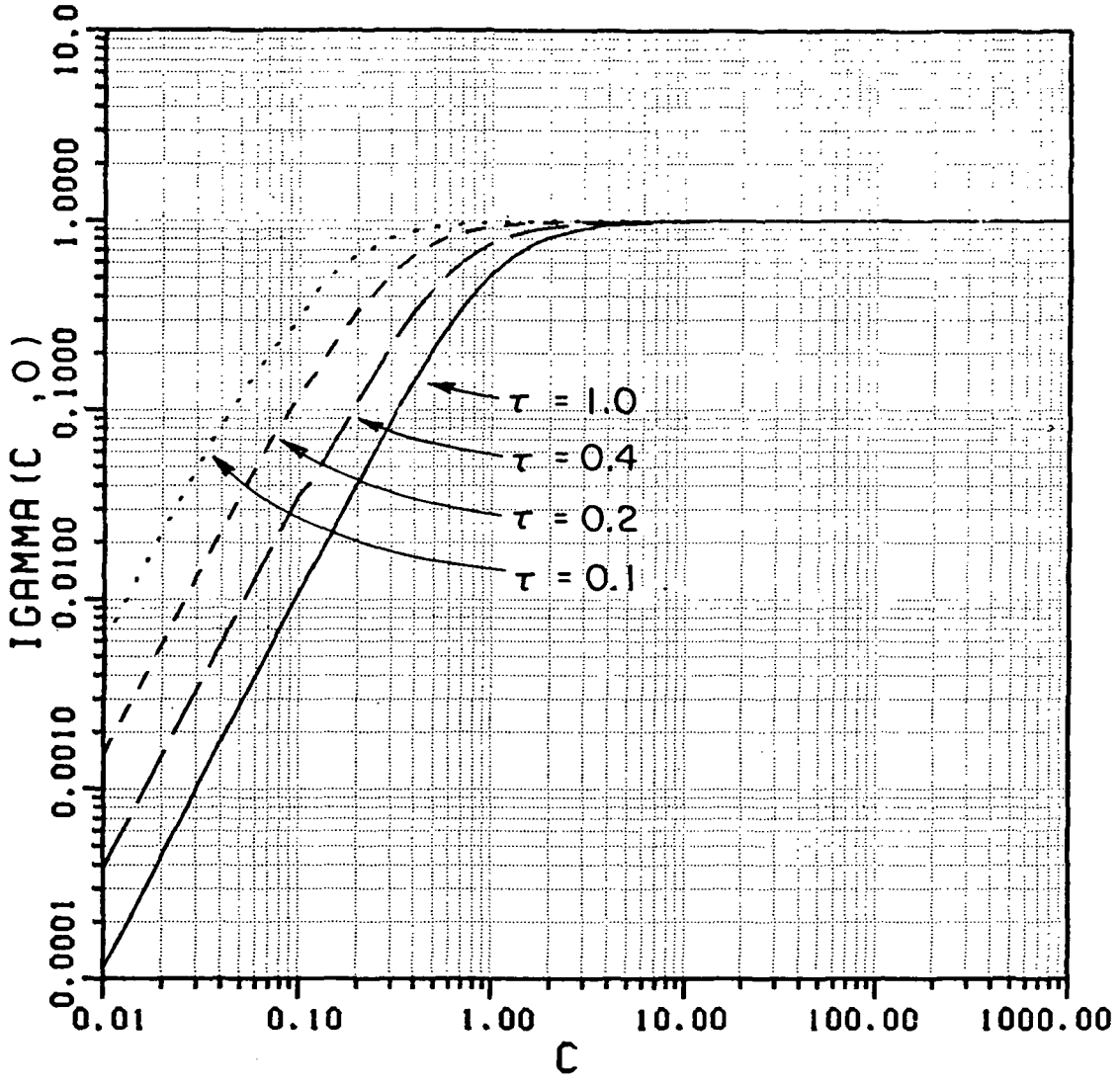

Figure 5.5. Correlation integral $I_\gamma(C,0)$ for a Gaussian illuminated circular receiving aperture antenna for on-axis incidence.

Inspection of Figure 5.5 and Equation (5.4.6a) shows that if τ is small, its effect would dominate over the effect of C, provided C is reasonably large. Also, Figures 5.5 and 5.2 are seen to be of the same form. Therefore, a simple relationship was sought between the uniform and Gaussian illumination cases.

It was determined empirically, by inspection of Figure 5.5, that for $\tau < 1$, the critical value of C, i.e., that C at which the correlation integral was $\frac{1}{2}$, was given approximately by

$$C_{crit} \approx \sqrt{\tau} \, . \qquad \tau < 1 \qquad (5.5.5)$$

Therefore, the equivalent uniform illumination correlation ratio is

$$C_{eff} \approx \frac{C}{\sqrt{\tau}} \qquad \tau < 1 \qquad (5.5.6)$$

and, hence,

$$C_{eff} \approx \frac{2\ell_n}{\sqrt{\tau D}} \, . \qquad (5.5.7)$$

This implies that the effective diameter

$$D_{eff} \approx \sqrt{\tau D} \, . \qquad (5.5.8)$$

Thus, all results derived for the uniform illumination case may be used for the Gaussian illuminated aperture, provided that the effective diemeter, D_{eff}, and correlation ratio, C_{eff}, are used instead of D and C.

Finally, antenna designers usually prefer to work with the feed power taper, T_p, instead of the illumination taper constant τ. T_p is defined as the ratio of the maximum value of the feed illumination power pattern, to the value in the direction of the rim of the aperture, and is expressed in dB. It is easily shown that,

$$T_p \approx \frac{8.686}{\tau^2} \quad \text{dB} \; . \qquad (5.5.9)$$

Summarizing this chapter, the general circular receiving aperture was evaluated for any arbitrary angle of arrival of a wave perturbed by a turbulent atmosphere, within the main beam of the antenna. Both uniform and Gaussian tapered feed illuminations were then completely evaluated. Next the special case of on-axis incidence was studied for both illuminations. The Gaussian tapered beam was related to the uniform aperture by a simple expression. This permits the results obtained for the uniform aperture case to be applied to the Gaussian tapered circular aperture as well.

CHAPTER VI

EXPERIMENTAL RESULTS

In this chapter, the theoretical model developed in the previous chapters is matched to experimental work with satellite communications links. Experiments performed at The Ohio State University to measure the variance and the level of the received signal over different earth-space paths are used to assign numerical values to key parameters of the model. The model is then used to predict and is compared with the results of similar measurements made elsewhere, to establish its validity under different conditions.

6.1 General Remarks

An important simplifying assumption used in this work is that the turbulence in the earth's atmosphere is homogeneous and isotropic over the path of the communications link. This is reasonable over short terrestrial paths. Slant or earth-space paths encounter gradients in temperature, pressure, water vapor density and, hence, refractivity. It is necessary, therefore, to assume an equivalent homogeneous isotropic atmosphere for the purposes of the model, not only for earth-space paths, but also for comparison with terrestrial results. Its parameters would be, in some sense, an average of the parameters of the earth's atmosphere

over the path, for long term statistical purposes. The next two sections detail the experimental work performed at O.S.U. to determine these parameters.

The primary experimental measurements used for this purpose were made at The Ohio State University ElectroScience Laboratory in Columbus, Ohio, when the Applications Technology Satellite, ATS-6, was moved from a geosynchronous position at 94^{o} W. longitude to 35^{o} E. longitude in 1975, and back in 1976 [35,36]. The elevation angle of the satellite, viewed from Columbus, Ohio, (83^{o} W. longitude) varied smoothly between 0^{o} and 43^{o}. The scintillation of the received signal amplitude as well as the average signal level were measured simultaneously at 30 GHz and 20 GHz with a 4.5 m (15 feet) parabolic antenna during the descent (1975) and at 30 GHz (4.5 m antenna) and 2 GHz (9 m antenna) during the ascent (1976). The corresponding power taper, T_p, of the 4.5 m antenna was 22 dB, while that of the 9.1 m antenna was 18 dB.

The receivers employed square-law detectors and, hence, may be classed as asynchronous receivers. The voltage outputs were sampled at 10 samples/second. The statistics of the equivalent antenna terminal voltage, v, as measured by the asynchronous AM receivers, were calculated for N samples after correcting for receiver calibration characteristics.

6.2 Signal Amplitude Variance

The normalized experimental received signal amplitude variance, s^2, was calculated by dividing the amplitude variance by the dc power level and was expressed in dB below the dc power level. If v_i is the i^{th} sample of v, from [35]

$$s^2 = 10 \log_{10} \sum_{i=1}^{N} \frac{(v_i - \langle v \rangle)^2}{N \langle v \rangle^2} \quad \text{dB} \qquad (6.2.1)$$

where

$$\langle v \rangle = \sum_{i=1}^{N} \frac{v_i}{N} \quad . \tag{6.2.2}$$

N = 2048 for the 1976 data. This corresponds to an averaging time of 204.8 seconds for each set of samples.

The data were taken under conditions of clear air at 33 elevation angles and the time average variances were calculated as the satellite ascended. The results were fitted to power law curves of the form

$$s^2 = A\, L^B \quad , \tag{6.2.3}$$

where A and B are constants and L (km) is the equivalent path length through a homogeneous atmosphere. The atmospheric path lengths were calculated assuming a spherical earth of radius R_e, given by 4/3 the actual radius, or 8479 km, to correct for standard refraction, and an atmosphere of height, h. The equivalent path length is then given by

$$L = \sqrt{[h^2 + 2hR_e + R_e^2 \sin^2\varepsilon]} - R_e \sin\varepsilon \tag{6.2.4}$$

where ε is the elevation angle.

A regressive fit was made to all the variance data to determine the values of A and B, while varying h to minimize the mean square error. The results at 30 and 2 GHz were [35],

$$s_{30}^2 = 10^{-6.4} L^{2.48 \pm .3} \tag{6.2.5}$$

$$s_2^2 = 10^{-6.5} L^{1.87 \pm .2} \tag{6.2.6}$$

$$h = 6.0 \pm 1 \text{ km} . \tag{6.2.7}$$

The fairly large error bounds do not indicate uncertainty in the data itself, but take into account the limited duration of the data periods and the correcting effect that observations over extended periods of time under different weather conditions would have on the results.

The same analysis was performed on the 1975, ATS-6 descending, data [36], with N = 1024, i.e., an averaging time of 102.4 seconds. The corresponding results for the 30 and 20 GHz data were,

$$s_{30}^2 = 10^{-6.2} L^{2.35 \pm .1} \tag{6.2.8}$$

$$s_{20}^2 = 10^{-6.39} L^{2.29 \pm .1} \tag{6.2.9}$$

$$h = 5.9 \pm 1 \text{ km} . \tag{6.2.10}$$

Consequently, the height of the equivalent homogeneous atmosphere in the present model was also taken as 6 km. The signal amplitude variance as calculated by the present model (4.7.2) was then fitted in the minimum mean-square-error sense to the power law curves (6.2.5) - (6.2.9). The correlation length of the atmosphere, ℓ_n, and the variance of the refractive index fluctuations, σ_n^2, were varied simultaneously to minimize the deviation from the power law curves. Subsequently, the height of the

equivalent atmosphere, h, for the model was also varied in an effort to further minimize the deviation. However, it was found that 6 km was the best overall compromise. The final results were

$$\sigma_n^2 = 4.0 \times 10^{-13} \tag{6.2.11}$$

$$\ell_n = 46 \text{ m} \tag{6.2.12}$$

$$h = 6.0 \text{ km} . \tag{6.2.13}$$

These results will be used in the subsequent discussion unless stated otherwise.

The question now arises as to the reasonableness of these values. A search through the literature provided very few direct statements of these values. Shifrin [37] indicates that σ_n^2 could take values from 2.5×10^{-11} to 2.5×10^{-13}. Ishimaru [28] indicates that σ_n^2 is of the order of 10^{-12}. Shifrin also gives the value of ℓ_n as ranging from 5 m to 100 m.

Some work has been done, however, to measure the atmospheric structure constant, C_n^2, of the Kolmogorov spectrum. Chadwick and Moran [38] and Gossard [39,40] are examples of recent publications. Height distributions are also given in [39]. An alternative method used, therefore, was to calculate the value of the equivalent structure constant, C_{ng}^2, for the Gaussian spectrum, as defined in (3.7.3) and compare this with the published measurements instead. Then, from (6.2.11), (6.2.12) and (3.7.3),

$$C_{ng}^2 = 5.3 \times 10^{-14} \qquad m^{-\frac{2}{3}} . \tag{6.2.13}$$

It is commonly accepted that near the surface C_n^2 varies over about two orders of magnitude. Average values tend to vary between 10^{-14} and 10^{-17} depending on the height at which the measurement is made. The above value of the equivalent structure constant appears to be reasonable, especially since it represents an average over a wide range of path lengths and heights.

Figure 6.1 shows the predicted signal amplitude variance at 2, 20 and 30 GHz using the appropriate antennas, together with the power law approximations to the 1975 and 1976 data. The agreement is reasonably good over a range of frequencies of 15 to 1 and is a further confirmation of the values of the chosen parameters.

It must be remembered, however, that the power law curves are approximations only and express only a path length dependence. They cannot, therefore, fully represent the variation of the signal variance with elevation angle. Figures 6.2 and 6.3 show the actual variances measured during the 1976 experiment, at each elevation angle, at 30 GHz and 2 GHz, respectively. The maximum and minimum observed values are plotted, together with the long term average predicted by the model. The results show a good fit. Indeed, the agreement here appears to be better than that shown in Figure 6.1.

As a further check, the model was used to calculate the variance for the IDCSP X-band beacon measurements reported by R.K. Crane [12]. A 60-foot parabolic antenna was used at 7.3 GHz over elevation angles from 0.5 to 10 degrees. The results were recast to be consistent with the definition of variance in this report (D.M. Theobold [36]). The prediction is shown in Figure 6.4. The agreement is again quite good.

Other measurements were made at The Ohio State University Electro-Science Laboratory using the Communications Technology Satellite, CTS, at 11.7 GHz and the COMSTAR D_3 Satellite at 28.56 GHz [41]. Measured and predicted amplitude variances are summarized in Table 1. The CTS

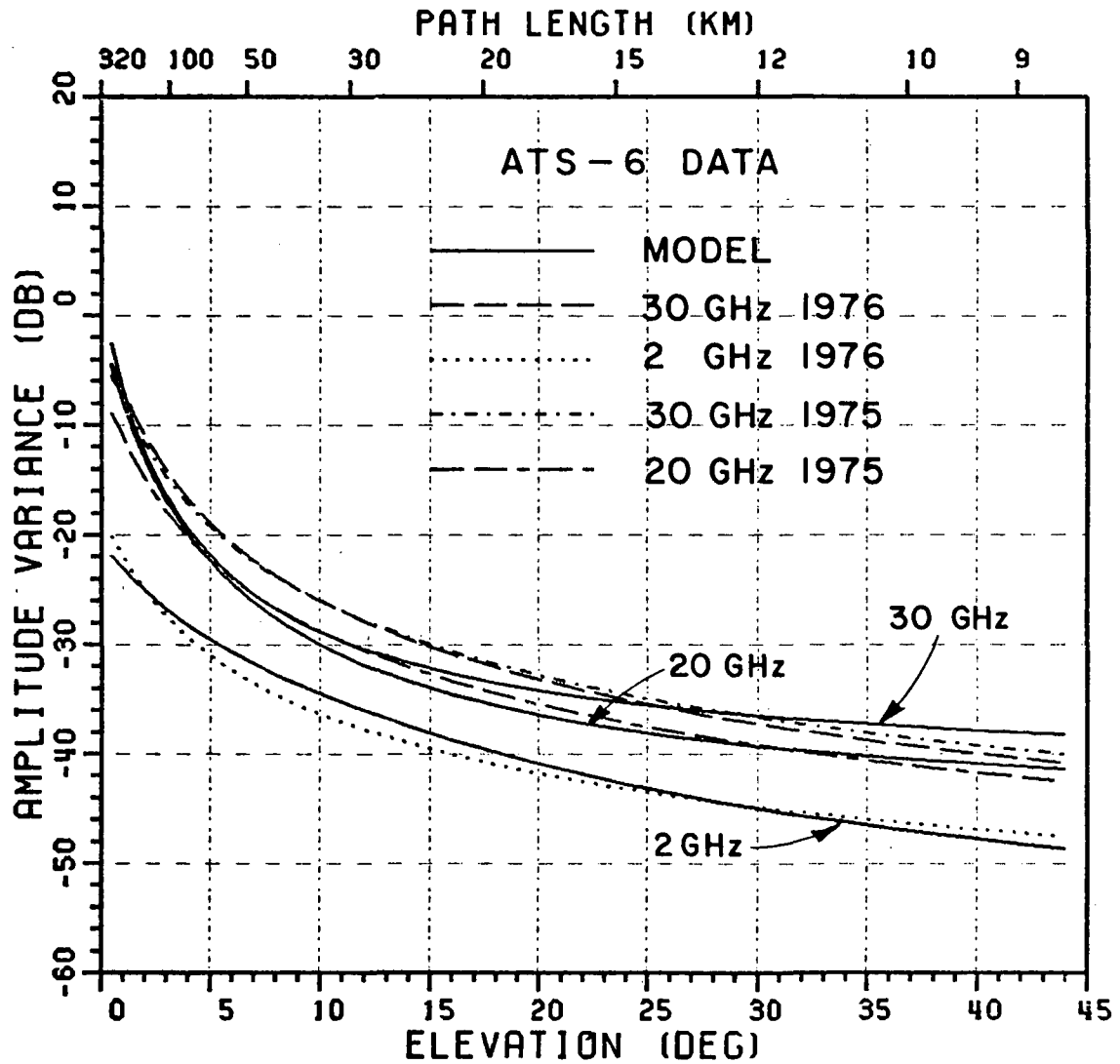

Figure 6.1. ATS-6 measured amplitude variance at 2, 20, and 30 GHz compared to theoretical model.

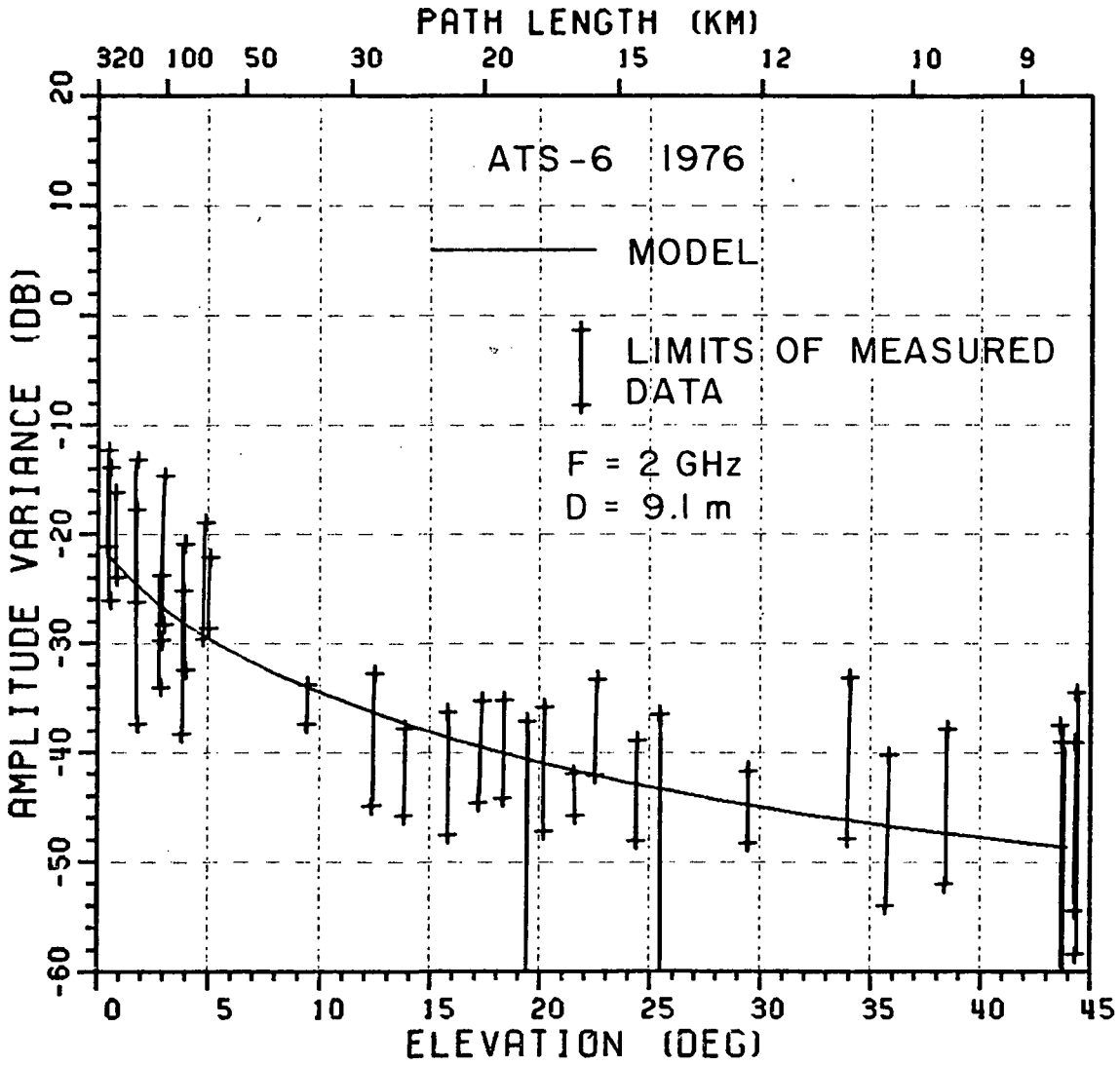

Figure 6.2. ATS-6/1976 limits of measured amplitude variance at 2 GHz compared to theoretical model.

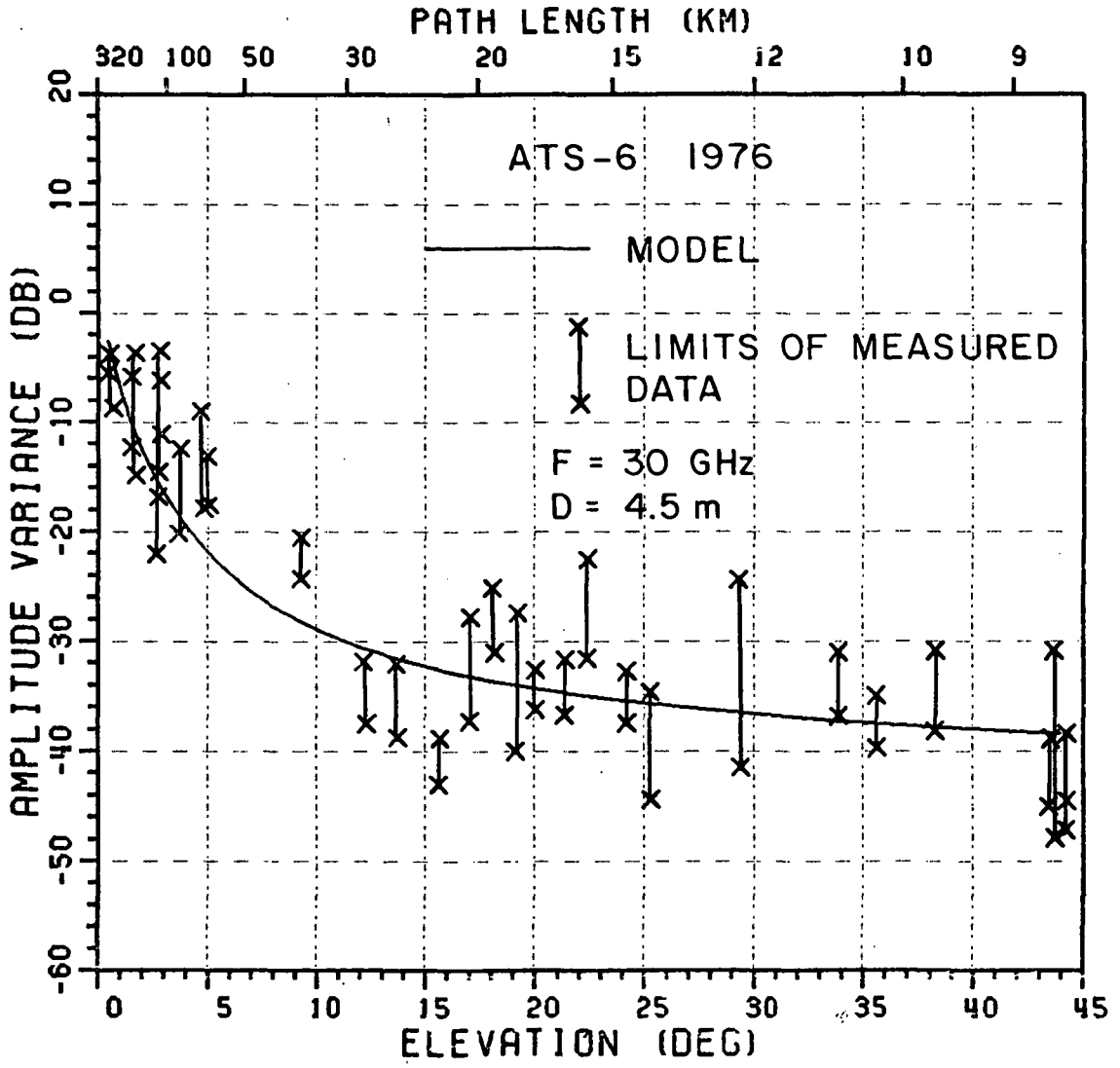

Figure 6.3. ATS-6/1976 limits of measured amplitude variance at 30 GHz compared to theoretical model.

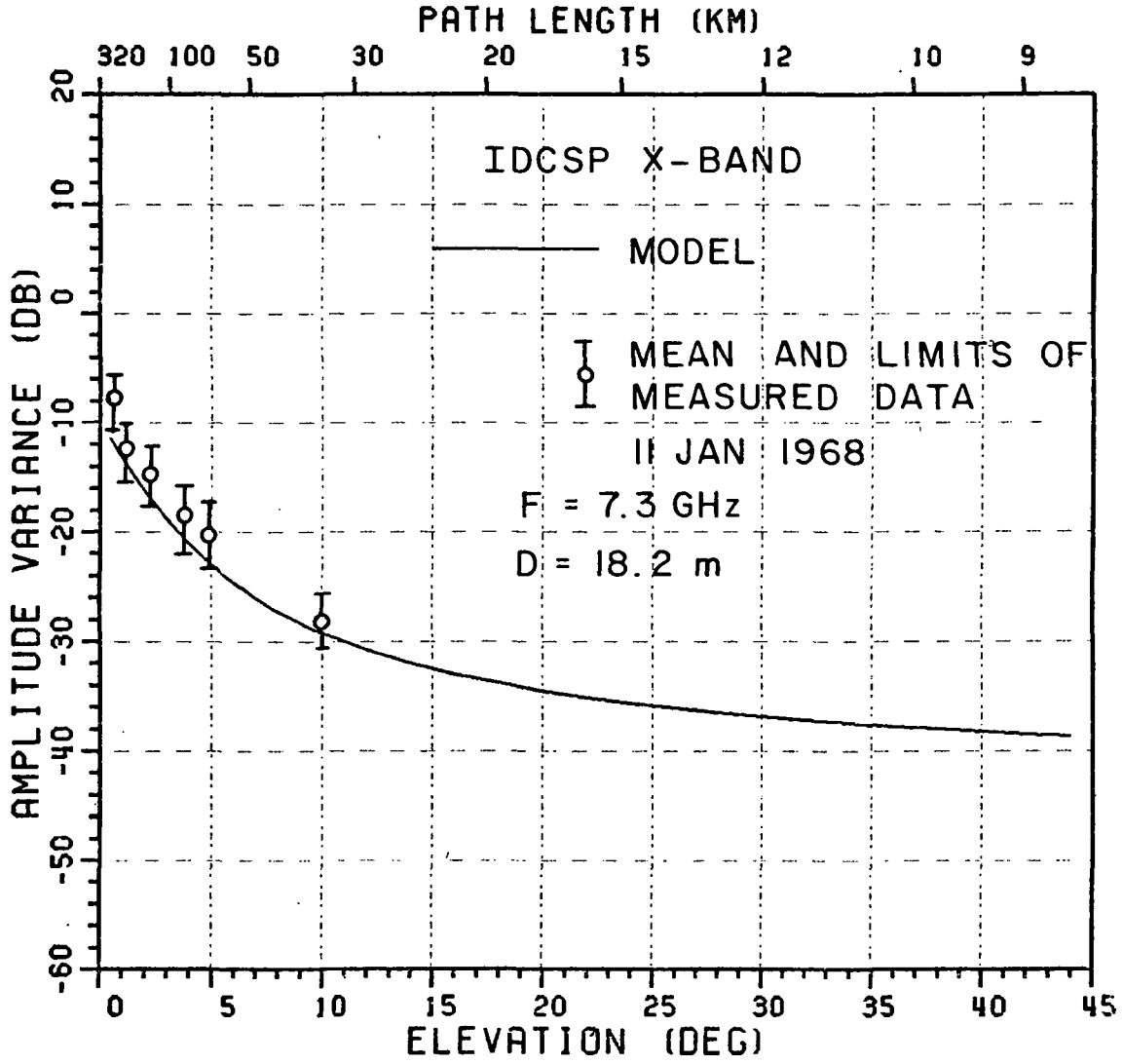

Figure 6.4. IDCSP X-band mean and limits of measured amplitude variance compared to theoretical model.

TABLE 1

SOME COMPARISONS OF THE THEORY AND EXPERIMENTAL RESULTS

Satellite	Frequency (GHz)	Receiver Antenna diam (m)	Elevation Degrees	Variance (dB) Measured	Model
CTS	11.7	0.6	32.7	- 36	- 42
COMSTAR D_3	28.56	0.6	43	- 42	- 45

measurements were heavily contaminated by system noise due to the low link margin. The other measurement with the 0.6 m antenna is also influenced by system noise to some degree. Under the circumstances, the agreement is reasonable.

Thus, the model appears to predict the signal amplitude variance, s^2, satisfactorily as a function of frequency, path length, and aperture size.

6.3 Signal Level Degradation

The experimental received dc signal power, P_R, as measured by the receiver was defined as

$$P_R = \langle v \rangle^2 \tag{6.3.1}$$

where $\langle v \rangle$ has been defined in (6.2.2). Since the receivers used in these experiments incorporated square-law detectors, the corresponding

theoretical result for the received power level is defined by (4.6.3).

The average received dc power was computed as a function of elevation angle from (4.6.3) for the receiving systems used in the ATS-6 return measurements [35]. Gas loss was added to account for the attenuation caused by the atmosphere. The 6 km equivalent atmosphere was assumed for this purpose. The results were normalized to the power that would be received at zenith and are shown in Figure 6.5.

In addition to the 2 GHz and 30 GHz data, median signal levels as a function of elevation angle, measured by McCormick and Maynard at the Communications Research Center, in Ottawa, using the US TACSATCOM-1 7.3 GHz beacon [42] are also available. A 9.1 m antenna was used. Measurements were made over elevation angles from 6^{o} to 0.5^{o} as the satellite moved eastward. The data has been recast to agree with the definitions used in this report by Theobold [36]. These measurements and predicted results are also included in Figure 6.5.

The theoretical results were calculated at 2, 7.3 and 30 GHz for 9.1, 9.1, and 4.5 m antennas, respectively. These correspond to 60, 220, and 450 wavelength antennas, with relative correlation ratios of 10.1, 10.1, and 20.4, respectively.

The agreement is seen to be quite good. The model thus appears to predict long term average power level degradation as well.

Figure 6.6. shows the average power degradation, as calculated from (4.8.2) only, excluding the gas loss. When compared with Figure 6.5, gas loss is seen to be the dominant cause of reduction in power levels at low elevation angles. However, the turbulence contribution is also significant. It will also be shown later that the effect can be considerably larger in millimeter wave systems.

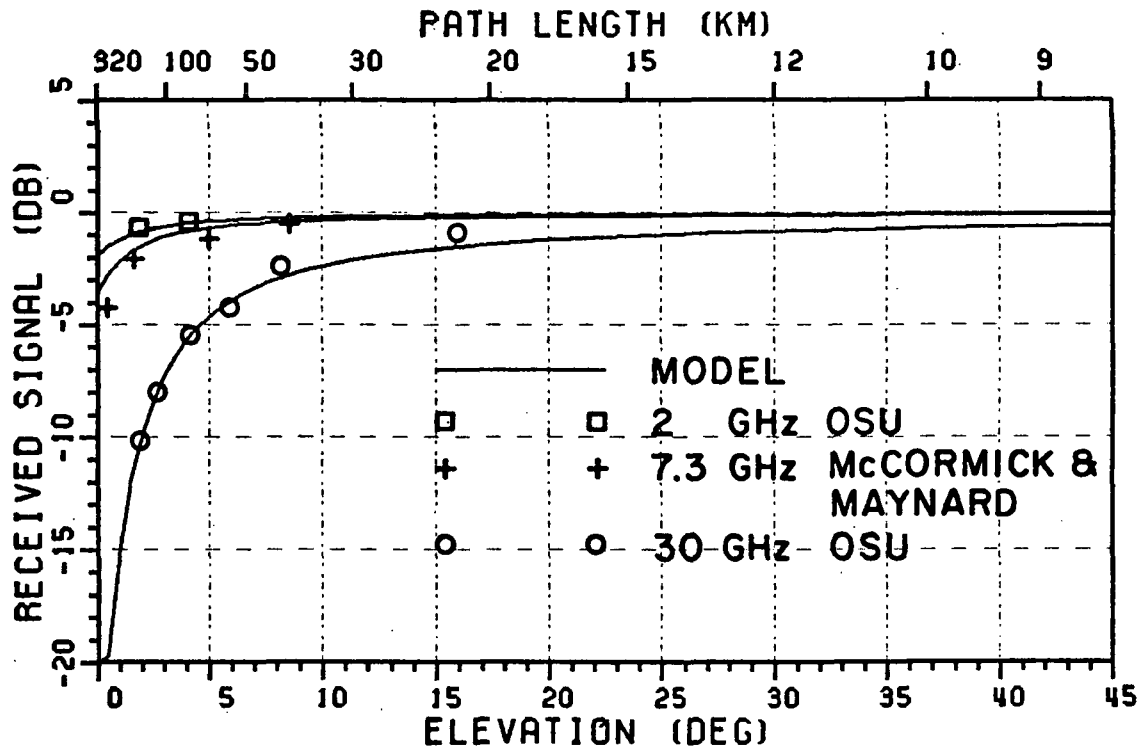

Figure 6.5. ATS-6 and TACSATCOM-1 measured received signal levels compared to theoretical model.

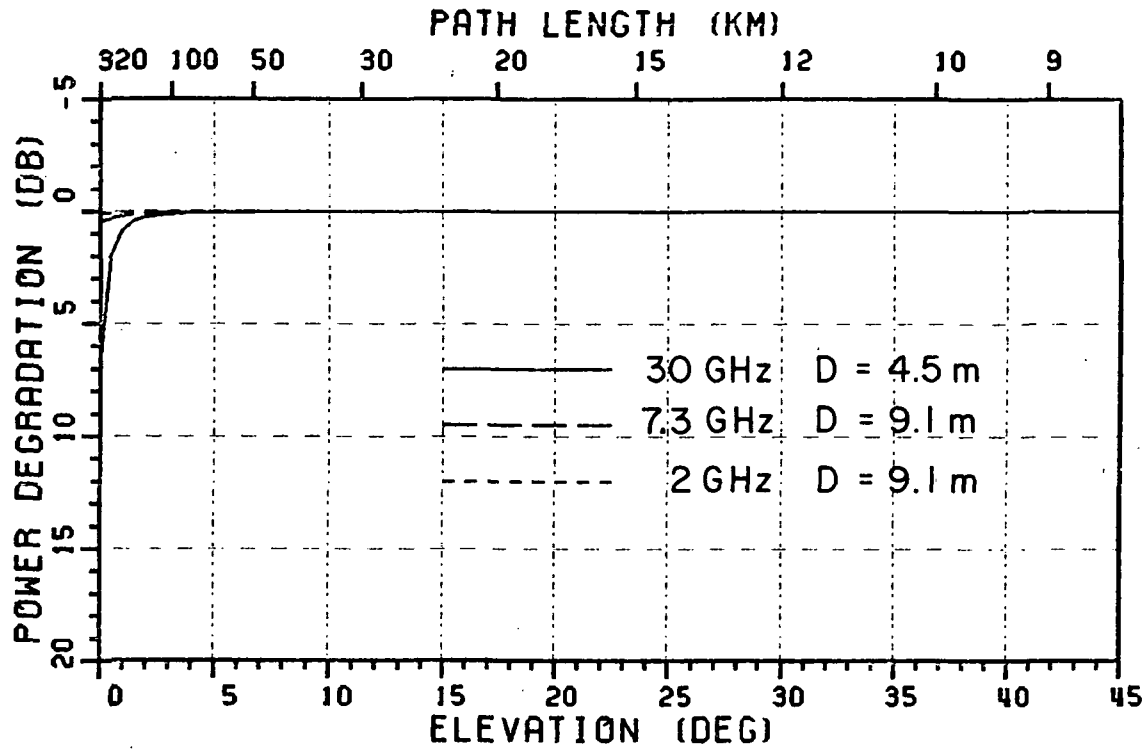

Figure 6.6. ATS-6 and TACSATCOM-1 degradation component of received signal level.

In summary, numerical values were derived for the constants of the model by fitting it to available experimental data. The data used were from different locations. The relevant parameters are given by (6.2.11)-(6.2.13). The model predicts long term average signal variance and received power over a wide range of frequencies and antenna sizes.

CHAPTER VII

DISCUSSION OF THE MODEL

7.1 Introduction

The key parameters of the long term average behavior of the model have now been estimated. Using these estimates, cases of interest are studied to gain insight into the behavior of the model as well as to predict the properties of the communications system.

Four frequencies have been chosen for this purpose. These are 3, 12, 30 and 90 GHz. They span the range of current interest and, in the case of 90 GHz, represent a frequency band in which increasing interest is being shown. While the validity of the model at 90 GHz is, at present, unknown it should provide at least an initial estimate for the link designer. As data become available, they could be easily compared with the given curves for verification.

Four representative antenna sizes have also been chosen for detailed study. These are 1 m (3.3 ft.), 4.5 m (15 ft.), 9.1 m (30 ft.), and 30 m (100 ft.), respectively. The first three are popular sizes. The 30 m antenna has been used at the lower microwave frequencies, especially in class A earth stations. It is unlikely that this size will be used extensively at 90 GHz, as the required tolerances become prohibitive. However, it represents an extreme case and will be a severe

test of the soundness of the model. It will also allow some properties of the propagation link, which might otherwise be hidden, to be brought out. All results presented at 90 GHz for the 30 m antenna should be viewed in this light. Also, whenever possible, the parameter under study is plotted at 30 GHz with the antenna aperture size varying continuously from 10 cm to 100 m. Obviously, the comments made above apply to the larger sizes in these plots as well.

Average conditions of turbulence will be always assumed, unless specifically stated otherwise. However, some properties of the link such as antenna gain degradation, which may not be significant under quiet conditions, may have a major impact on the performance of the system under conditions of strong turbulence. Hence, some cases are evaluated with this in mind, in order to estimate the worst case behavior of the link.

Some general properties of the formulated model atmosphere will be first discussed. Next, amplitude variance will be studied, both for the synchronous and the asynchronous AM receiver. The study will be repeated for the degradation of the average received signal power. Finally, the gain degradation of the antenna will be examined under conditions of strong turbulence.

7.2 The Atmosphere

The long term average parameters of the atmosphere, modeled as an equivalent homogeneous isotropic Gaussian spectrum, were estimated to be, (6.2.11) - (6.2.13),

$$\sigma_n^2 = 0.4 \times 10^{-12} \tag{7.2.1}$$

$$\ell_n = 46 \text{ m} \tag{7.2.2}$$

$$h = 6 \text{ m} \quad . \tag{7.2.3}$$

The corresponding correlation coefficient is shown in Figure 7.1. The figure also shows the correlation function of the equivalent Von Karman spectrum for homogeneous turbulence, having the same correlation length. Figure 7.2 shows the corresponding spectra for the two models. If the Von Karman spectrum is accepted as being closer to the natural spectrum, it will be seen that errors may occur in the Gaussian model in the geometrical optics region and in the long path region of a propagating wave.

Figure 7.3 shows the path length through this 6 km equivalent atmosphere over a 4/3 radius earth, for elevation angles from 0^{o} to 45^{o}. The maximum length (at 0^{o}) is about 320 km. Thus, the ratio of the path length along the horizon to that at zenith is, approximately, 53. Therefore, a power quantity which is directly proportional to the path length will vary by about 17 dB from zenith to the horizon due to the variation in path length alone.

Figure 7.4 shows the wave variances (3.5.13b) of waves at the four frequencies of interest, namely 3, 12, 30, and 90 GHz, as they propagate through this atmosphere. It should be remembered that the wave variance is an artifical construct of no physical significance, being defined simply as the sum of the log amplitude and phase variances. The path length characteristic of Figure 7.3, is clearly mirrored in these curves, as expected. The k^2 dependence of values is also seen.

Figure 7.5, showing the phase variance of the propagating waves, is very similar to Figure 7.4. This is because the long path region has not been reached. Consequently, the phase variance is much larger than the log-amplitude variance and dominates in the wave variance. Some differences are becoming noticeable at 3 GHz at low elevation angles.

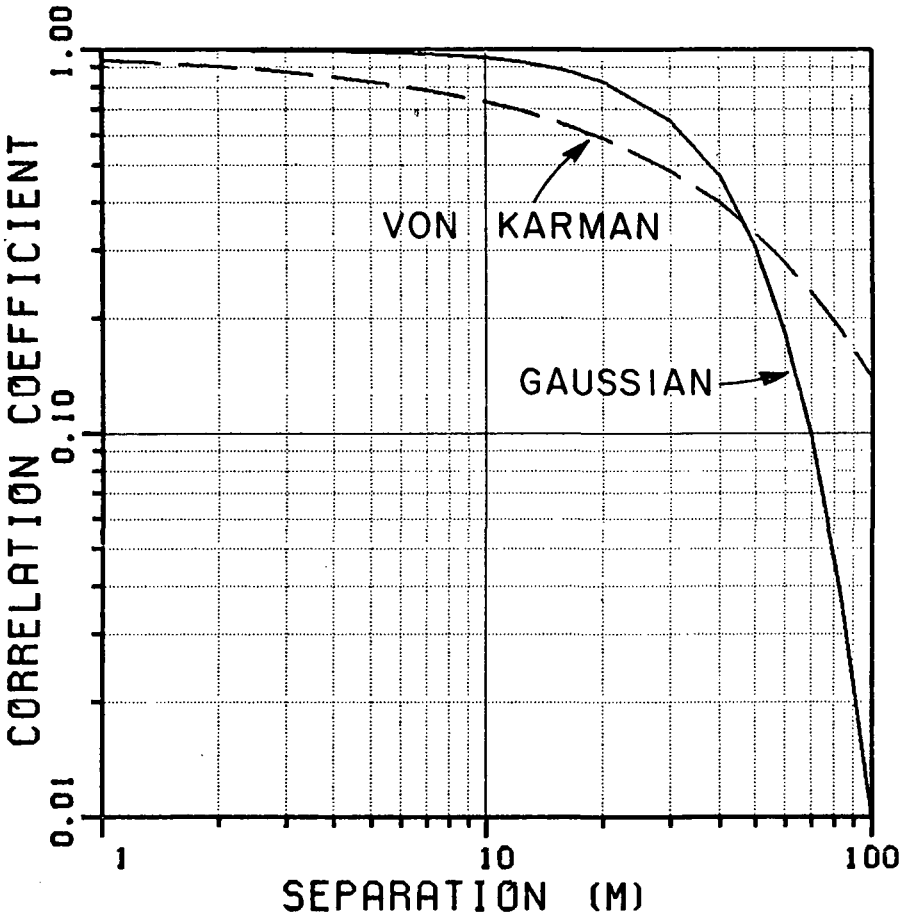

Figure 7.1. Correlation coefficient of the model atmosphere and the equivalent Von Karman model.

$\sigma_n^2 = 0.4 \times 10^{-12}$; $\ell_n = 46$ m; $L_0 = 64$ m; $\ell_0 = 10$ mm.

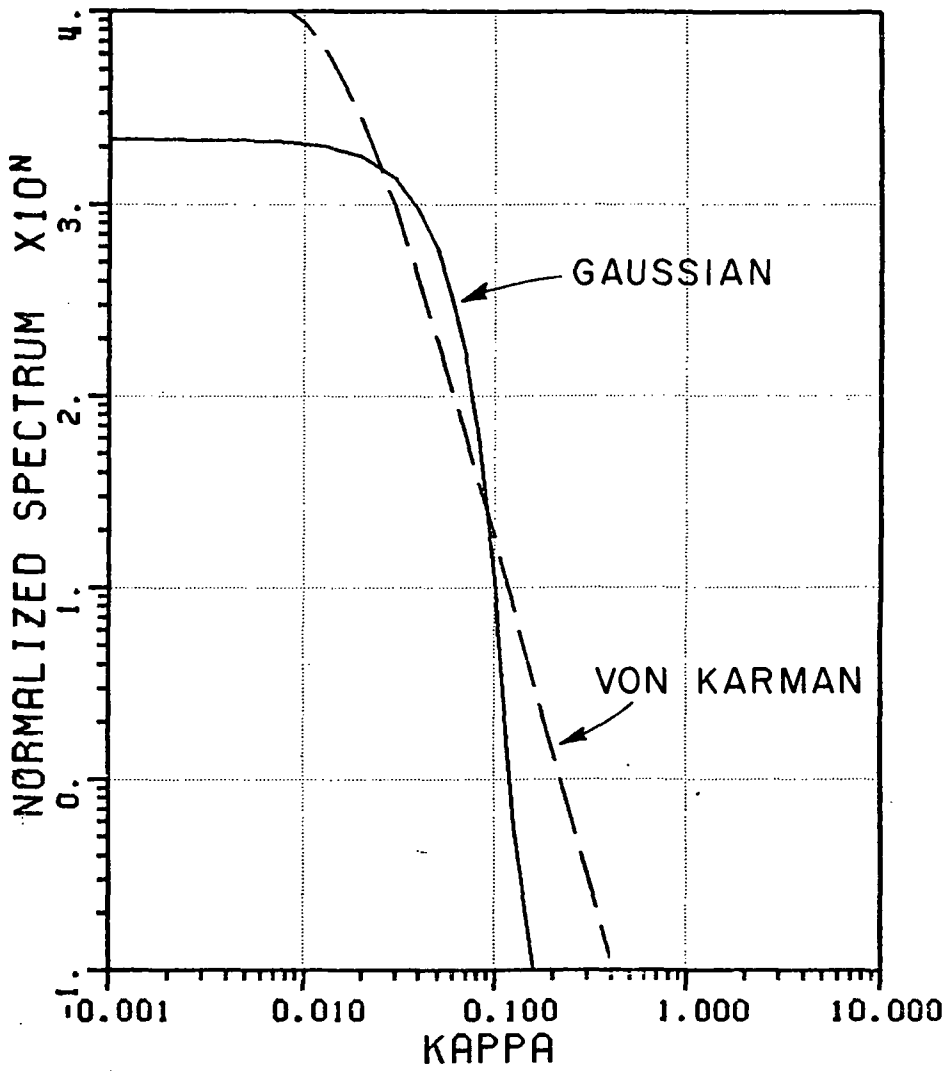

Figure 7.2. Spectrum of the model atmosphere and the equivalent Von Karman model.

$\sigma_n^2 = 0.4 \times 10^{-12}$; $\ell_n = 46$ m; $L_0 = 64$ m; $\ell_0 = 10$ mm.

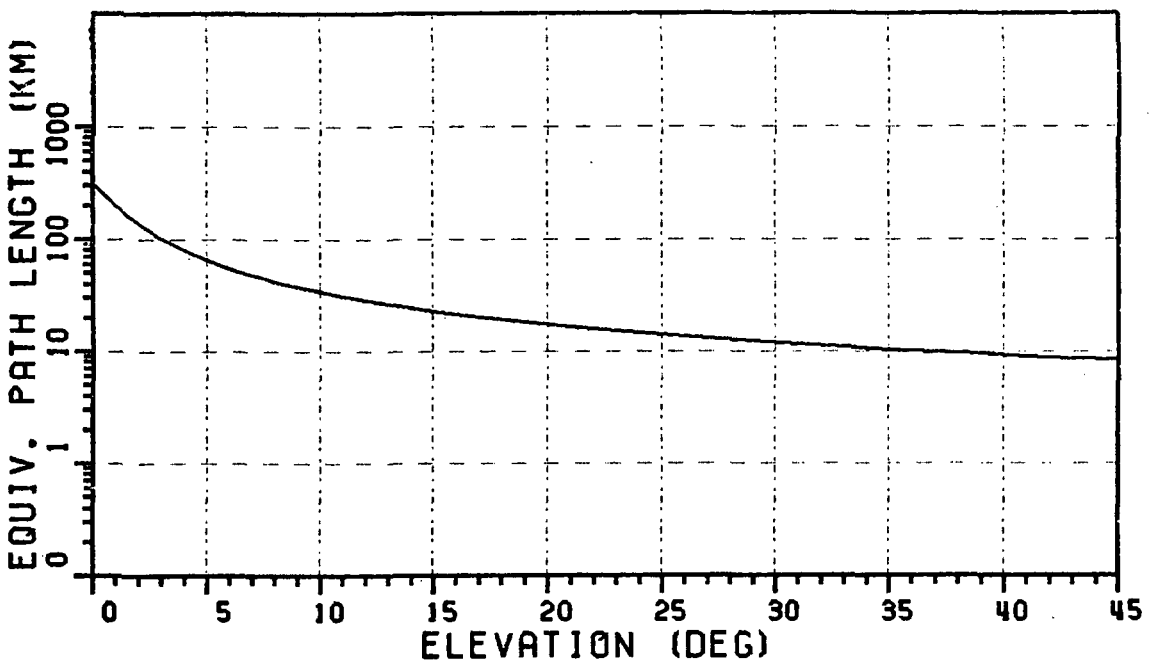

Figure 7.3. Path length through the model 6 km atmosphere.

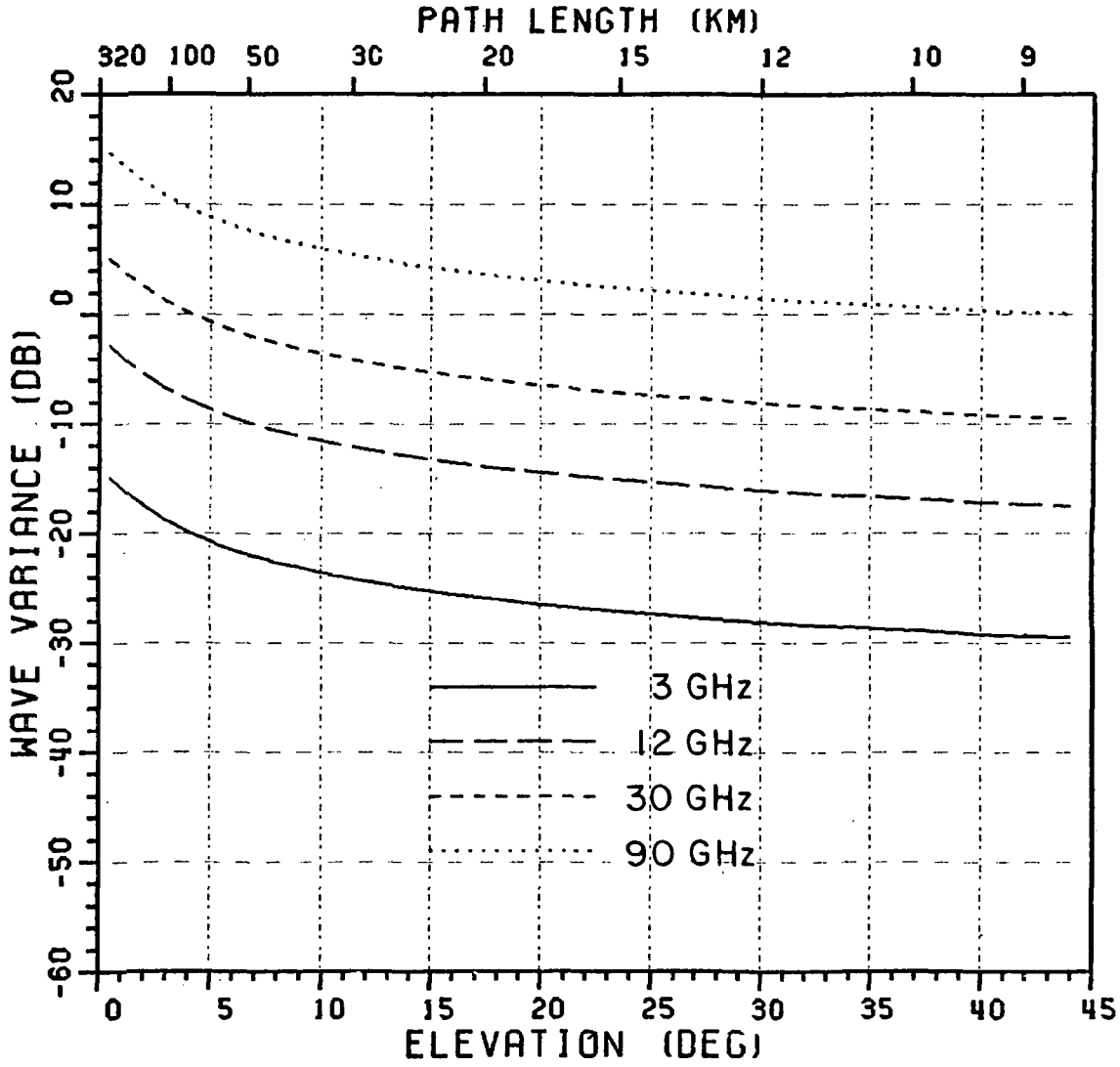

Figure 7.4. Wave variance dependence on frequency.

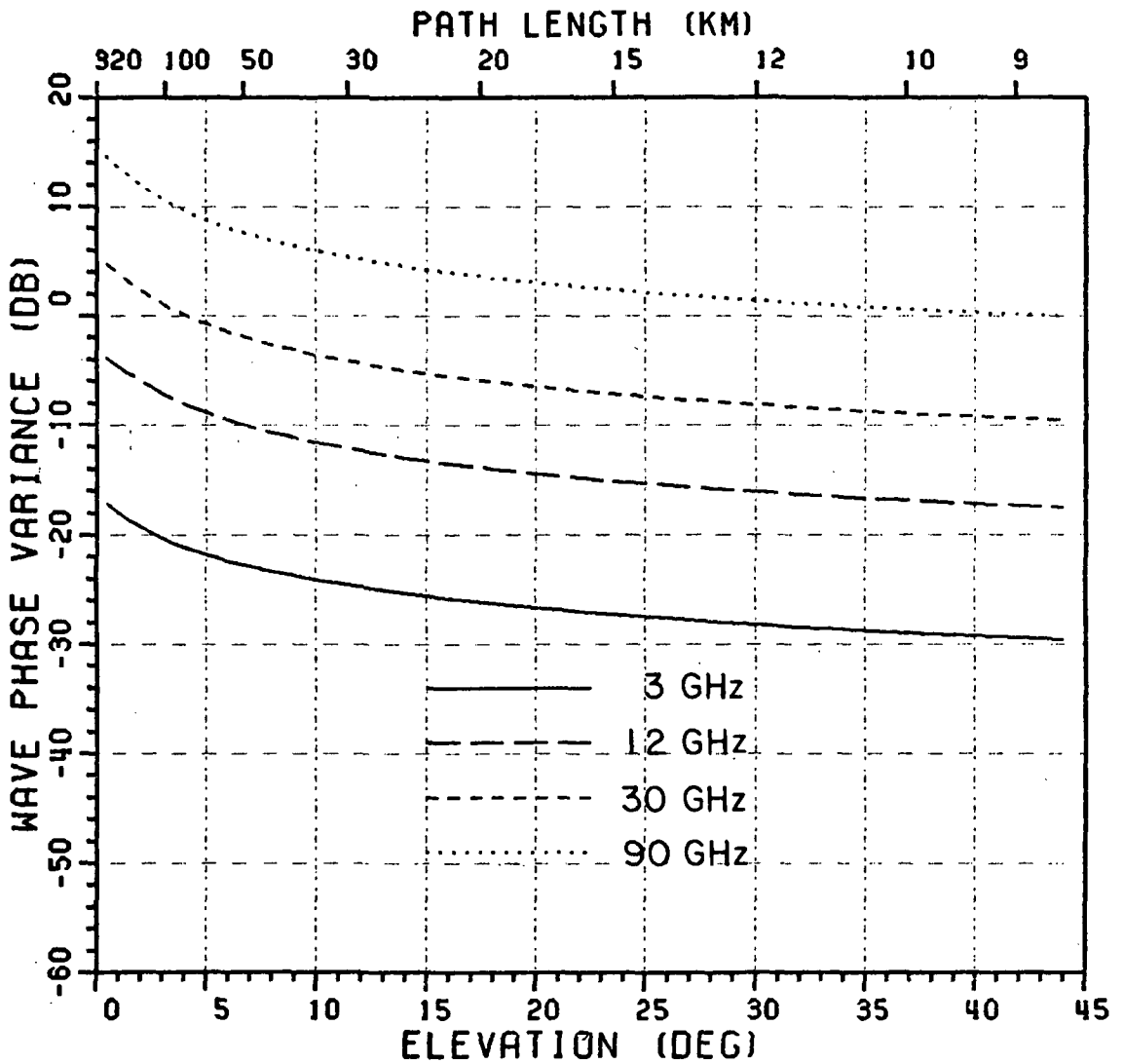

Figure 7.5. Wave phase variance dependence on frequency.

The log-amplitude variance is shown in Figure 7.6. The characteristics are markedly different from those of the previous two variances. Numerical values are several orders of magnitude below the phase variances. Thus, it may be expected that the phase ripple across the wave front should be a dominating feature of the wave. Consequently, there would be significant phase perturbation of the antenna terminal voltage as well as some amplitude scintillation caused by the incoming rays not adding in phase. Both of these effects would affect the scintillation measured by a synchronous, or phase sensitive, receiver.

A receiver whose demodulating circuits are sensitive to amplitude scintillations alone should, hence, perceive a much smaller scintillation. This explains the curves of measured scintillation in Chapter Six.

7.3 Signal Amplitude Variance

Figure 7.7 shows the variance of the amplitude scintillations measured by an asynchronous receiver at the four frequencies of interest. The diameter of the circular aperture has been fixed at 4.5 m for these curves. It is interesting to note that the variance is beginning to saturate at low elevation angles. This will be discussed in greater detail shortly.

Figure 7.8 shows the corresponding curves for a system with a synchronous receiver. The variance seen by this receiver is several orders of magnitude higher than the preceding case for the reasons explained before, i.e., the phase perturbations across the aperture introduce amplitude scintillation and phase fluctuation of the antenna terminal voltage. Therefore, the synchronous receiver, which is sensitive to phase fluctuations as well, would see a much higher fluctuation of the terminal voltage. The characteristics of the phase fluctuations clearly dominate the results.

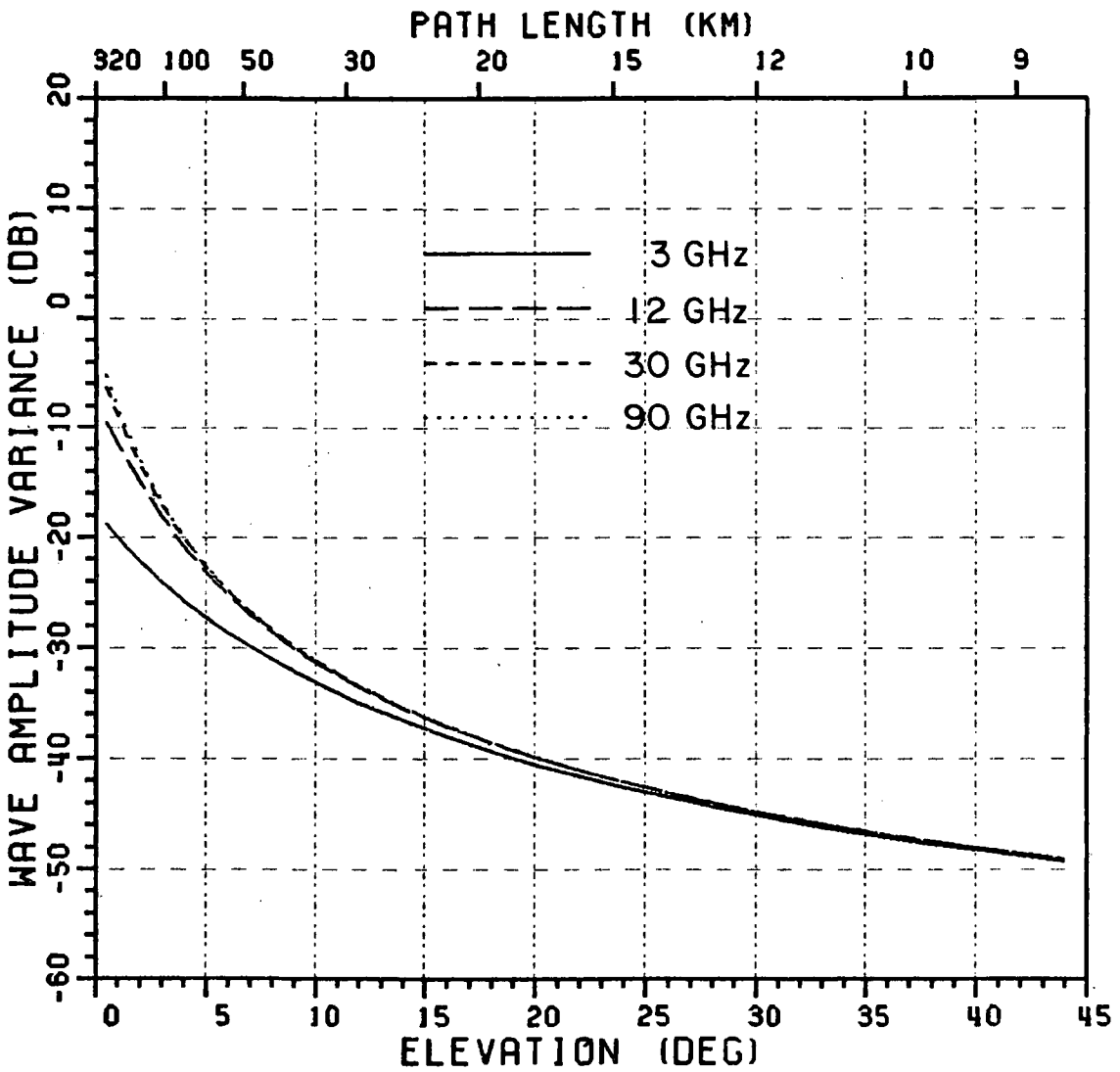

Figure 7.6. Wave amplitude variance dependence on frequency.

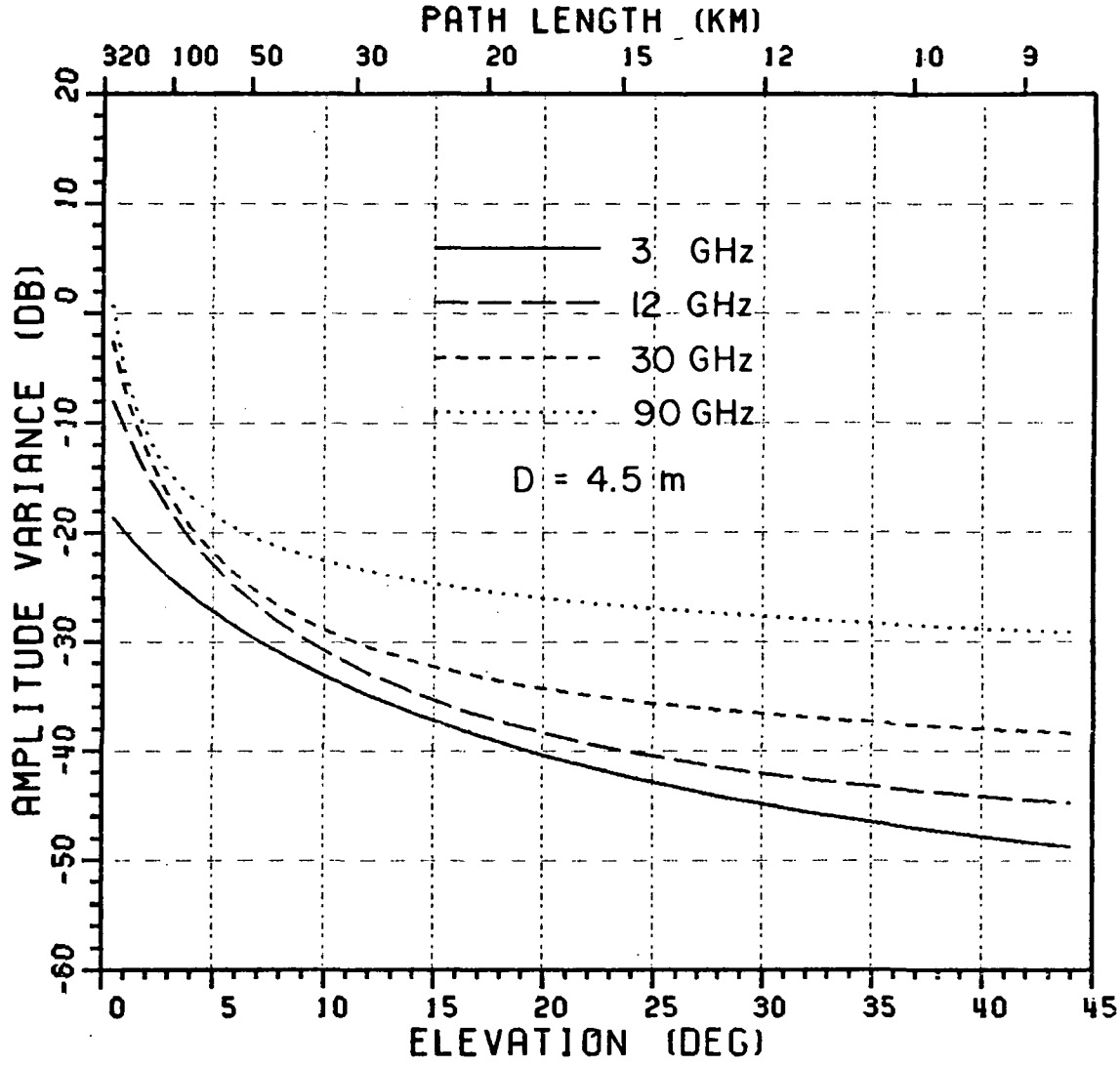

Figure 7.7. Frequency dependence of signal amplitude variance, measured by an asynchronous receiver. D=4.5 m, F=3, 12, 30 and 90 GHz.

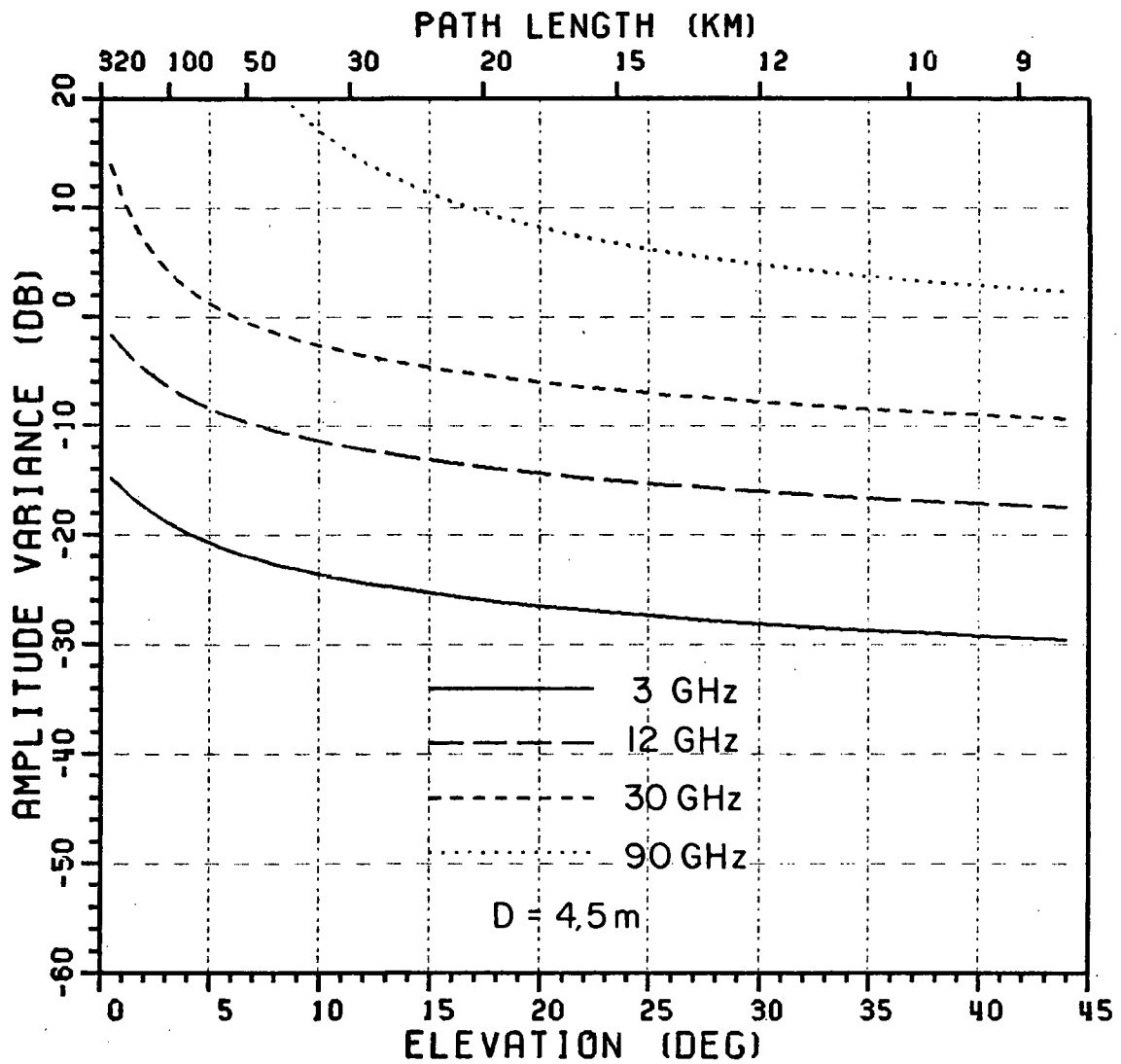

Figure 7.8. Frequency dependence of signal amplitude variance, measured by a synchronous receiver. D=4.5 m, F=3, 12, 30 and 90 GHz.

Curves for the variance of the voltage measured by synchronous receivers also may be seen to show the variance of the field in the focal plane of a focusing antenna, as noted in Section (2.6). It should be useful to bear this in mind during this discussion.

The results shown above are for long term average conditions only. An attempt was made to estimate results for extreme conditions. It was felt that the extreme cases in the atmosphere occur first under very quiet conditions, i.e., when the refractive index variance is at a minimum. It would then appear, intuitively, that the correlation length would be very high. The other extreme would be when σ_n^2 is very high. It is reasonable to expect that the correlation length should then be low. This would also pose the worst case for the antenna. To obtain these conditions, the refractive index variance was changed by a factor of 10 about its median value and the correlation length was also varied by a factor of 10. The corresponding values of C_{ng}^2 were also computed for comparison purposes.

Case 1: Quiet atmosphere

$$\sigma_n^2 = .04 \times 10^{-12}$$

$$\ell_n = 100 \text{ m}$$

$$C_{ng}^2 = .3 \times 10^{-14} \qquad m^{-\frac{2}{3}}$$

Case 2: Disturbed atmosphere

$$\sigma_n^2 = 4.0 \times 10^{-12}$$

$$\ell_n = 10 \text{ m}$$

$$C_{ng}^2 = 1.4 \times 10^{-12} \qquad m^{-\frac{2}{3}} \; .$$

The equivalent structure constant is for comparison purposes only. The results are shown for the two receiver systems in Figures 7.9 and 7.10 at 30 GHz for an aperature diameter of 4.5 m. These may be reasonably expected to be the extreme conditions to which the links could be expected to be subjected under clear air conditions.

The validity of the present model under conditions of strong turbulence is not known. Much depends on the validity under these conditions of the amplitude and phase filter functions used to calculate the log amplitude and phase variances. Furthermore, the expressions for the average power and signal variance measured by an asynchronous receiver may not contain a sufficient number of terms of the Taylor series expansion used to remain accurate. An injudicious choice of the refractive index variance and correlation length can cause these expressions to blow up. Unfortunately, improving their accuracy necessitates the evaluation of ever higher moments of the asynchronous received voltage. A reference to Appendix A4 quickly discourages this approach.

Therefore, all results shown for the strong turbulence case must be used with care until their validity is verified by theoretical or experimental methods.

The dependence of amplitude variance on aperature size is examined in Figure 7.11 for the asynchronous receiver case. Only 1 m and 9.1 m diameter apertures, which encompass the range of popular sizes, are considered at each frequency. The results are shown separately in Figures 7.12 to 7.15. There is a clear increase in the measured scintillation with the larger aperture.

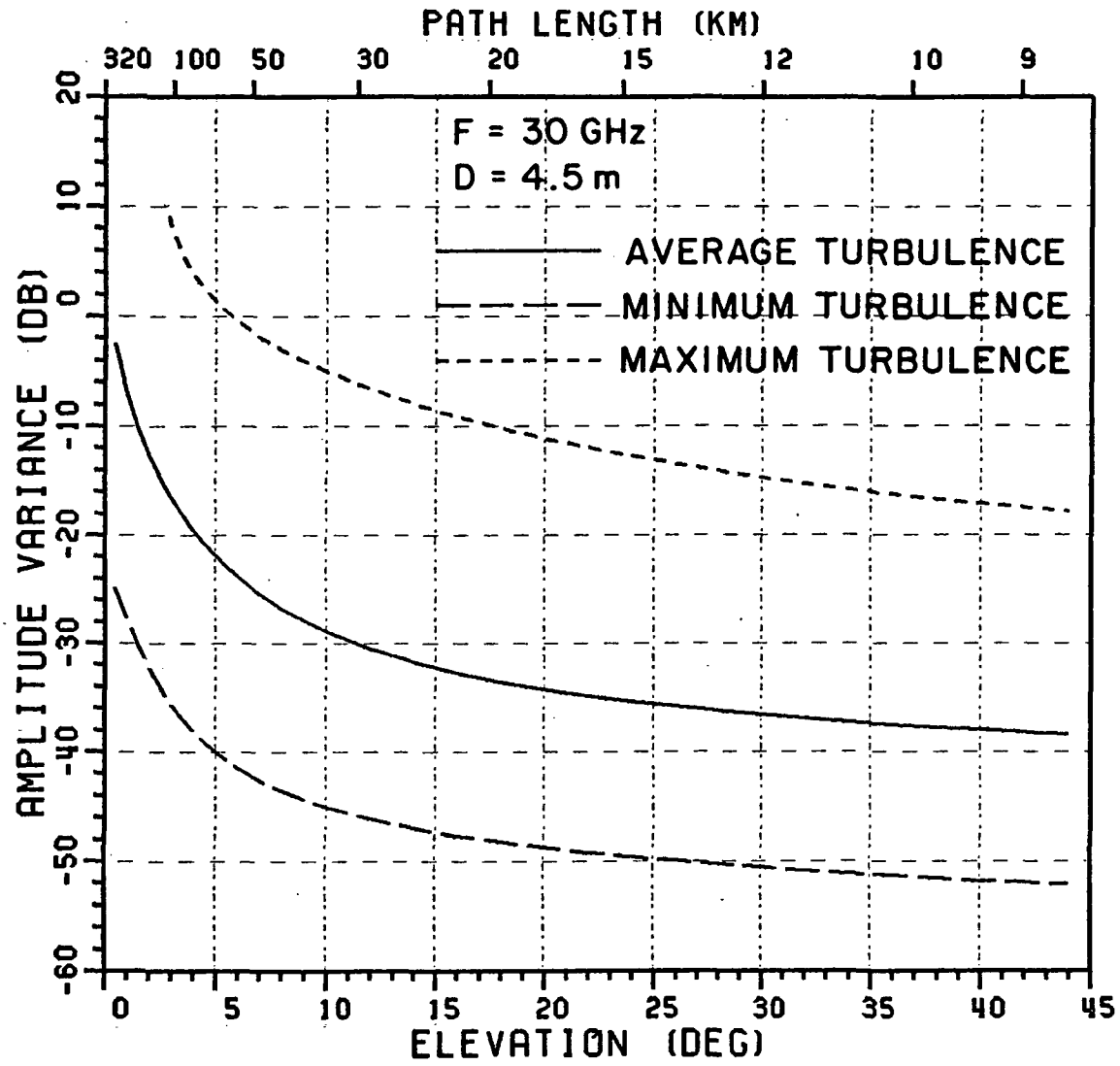

Figure 7.9. Change of variance with extremes of turbulence, F=30 GHz; D=4.5 m; asynchronous receiver.

Average turbulence: $\sigma_n^2 = 0.4 \times 10^{-12}$; $\ell_n = 46$ m.

Minimum turbulence: $\sigma_n^2 = .04 \times 10^{-12}$; $\ell_n = 100$ m.

Maximum turbulence: $\sigma_n^2 = 4.0 \times 10^{-12}$; $\ell_n = 10$ m.

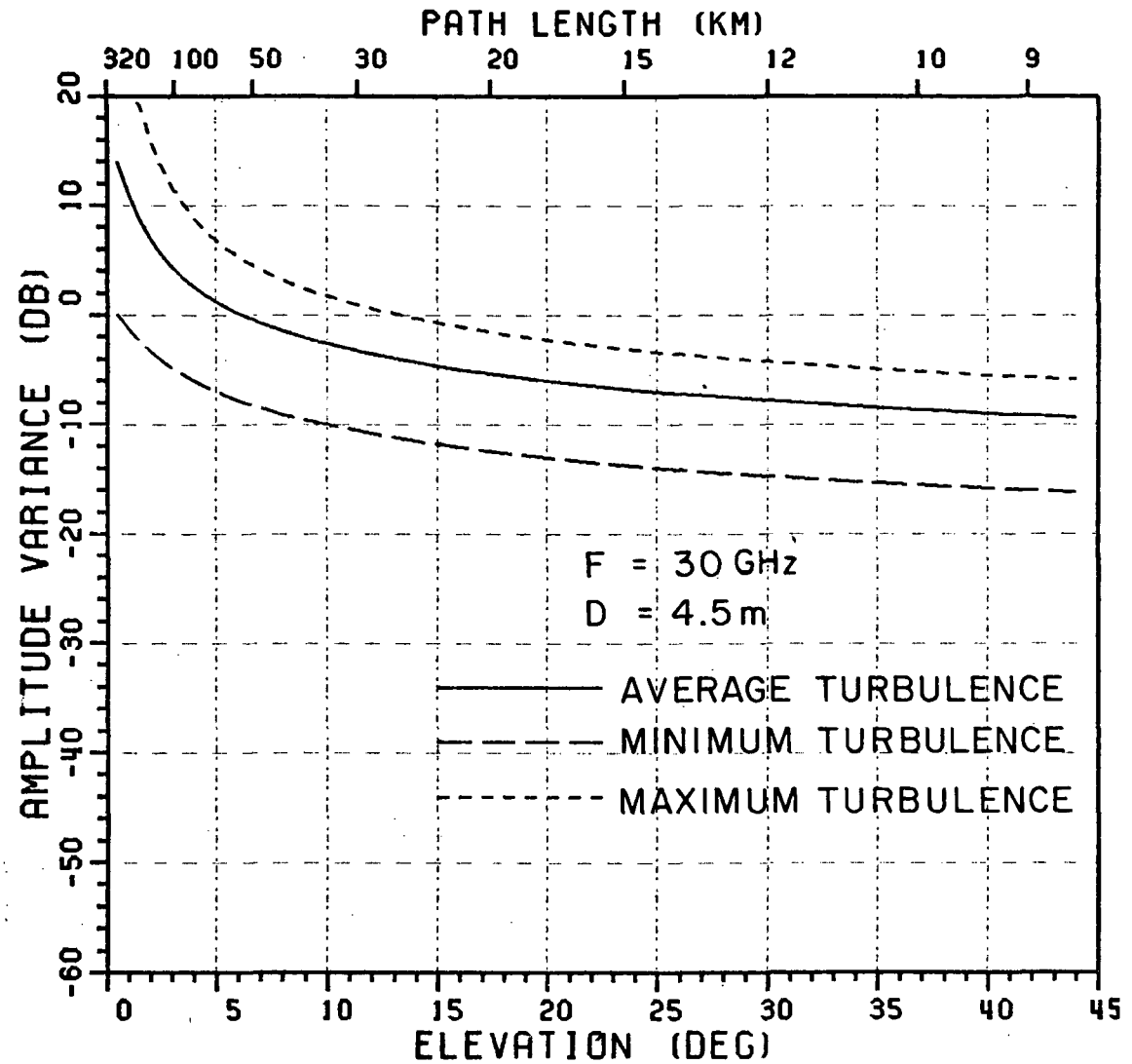

Figure 7.10. Change of variance with extremes of turbulence, F=30 GHz; D=4.5 m; synchronous receiver.

Average turbulence: $\sigma_n^2 = 0.4 \times 10^{-12}$; $\ell_n = 46$ m.

Minimum turbulence: $\sigma_n^2 = .04 \times 10^{-12}$; $\ell_n = 100$ m.

Maximum turbulence: $\sigma_n^2 = 4.0 \times 10^{-12}$; $\ell_n = 10$ m.

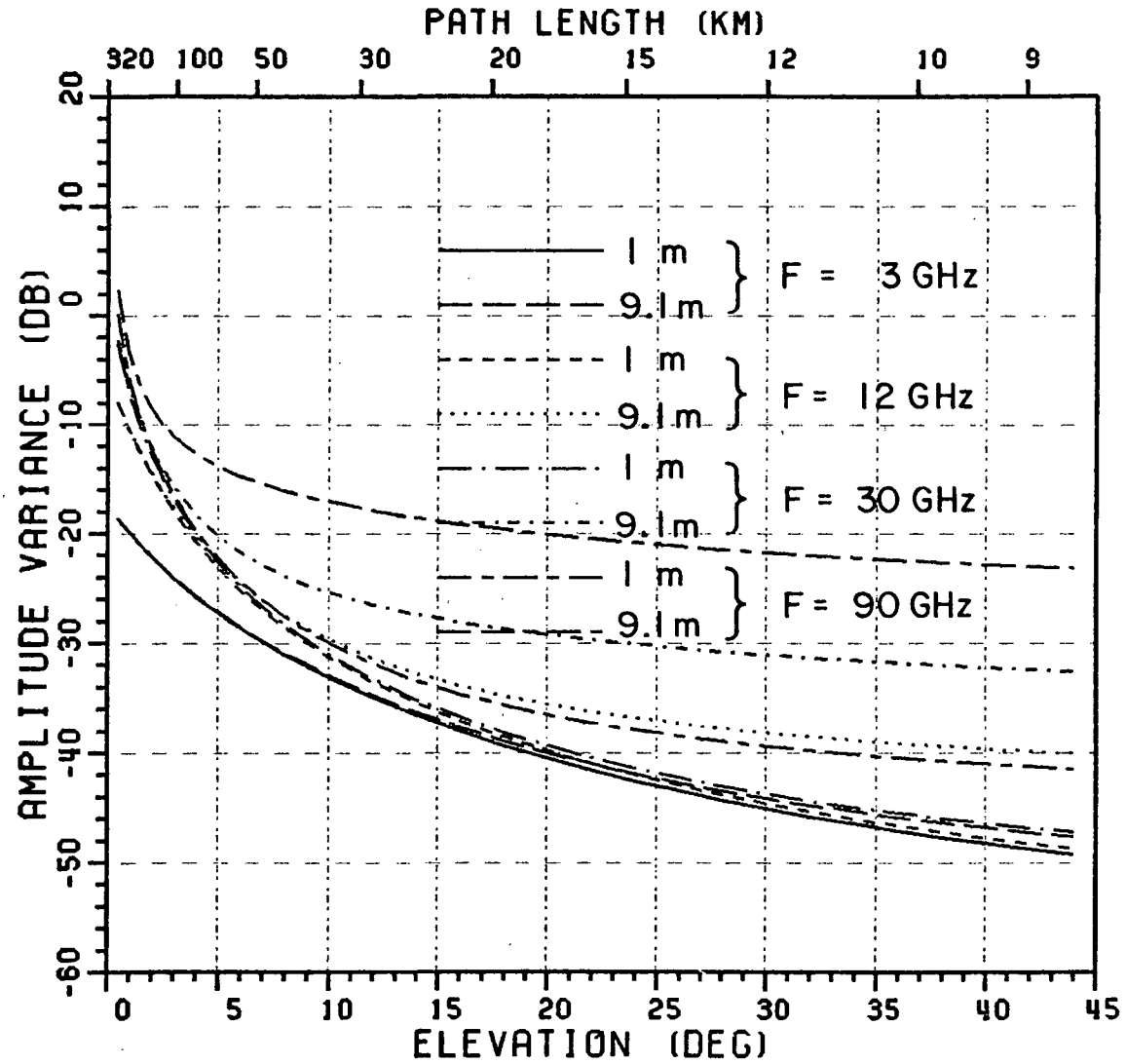

Figure 7.11. Dependence of variance on antenna aperture size, at 3, 12, 30 and 90 GHz; asynchronous receiver.

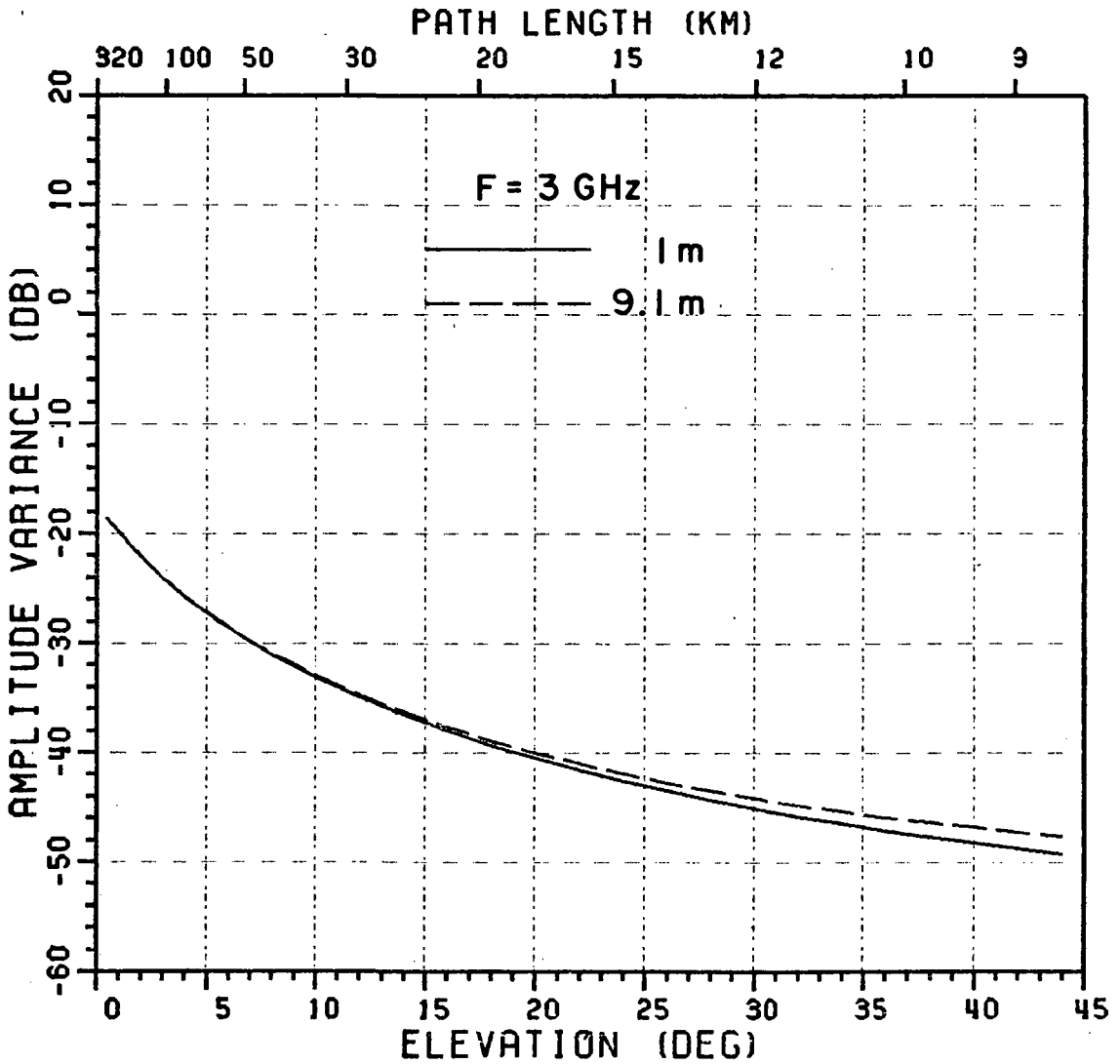

Figure 7.12. Dependence of variance on antenna aperture size, at 3 GHz; asynchronous receiver.

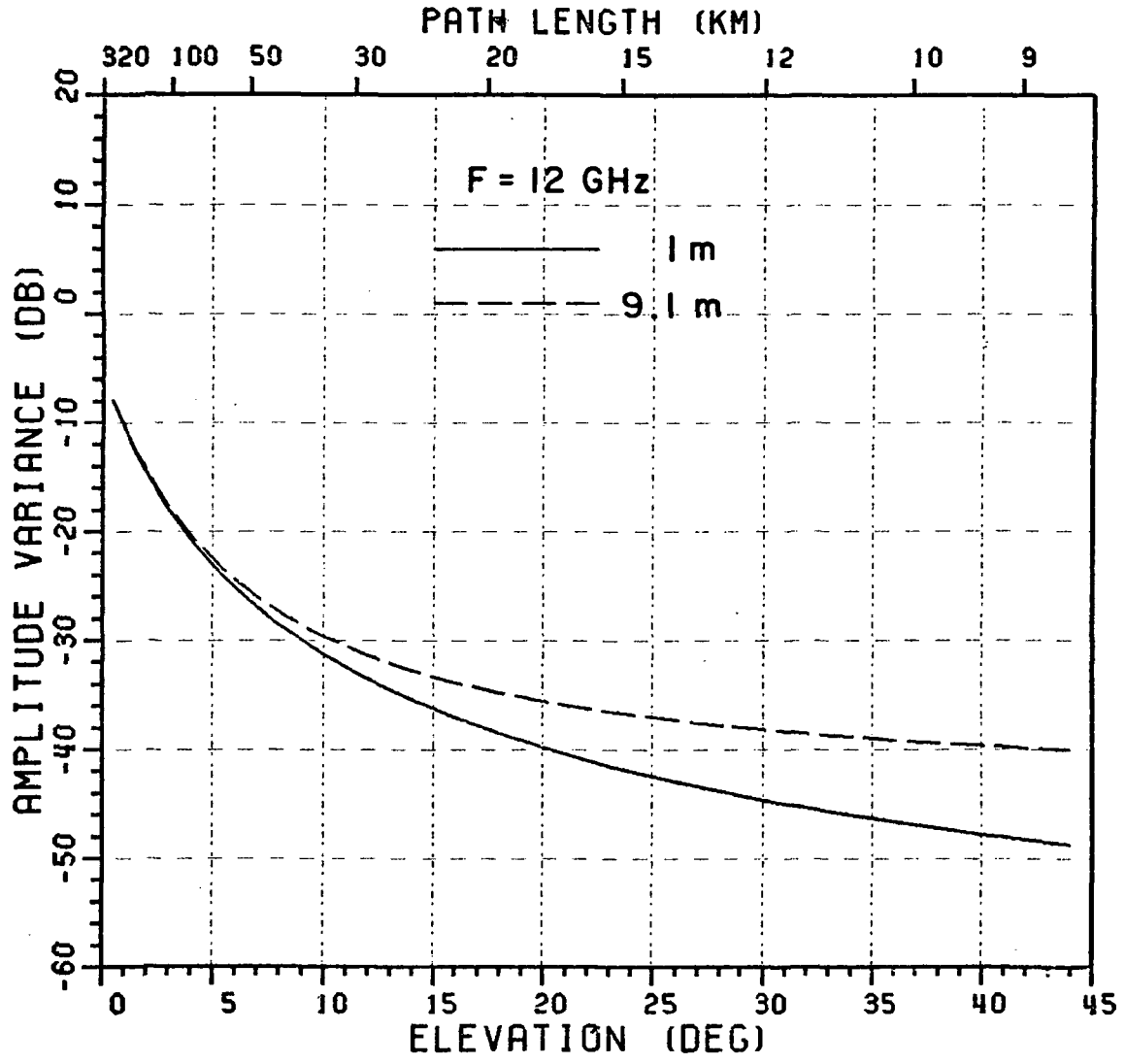

Figure 7.13. *Dependence of variance on antenna aperture size, at 12 GHz;* asynchronous receiver.

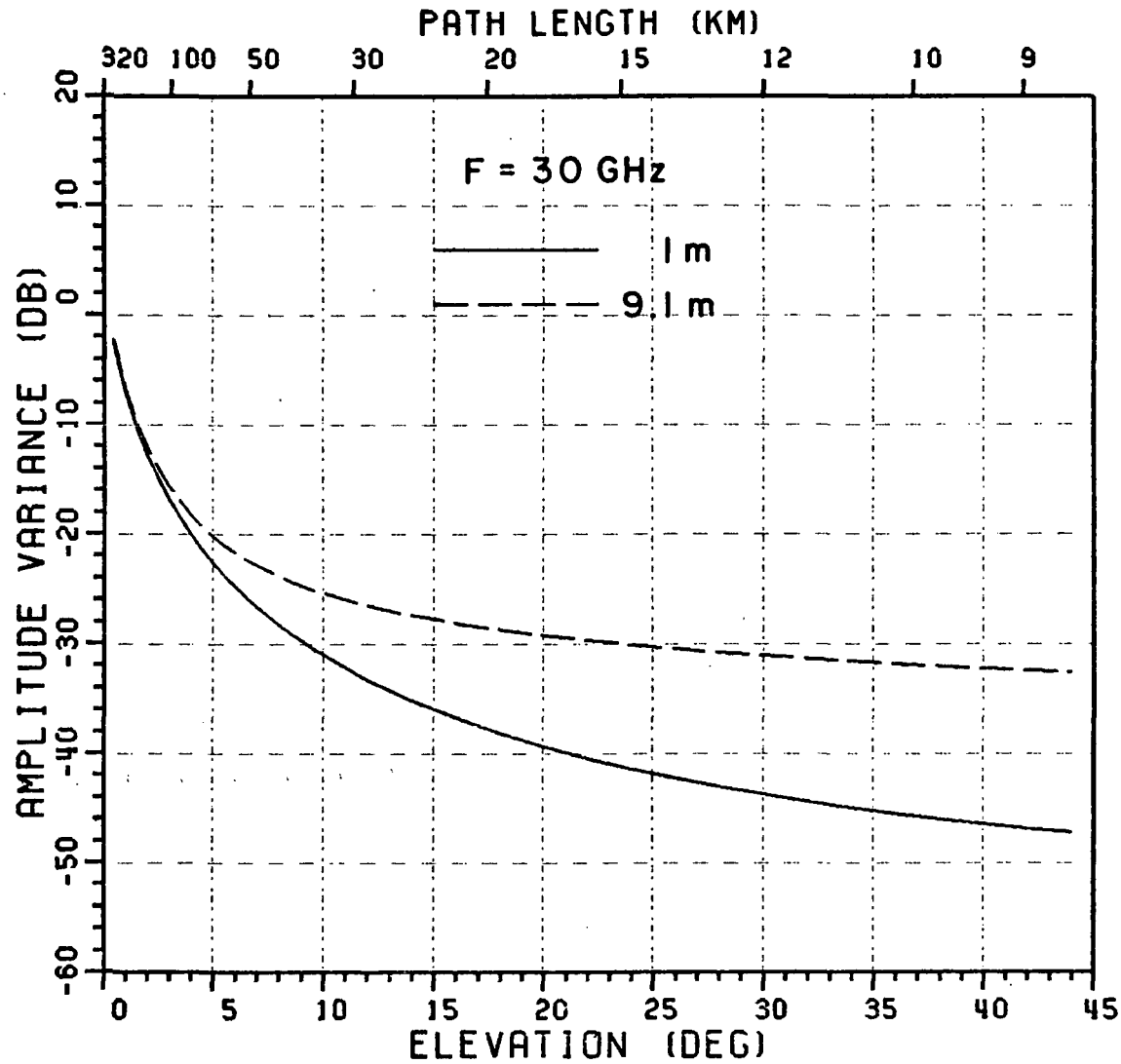

Figure 7.14. Dependence of variance on antenna aperture size, at 30 GHz; asynchronous receiver.

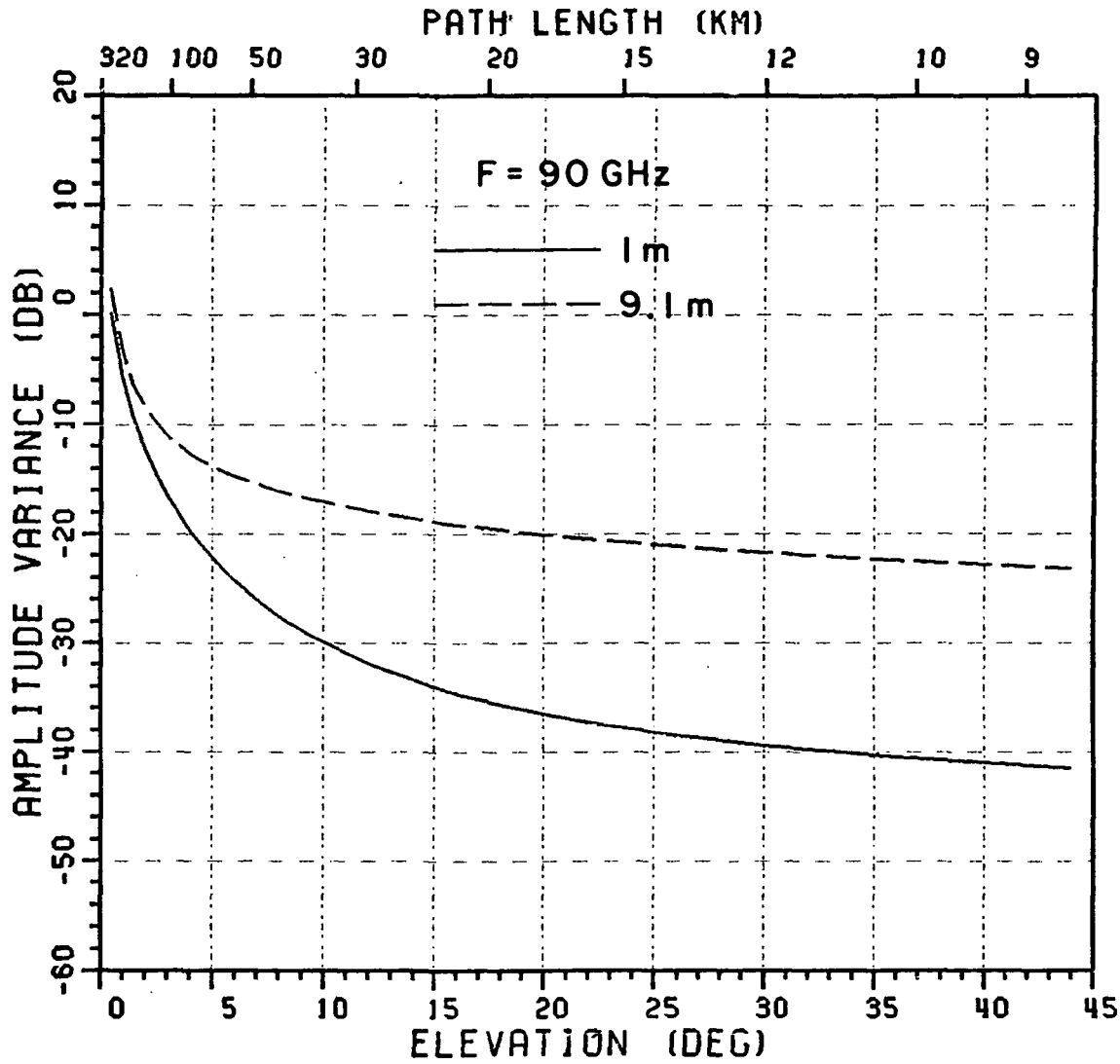

Figure 7.15. Dependence of variance on antenna aperture size, at 90 GHz; asynchronous receiver.

Figure 7.16 is a different presentation of the variance of the received signal measured by an asynchronous AM receiver. The measured amplitude variance is displayed in the figure as a function of aperture size, at selected elevation angles. The path length (km) through the equivalent homogeneous atmosphere is given in parentheses. The atmosphere is assumed to be under conditions of average turbulence.

The normalized amplitude variance is initially constant at any given elevation angle. However, it increases rapidly with the size of the aperture beyond some critical value in the range of 1 m to 10 m. Another important characteristic is the evidence of aperture averaging at the larger aperture sizes over the longer propagation paths. There is a clear reduction in the increase of the amplitude variance with aperture size, compared with that at higher elevation angles.

It is essential to note that this should not be classed simply as a D/λ effect. A fundamental feature of the present model is that the diameter of the antenna is related not only to the wave length, λ, but also to the size of the correlation length of the atmosphere. Consequently, two systems, having the same electrical aperture size, but at different frequencies, may have marked differences in behavior because of the different physical aperture sizes and, hence, different relative correlation ratios to the atmospheric turbulence scale size. In other words, since the incoming wave front is no longer plane, the number of ripples across the aperture would be different at different frequencies for antennas of the same electrical aperture size, thus affecting the results by different amounts.

The asynchronous receiver eliminates the phase information in the measured signal. Therefore, it is difficult to relate the observed results directly to the properties of the received wave. Equation (4.7.2) exemplifies this problem. The synchronous receiver, on the other hand, retains more information from the received signal. Hence, the amplitude variance measured by a synchronous AM receiver is studied next.

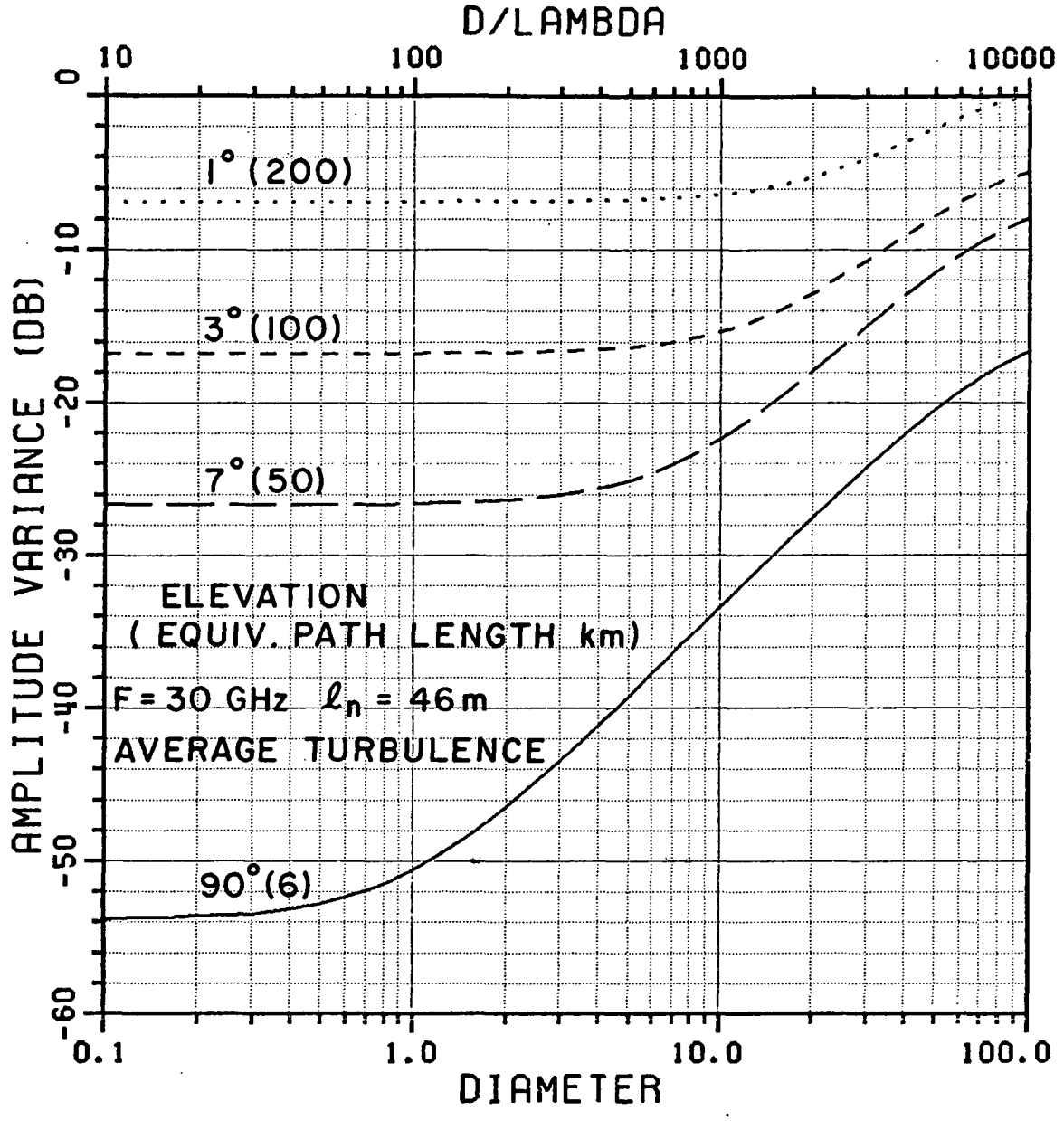

Figure 7.16. Dependence of variance on antenna aperture size, at selected elevation angles; F=30 GHz; asynchronous receiver. The equivalent path length is shown in parentheses.

Figure 7.17 shows the amplitude variance as a function of elevation angle for aperture sizes of 1 m and 9.1 m only, at the four selected frequencies for synchronous receiver systems. Average conditions of turbulence are assumed as before. There is no noticeable effect on the variance with change in aperture sizes in this range. Therefore, the normalized amplitude variance (4.4.3) was next plotted in Figure 7.18 for aperture sizes from 10 cm to 100 m at 30 GHz, as in Figure 7.16.

While there is the expected change of the variance with elevation angle, the aperture size dependence is weaker. Furthermore, instead of increasing with aperture size, as in Figure 7.16, the variance remains constant for small apertures and then actually decreases with larger aperture sizes.

Unfortunately, the normalization of the variance to the measured dc power, while useful as an experimental procedure, introduces an additional variable, thereby making comparison of Figures 7.16 and 7.18 and the interpretation of the results difficult. The true fluctuating power in the received signal, P_{fl} (4.3.19), is a more useful aid to understanding the mechanisms involved.

Figure 7.19 shows the measured fluctuating power, P_{fl}, normalized to the plane wave power, P_{RO}, received in the absence of turbulence. The latter is, by definition, independent of the turbulence and the elevation angle. P_{fl} cannot, obviously, exceed P_{RO}. The curves are drawn under conditions of average turbulence in the same format as Figures 7.16 and 7.18.

At high elevation angles the fluctuating power increases with path length as expected. However, an interesting behavior is revealed by the 0^{o} and 1^{o} curves, which actually cross over and indicate smaller values of the received fluctuating power at long path lengths for a given large aperture size, than at shorter path lengths. To bring out this effect, the same cases are plotted for maximum turbulence conditions in Figure 7.20,

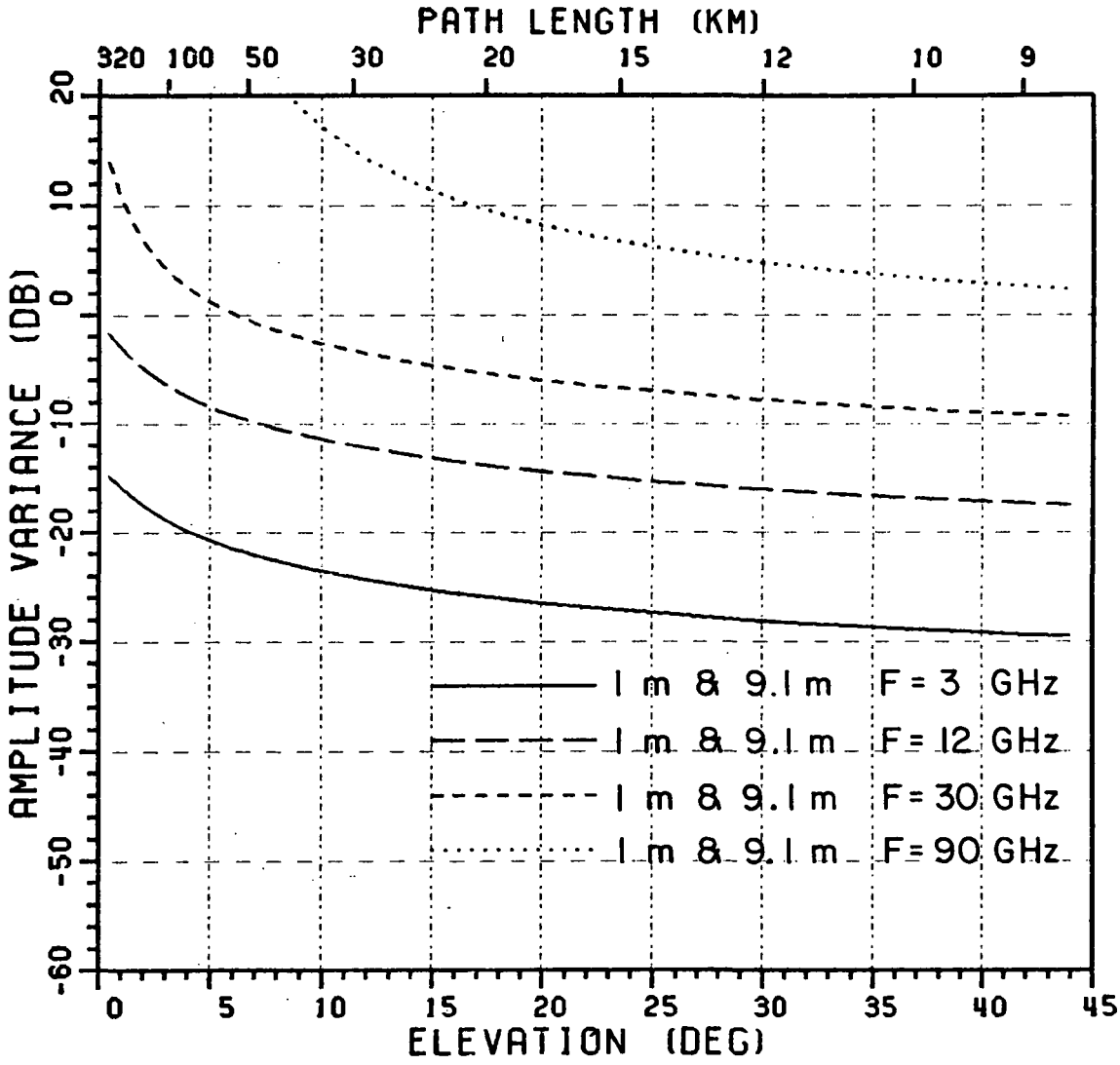

Figure 7.17. Dependence of variance on antenna aperture size, at 3, 12, 30 and 90 GHz; synchronous receiver.

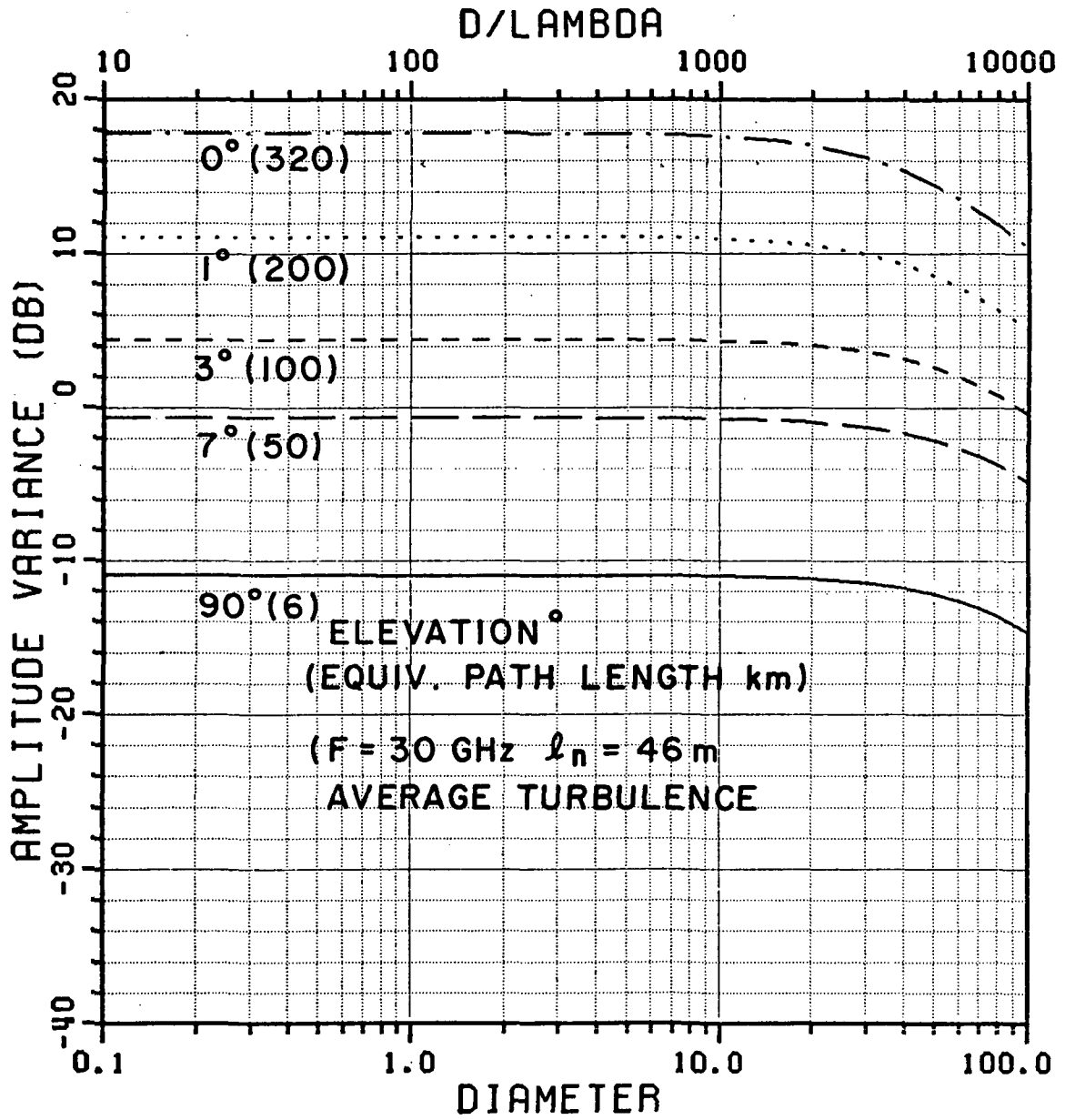

Figure 7.18. Dependence of variance on antenna aperture size, at selected elevation angles; F=30 GHz; synchronous receiver. The equivalent path length is shown in parentheses.

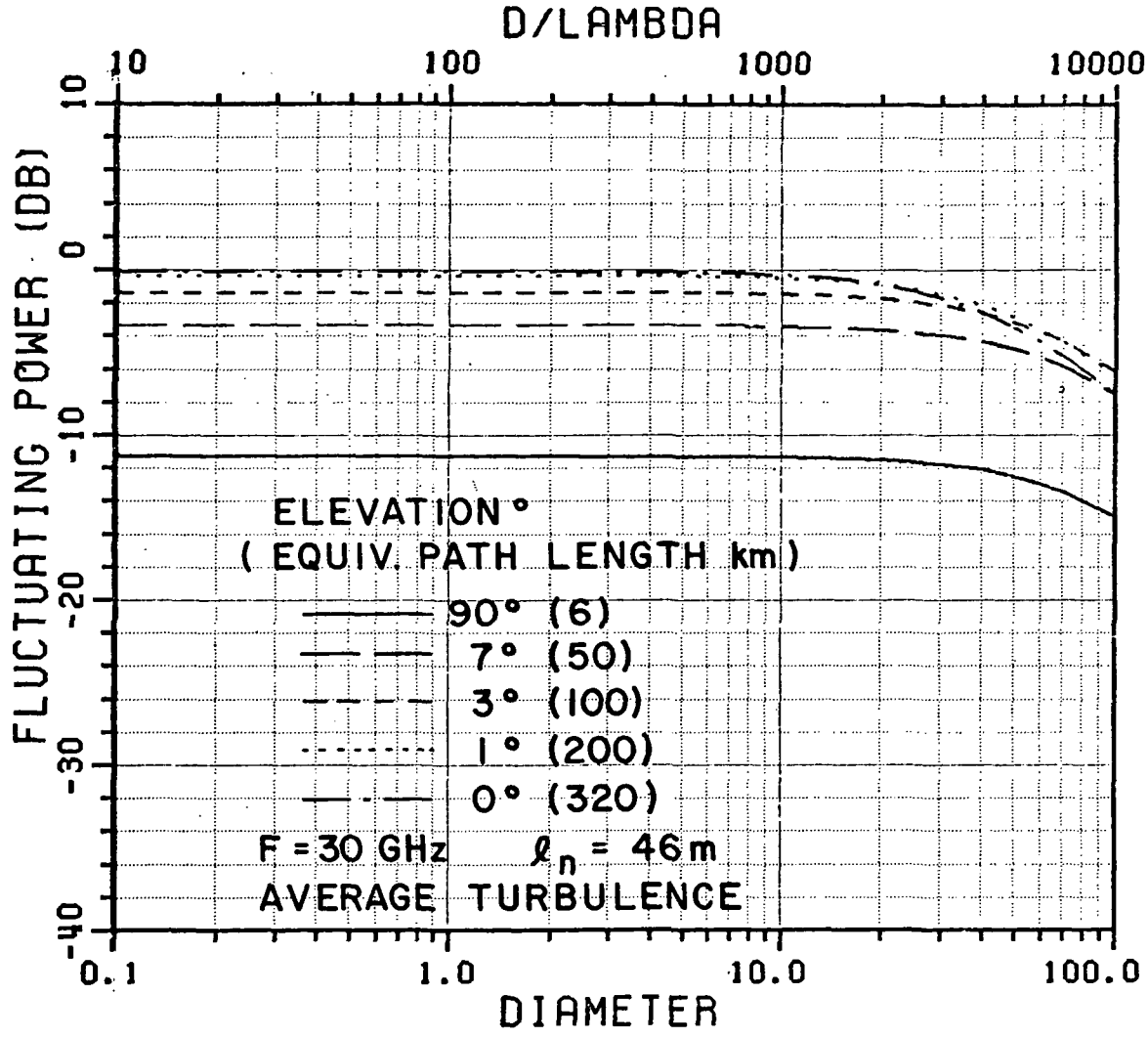

Figure 7.19. Dependence of the fluctuating component of the received power on antenna aperture size at selected elevation angles in average turbulence; F=30 GHz; synchronous receiver.

$\sigma_n^2 = 0.4 \times 10^{-12}$; ℓ_n = 46 m .

The equivalent path length is shown in parentheses.

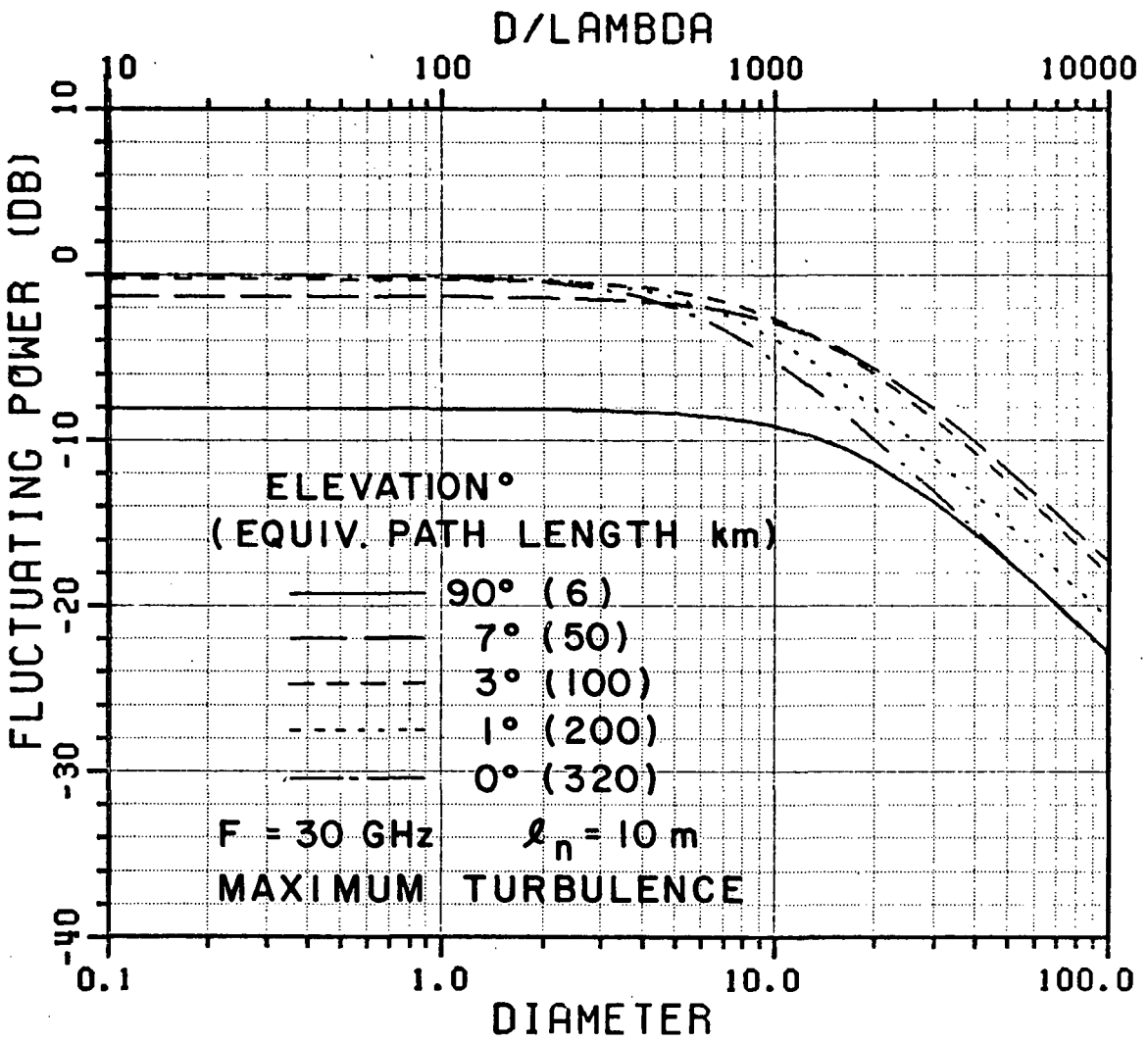

Figure 7.20. Dependence of the fluctuating component of the received power on antenna aperture size at selected elevation angles in maximum turbulence; F=30 GHz; synchronous receiver.

$\sigma_n^2 = 4.0 \times 10^{-12}$; ℓ_n = 10 m.

The equivalent path length is shown in parentheses.

where the phenomenon is magnified and visible at shorter path lengths as well. It is also apparent that the crossover occurs at antenna sizes close to the size of the correlation length of the refractive index fluctuations. It is suggested that the path length at which the effect becomes noticeable is such that the scale size of the turbulence becomes comparable to the size of the Fresnel zone of the antenna.

Figures 7.16 through 7.20 illustrate the phenomenon known as aperture averaging. Over short path lengths, the phase fluctuations are well correlated over the Fresnel zone of the antenna. Therefore, increasing the path length, which increases the magnitude of the amplitude and phase fluctuations results in an increased signal variance. However, when the path length is sufficiently large and the antenna is also large, the phase correlation length becomes comparable to or less than the Fresnel size of the antenna. Now, different rays reaching the antenna are uncorrelated, causing partial cancellation of the fluctuating component of the signal. This also reduces the variance of the antenna terminal voltage.

An alternative viewpoint is to look at the antenna as a spatial filter. Referring to Chapter 4.3 - 4.4, it is seen that if the antenna is small compared to the scale size of the turbulence, the amplitude variance measured by a synchronous receiver is, in fact, the true fluctuating power in the wave. This, clearly, will be a function of the atmospheric turbulence only, as long as there is no significant scattering out of the beam of the antenna.

7.4 Signal Level Degradation

The degradation in received power as perceived by the receiver was examined under the same conditions and for the same dependences as the amplitude variance. The following is a summary of the findings of the resulting degradation.

Figures 7.21 and 7.22 show the frequency dependence of the power degradation for the asynchronous and synchronous receiving systems, respectively. The former does not show significant effects except at very low elevation angles. The latter, as shown before, measures the true non-fluctuating component of the incoming wave. Thus, degradation effects are significant at all elevation angles.

The aperture size dependence of the average power degradation experienced by an asynchronous receiver at 30 GHz is shown in Figures 7.23 and 7.24. It is displayed as a function of elevation angle in Figure 7.23 for the maximum turbulence case. It is also plotted with aperture size as the primary variable in Figure 7.24 for the average turbulence case. Even if the 0^{o} values are excluded, it is significant that there may be more than a tenfold decrease in the received average power at low elevation angles in strong turbulence, over that received under average turbulence conditions. Hence, system margins may easily be degraded in heavy turbulence. The likelihood of such an occurrence is, of course, not estimated in this report.

Average power degradation for a synchronous receiver is shown in Figure 7.25. It is included for completeness and for purposes of comparison only. There is no aperture size dependence of power degradation for synchronous receiver systems. This is seen in Equation (4.3.17). The dc power measured by the synchronous receiver is the true coherent power in the wave. This is, clearly, independent of the receiving system and is a function of the atmospheric link only.

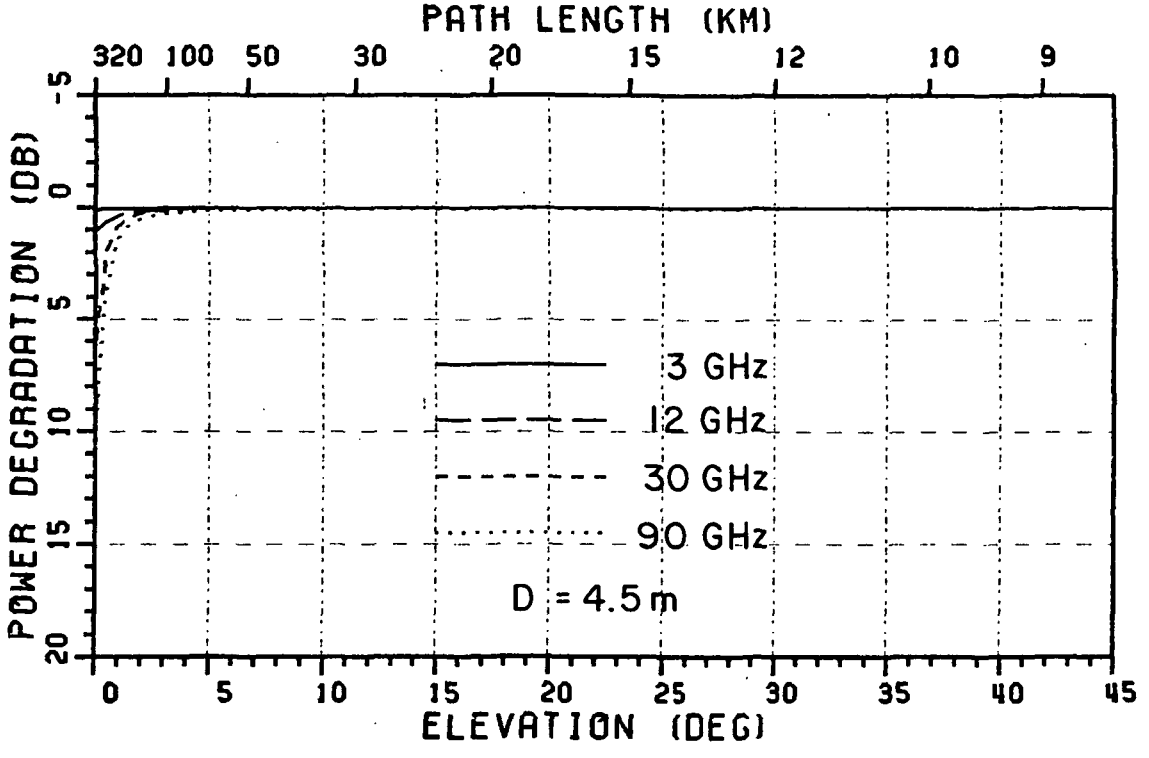

Figure 7.21. Frequency dependence of average power degradation, D=4.5 m; asynchronous receiver.

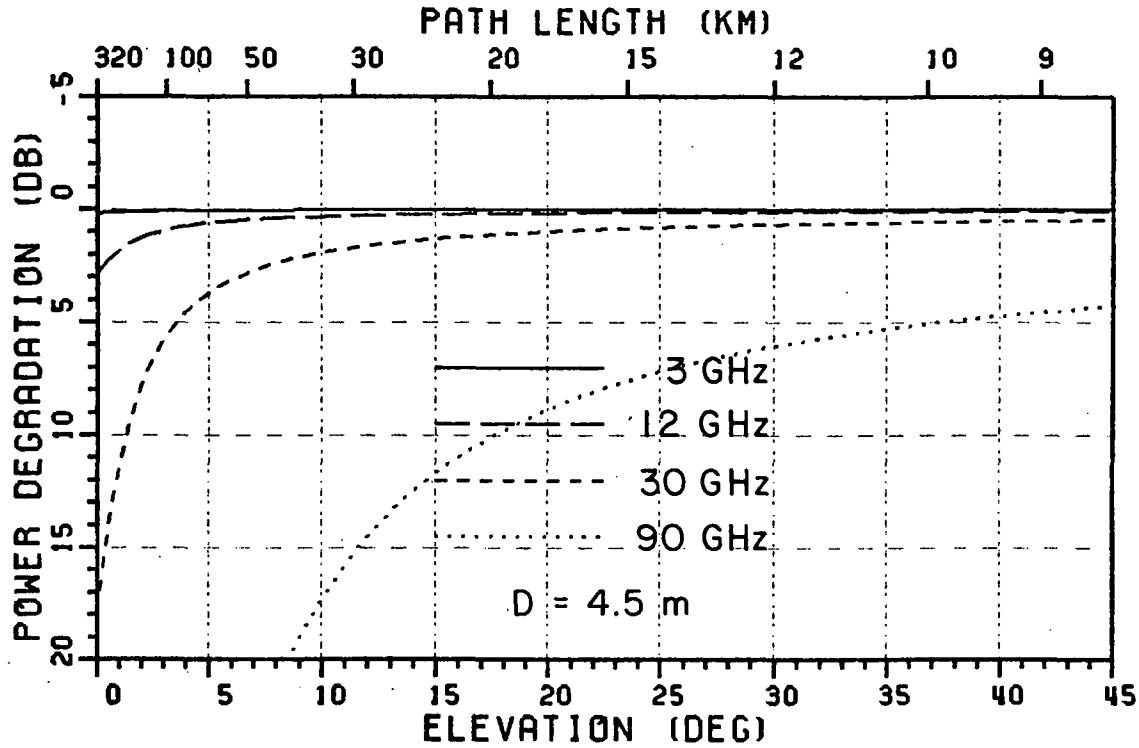

Figure 7.22. Frequency dependence of average power degradation, D=4.5 m; synchronous receiver.

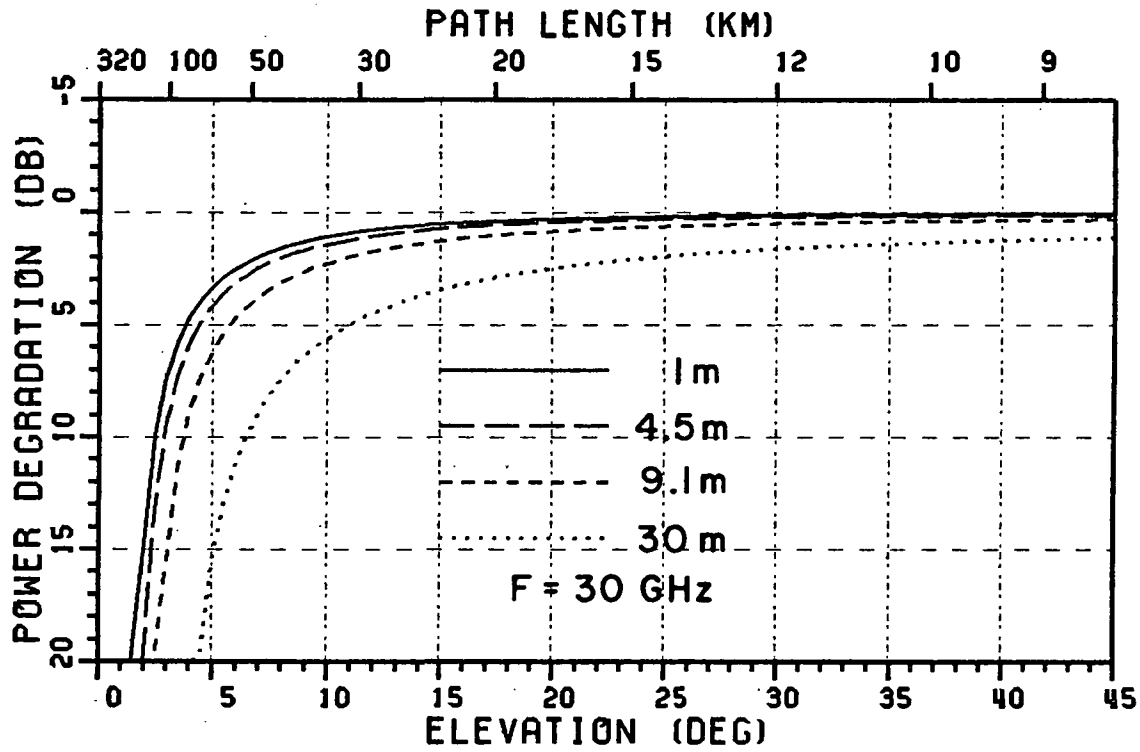

Figure 7.23. Aperature size dependence of average power degradation, in maximum turbulence; F=30 GHz; asynchronous receiver.

$\sigma_n^2 = 4.0 \times 10^{-12}$; $\ell_n = 10$ m.

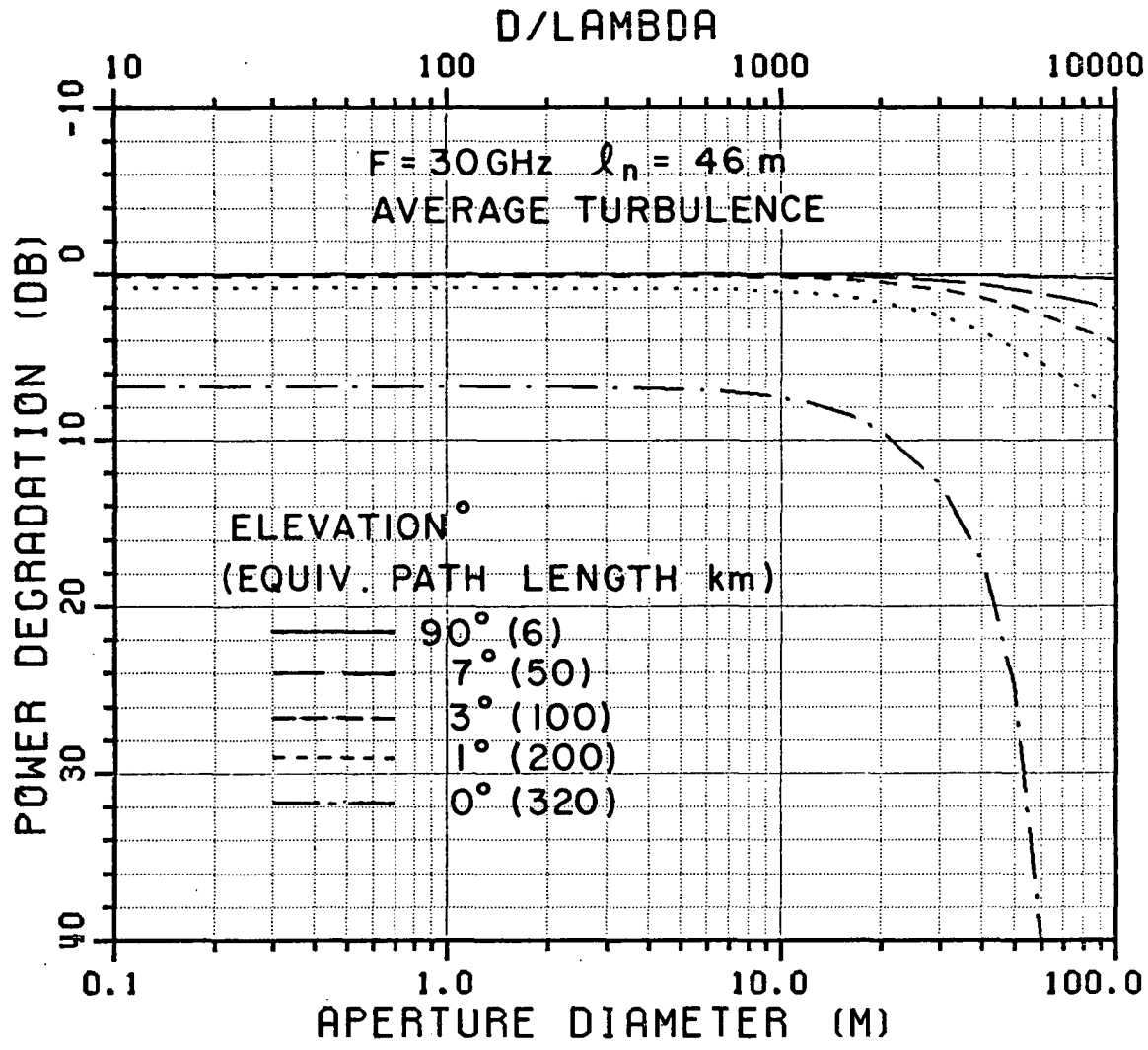

Figure 7.24. Dependence of the average received power on antenna aperture size at selected elevation angles in average turbulence, F=30 GHz; asynchronous receiver. The equivalent path length is shown in parentheses.

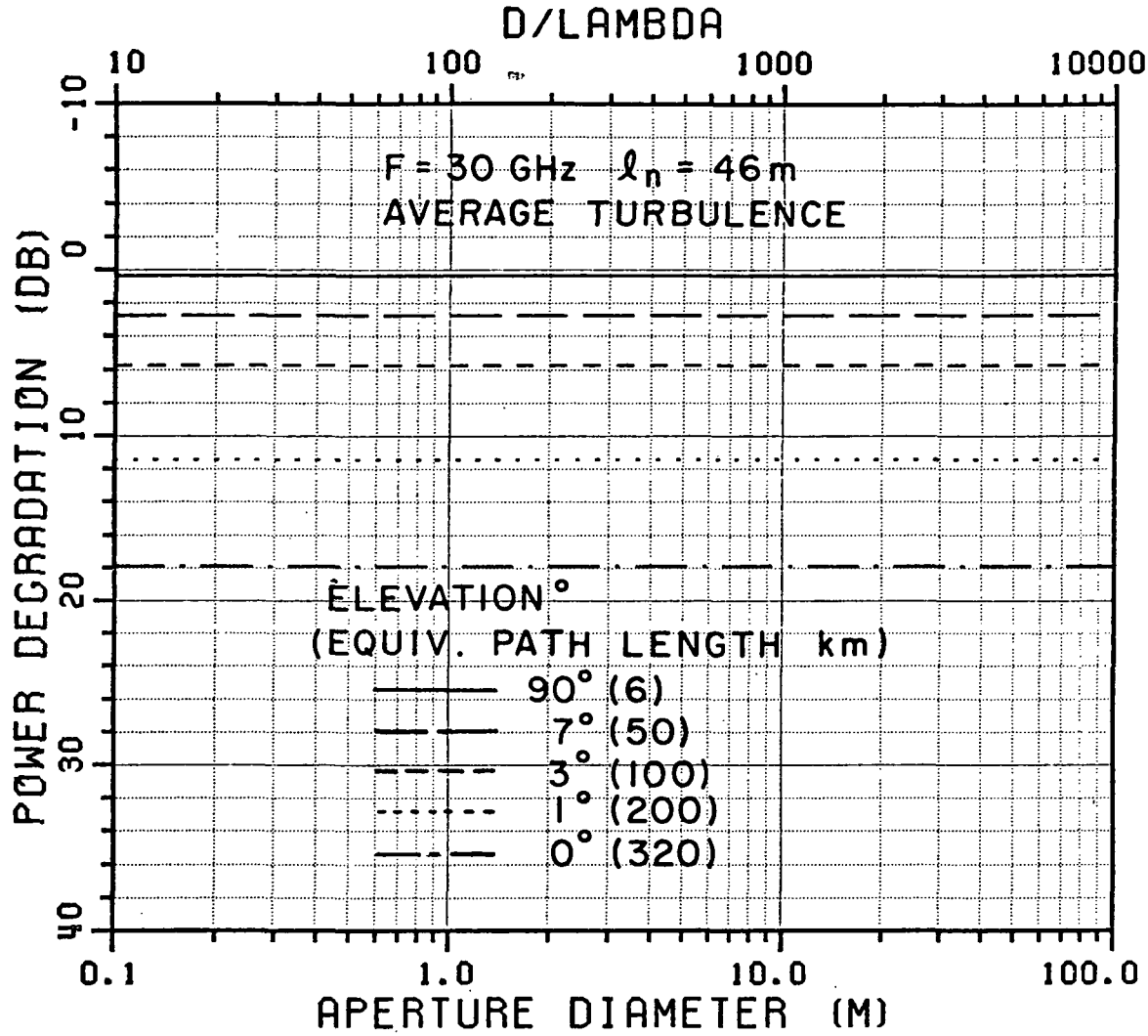

Figure 7.25. Dependence of the average received power on antenna aperture size at selected elevation angles in average turbulence, F=30 GHz; synchronous receiver. The equivalent path length is shown in parentheses.

7.5 Gain Degradation

The gain degradation, defined in Chapter 4.11, is examined briefly in this section under conditions of strong turbulence. Gain degradation has also been described as an 'aperture to medium coupling loss'. The gain is a measure of the total received power, i.e., the average as well as the fluctuating power is included in its definition. Gain degradation, hence, implies that some of the fluctuating power is not being added back into the output of the antenna. This can occur when the magnitude of the turbulence is such that some of the fluctuating power is scattered out of the beam of the antenna. Hence, a narrow beam antenna will suffer a greater gain degradation for a given degree of turbulence.

In contrast, it should be recalled that signal level degradation was defined as the reduction in only the dc component of the measured signal. It is affected by the type of receiver used as well. Gain degradation, however, is independent of the receiver system and depends on the size of the antenna and the characteristics of the turbulence only.

The frequency dependence of gain degradation is shown in Figure 7.26 with elevation angle, under conditions of strong turbulence. The aperture diameter is 4.5 meters. Figure 7.27 shows the aperture size dependence at 30 GHz, also under conditions of strong turbulence.

The aperture size dependence is displayed in a different format in Figure 7.28. The antenna gain is shown at 30 GHz as a function of elevation angle (or equivalent path length). A region of gain saturation is seen. Increasing the aperture size in this region does not result in an increase in gain. However, a further increase in size narrows the beam so much that almost none of the fluctuating power is captured by the antenna. Then the gain resumes its increase with aperture size, now receiving the coherent power in the wave only.

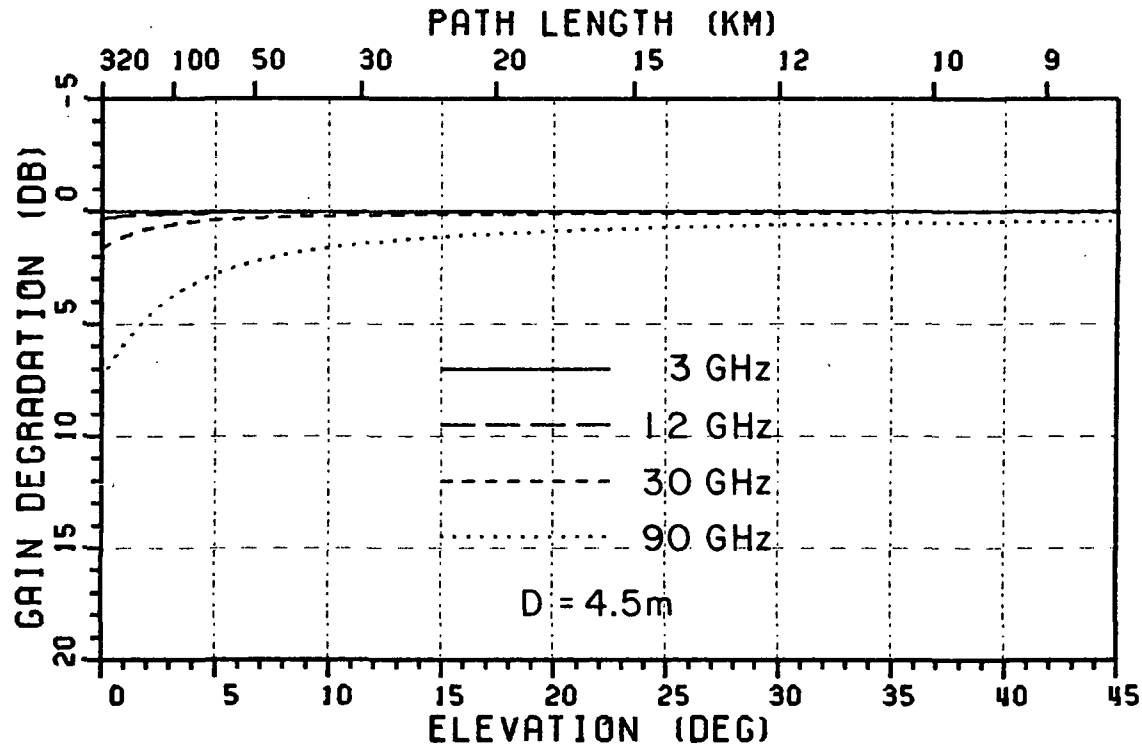

Figure 7.26. *Frequency dependence of antenna gain degradation, in maximum turbulence.*

$D = 4.5$ m; $\sigma_n^2 = 4.0 \times 10^{-12}$; $\ell_n = 10$ m.

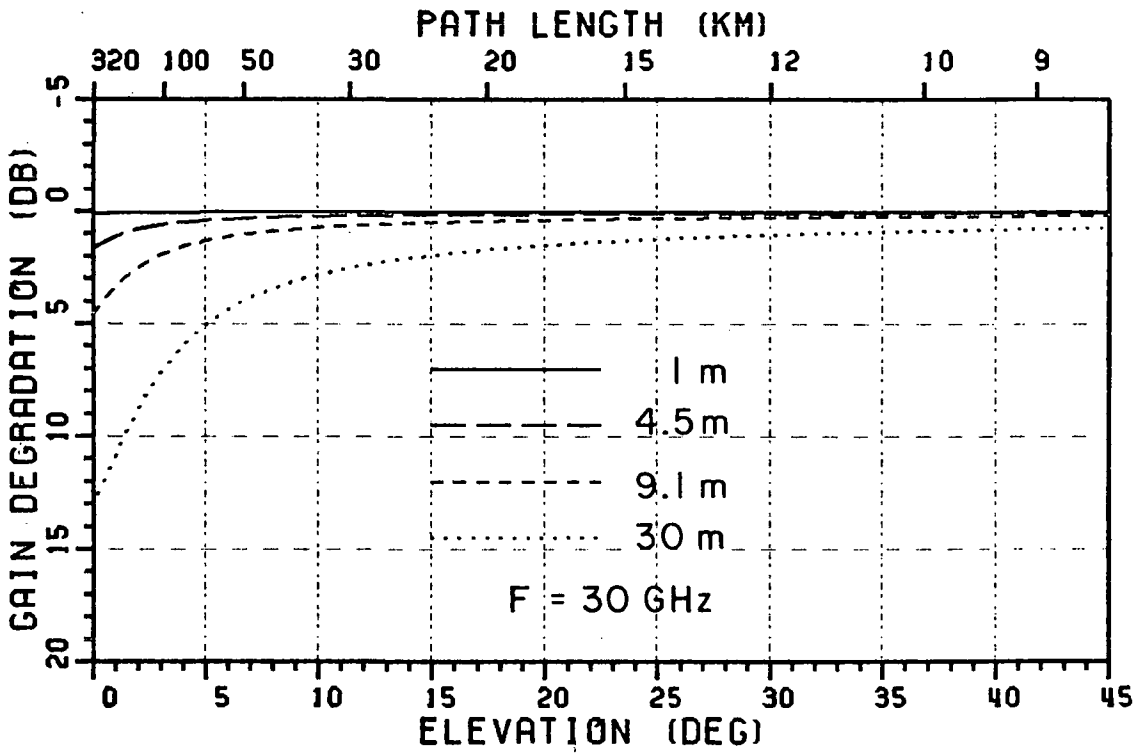

Figure 7.27. Aperture size dependence of antenna gain degradation in maximum turbulence.

F=30 GHz; $\sigma_n^2 = 4.0 \times 10^{-12}$; ℓ_n = 10 m.

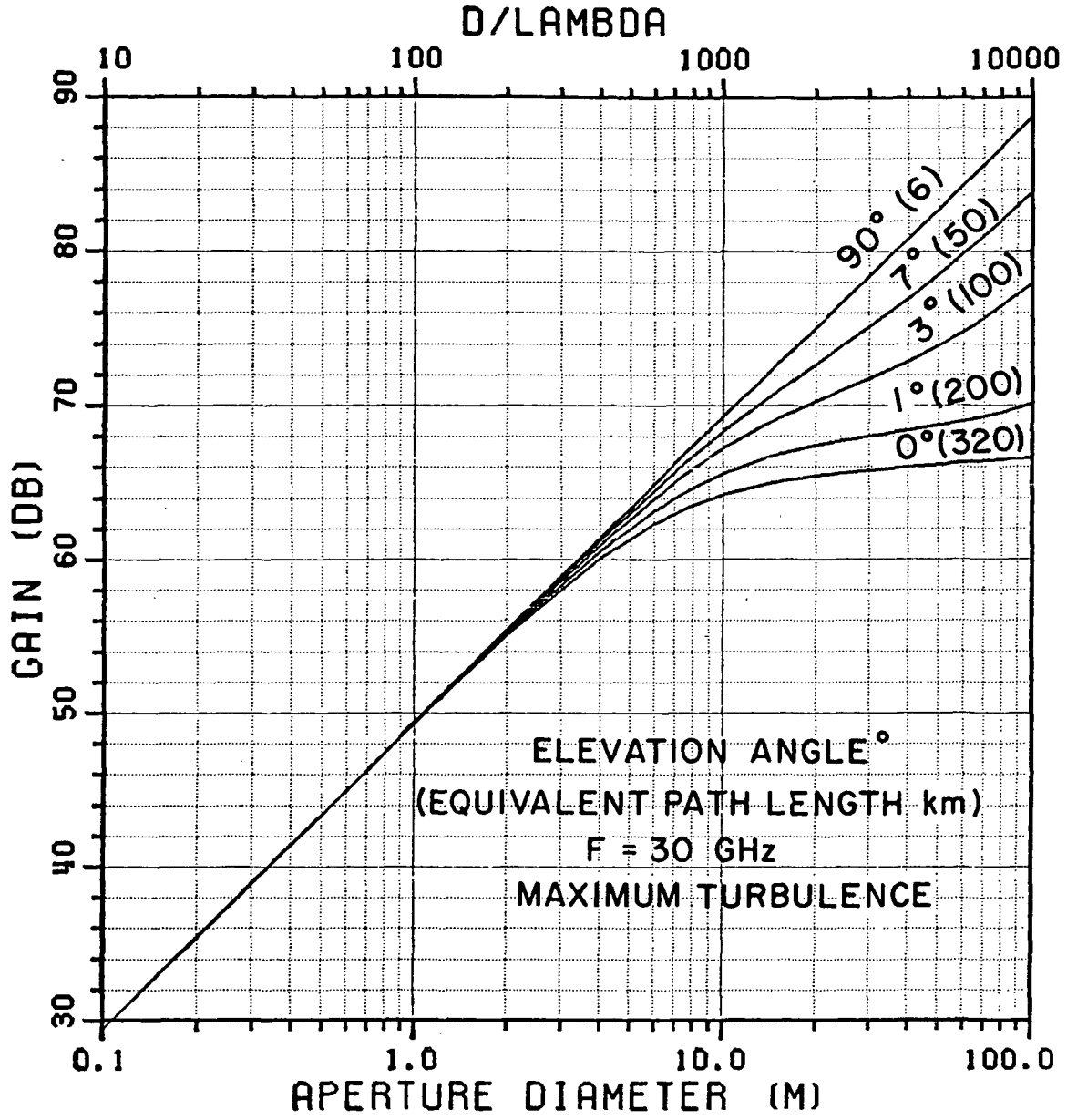

Figure 7.28. Dependence of antenna gain on aperture size, at selected elevation angles in maximum turbulence.

F=30 GHz; $\sigma_n^2 = 4.0 \times 10^{-12}$; $\ell_n = 10$ m.

The equivalent path length is shown in parentheses.

Figure 7.29 shows the same case as Figure 7.28, except that only the degradation is shown, instead of the total gain. Gain degradation in excess of 10 dB is possible, depending on the antenna size.

It must be reiterated that the results shown in this chapter should be used with caution. The Gaussian approximation to the Von Karman spectrum carries inherent inaccuracies. The expressions used may not be completely valid under conditions of strong turbulence. The results should be viewed primarily as illustrations of the processes taking place. However, the model permits at least an order of magnitude estimation of the effects of turbulence on the communications link. Its performance would be considerably better for predicting long term average behavior. In general, the use of numerical values should be combined with normal engineering practice, appropriate safety factors, and a healthy dose of skepticism!

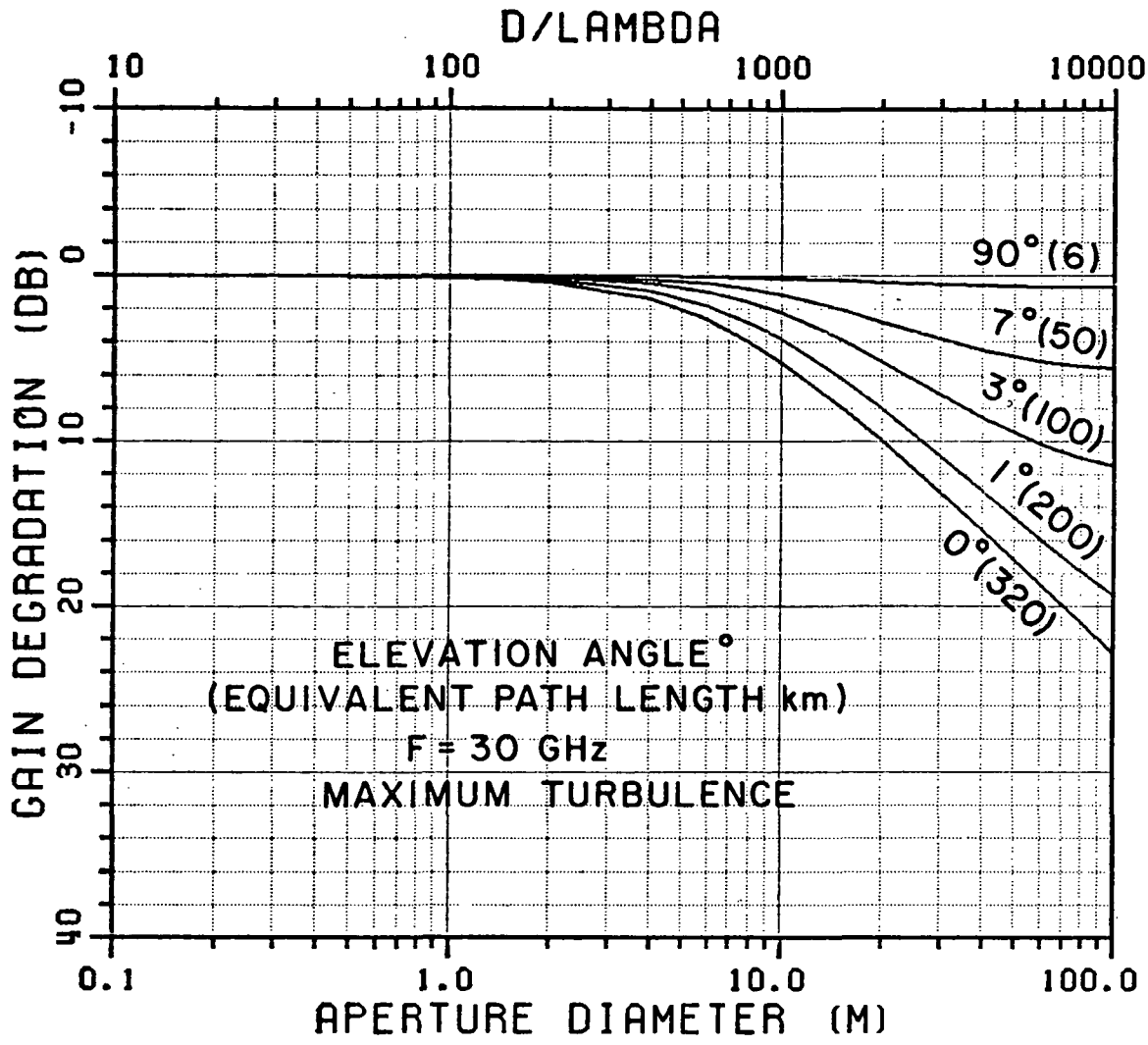

Figure 7.29. Dependence of antenna gain degradation on aperture size, at selected elevation angles, in maximum turbulence.

F=30 GHz; $\sigma_n^2 = 4.0 \times 10^{-12}$; $\ell_n = 10$ m.

The equivalent path length is shown in parentheses.

CHAPTER VIII

SUMMARY

The effects of atmospheric turbulence on microwave and millimeter wave communications systems, with special emphasis on satellite communications systems, has been examined.

A generalized theory of the receiving aperture antenna was first formulated. The results were extended to the case of an incident wave propagating through a turbulent medium.

The earth's atmosphere was considered next. The Von Karman model was discussed and approximated by the Gaussian spectrum. The behavior of the log amplitude and phase of a wave propagating through such an atmosphere were examined. Some new results were formulated for the correlation functions and variances of these statistical parameters.

The role of the receiver was studied next. It was shown that the effect of the receiver cannot be ignored in the presence of turbulence. The statistics of the received signal may be perceived very differently by the two general classes of receivers described as synchronous and asynchronous receivers, respectively. The total power, variance,

signal level and the degradation ofthe signal level measured by each of these receivers were then formulated. It was noted that the results for the synchronous receiver may also be used to study the field at the focal plane of a focusing antenna.

The particular case of the circular aperture was then considered. A complete result for the power received and the antenna gain was derived for both the uniform feed function and Gaussian tapered feed functions, provided the angle of arrival of the wave did not deviate significantly from the main beam. The particular case of on-axis incidence was studied in detail and some general characteristics of gain and gain degradation in turbulence were discussed. The Gaussian tapered aperture and the uniform aperture were shown to be simply related if the feed taper in the former is reasonably sharp.

Experimental results were next used to determine the numerical values of key parameters in the atmospheric model. It was shown that the atmosphere could be approximated by a uniform homogeneous isotropically turbulent atmosphere over the propagation path. Its equivalent height was found to be 6 km over an earth of effective radius equal to 4/3 the physical radius, or 8479 km. The variance of refractive index fluctuations of 0.4×10^{-12}, together with a correlation length of 46 meters, was found to be suitable for prediction of long term average behavior. The model adequately predicted link behavior over a frequency ratio of 15 to 1 and in different locations.

The link model was used to study signal variance, degradation of average power, and antenna gain degradation for frequencies from 3 GHz to 90 GHz and aperture diameters from 1 meter to 30 meters. The average power degradation indicates the reduction in the time average received signal level as measured by the receiving system. The gain degradation, on the other hand, is a measure of the reduction in the total power captured by the antenna. Their behavior was compared at the extremes of intensity of turbulence as well as for long term average values.

In general, the received signal variance increases with frequency. Its frequency dependence varies with the type of receiver used. The received power degradation also increases with frequency and changes with the type of receiver used. There is, however, no aperture size dependence of received power degradation when a synchronous receiver is used.

Regions of gain saturation are seen with large antennas. Examples of aperture averaging were also found when the antenna size and the Fresnel size of the propagation path were comparable to the scale size of the refractive index fluctuations.

It was shown that the synchronous receiver indicates a greater level of signal variance than the asynchronous receiver. Thus, the latter is preferable for communications links. However, the former should be preferably used to study atmospheric turbulence as its output contains phase as well as amplitude information. Care should also be taken to use the expressions appropriate to the particular receiver for evaluating signal level and variance.

Finally, the numerical results should be used with care and a clear understanding of the approximations involved. Normal engineering practice should be followed when applying the contents to system design.

APPENDIX A1

MODEL SUMMARY

A1.1 Field Quantities

The antenna aperture, S, lies in the x-y plane. $\overline{P} = (x,y)$ is any point on this surface. A plane wave incident on the turbulent atmosphere and travelling a distance L through it, reaches the aperture at a direction (θ,ϕ) with respect to the positive z axis.

Let

$$\overline{k}_s = (k_x,k_y) \ , \tag{A1.1.1}$$

where

$$k_x = k \sin\theta \cos\phi \tag{A1.1.2}$$

$$k_y = k \sin\theta \sin\phi \ . \tag{A1.1.3}$$

The incident field produces a random aperture field distribution

$$\tilde{\overline{E}}_r(\overline{P}) = \tilde{\overline{U}}(\overline{P})\ e^{-j\overline{k}_s\cdot\overline{P}} \tag{A1.1.4}$$

$$\tilde{U}(\overline{P}) = A_0\ e^{\tilde{\chi}(\overline{P})+j\tilde{\psi}(\overline{P})} \tag{A1.1.5}$$

$$\tilde{\overline{U}}(\overline{P}) = \hat{p}\,\tilde{U}(\overline{P}) \tag{A1.1.6}$$

χ = log amplitude

ψ = phase .

Let

$$U_0 = A_0\, e^{\chi_0+\sigma_\chi^2+j\sigma_\chi\sigma_\psi b_{\chi\psi}(\overline{P},\overline{P})} \tag{A1.1.7}$$

$$\chi_0 = \langle \chi \rangle \quad . \tag{A1.1.8}$$

The aperture illumination is described by the feed function $\overline{f}(\overline{P})$,

$$\overline{f}(\overline{P}) = \hat{p}_f\, f(\overline{P}) \quad . \tag{A1.1.9}$$

Both the polarization of the incident wave, $\hat{p}$, and the illumination, $\hat{p}_f$, are assumed to be independent of position at all times.

A1.2 The Atmosphere

The turbulence is homogeneous and isotropic over the path. The correlation function of the refractive index fluctuations is

$$b_n(\overline{P}_1,\overline{P}_2) = e^{\frac{-|\overline{P}_1-\overline{P}_2|^2/L_a^2}{C^2}} \tag{A1.2.1}$$

$C = \frac{\ell_n}{L_a}$ = The correlation ratio, is the correlation length of the turbulence, ℓ_n, normalized to a characteristic antenna dimension, L_a.

Also,

$$\sigma_\chi^2 = \frac{\sqrt{\pi}}{2} \sigma_n^2 \ell_n k^2 L \left[1 - \frac{\tan^{-1} W_g}{W_g}\right] \tag{A1.2.2}$$

$$\sigma_\psi^2 = \frac{\sqrt{\pi}}{2} \sigma_n^2 \ell_n k^2 L \left[1 + \frac{\tan^{-1} W_g}{W_g}\right] \tag{A1.2.3}$$

$$\sigma_w^2 = \sigma_\chi^2 + \sigma_\psi^2 \tag{A1.2.4}$$

$$= \sqrt{\pi}\, \sigma_n^2 \ell_n k^2 L \tag{A1.2.5}$$

$$\sigma_w^2(1 - b_n) = \sigma_\chi^2(1 - b_\chi) + \sigma_\psi^2(1 - b_\psi) \tag{A1.2.6}$$

$$W_g = \frac{4L}{k\ell_n^2} \quad , \tag{A1.2.7}$$

where

σ_n^2 = variance of atmospheric refracted index fluctuations.

σ_χ^2 = log amplitude variance.

σ_ψ^2 = phase variance.

σ_w^2 = wave variance.

W_g = Gaussian wave parameter.

b_χ = log amplitude correlation coefficient.

b_ψ = phase correlation coefficient.

Average Received Voltage

A1.3 Synchronous Receiver

$$< \tilde{V}_{syn} > = < \tilde{V}_r(\bar{k}_s) > = V_{d0}\, e^{-\frac{1}{2}\sigma_w^2}\, g_V(\bar{k}_s)\, \hat{p}\cdot\hat{p}_f \quad , \tag{A1.3.1}$$

where

$$g_V(\bar{k}_s) = \frac{I_V(\bar{k}_s)}{I_{V\ max}} \tag{A1.3.2}$$

is the voltage pattern function.

$$I_V(\bar{k}_s) = \int_S f(\bar{P})\, e^{-j\bar{k}_s\cdot\bar{P}}\, dS \tag{A1.3.3}$$

$$V_{d0} = U_0 K_V I_{V\ max}\, \hat{p}\cdot\hat{p}_f \quad . \tag{A1.3.4}$$

Asynchronous Receiver

$$\langle \tilde{V}_{asyn} \rangle = \langle |\tilde{V}_r(\bar{k}_s)| \rangle$$

$$= |V_{d0}||g_V(\bar{k}_s)| \left\{ \frac{1}{2}\left[1 + g_d\right] - \frac{1}{8}\left[1 - 2g_d + e^{4\sigma_x^2}\right] \right\} |\hat{p}\cdot\hat{p}_f| \quad . \tag{A1.3.5}$$

g_d is defined in (A1.4.3). It is the gain degradation factor.

A1.4 Total Received Power

$$P_R = P_{RO}\, g_0(\bar{k}_s) g_d\, |\hat{p}\cdot\hat{p}_f|^2 \quad , \tag{A1.4.1}$$

where

$$g_0(\bar{k}_s) = \left|g_V(\bar{k}_s)\right|^2 \tag{A1.4.2}$$

is the power pattern function.

$$g_d = e^{-\sigma_w^2} \frac{I_p(\bar{k}_s)}{I_{p0}(\bar{k}_s)} \tag{A1.4.3}$$

$$I_p(\bar{k}_s) = \iint_S \iint_S e^{\sigma_w^2 b_n(\bar{P}_1,\bar{P}_2)}\, f(\bar{P}_1) f(\bar{P}_2)^*\, e^{-j\bar{k}_s\cdot(\bar{P}_1-\bar{P}_2)}\, dS_1 dS_2 \tag{A1.4.4}$$

$$I_{PO}(\bar{k}_s) = \iint_S \iint_S f(\bar{P}_1) f(\bar{P}_2)^* \, e^{-j\bar{k}_s \cdot (\bar{P}_1 - \bar{P}_2)} \, dS_1 dS_2 \qquad \text{(A1.4.5)}$$

$$= |I_V(\bar{k}_s)|^2 \qquad \text{(A1.4.6)}$$

$$I_{PO\ max} = |I_V(\bar{k}_s)|^2_{max} \quad . \qquad \text{(A1.4.7)}$$

If the antenna is assumed to be matched to the load,

$$P_{RO} = \frac{|U_0 K_V I_{V\ max}\ \hat{p} \cdot \hat{p}_f|^2}{2|Z_1|^2} R_1 \qquad \text{(A1.4.8)}$$

is the power received on beam axis. Therefore,

$$P_{RO} = |\hat{p} \cdot \hat{p}_f|^2 \frac{|U_0|^2}{2\eta_0} A_{eO} \qquad \text{(A1.4.9)}$$

$$\frac{|U_0|^2}{2\eta_0} = \text{incident power density, } S_{inc} \ . \qquad \text{(A1.4.10)}$$

A_{eO} is given in (A1.7).

If we expand

$$e^{\sigma_w^2 b_n} = \sum_{m=0}^{\infty} \frac{(\sigma_w^2 b_n)^m}{m!} \quad , \tag{A1.4.11}$$

then

$$\frac{I_P(\bar{k}_s)}{I_{P0}(\bar{k}_s)} = \sum_{m=0}^{\infty} \frac{\sigma_w^{2m}}{m!} I_{Cm}(\bar{k}_s) \quad , \tag{A1.4.12}$$

where

$$I_{Cm}(\bar{k}_s) = \frac{I_{Pm}(\bar{k}_s)}{I_{P0}(\bar{k}_s)} \tag{A1.4.13}$$

$$I_{Pm}(\bar{k}_s) = \iint_S \iint_S b_n(\bar{P}_1,\bar{P}_2)^m \, f(\bar{P}_1) f(\bar{P}_2)^* \, e^{-j\bar{k}_s \cdot (\bar{P}_1 - \bar{P}_2)} \, dS_1 dS_2 \quad . \tag{A1.4.14}$$

Then

$$g_d = e^{-\sigma_w^2} \sum_{m=0}^{\infty} \frac{\sigma_w^{2m}}{m!} I_{Cm}(\bar{k}_s) \quad . \tag{A1.4.15}$$

$I_{Cm}(\bar{k}_s)$ is called the correlation integral across the aperture.

A1.5 Signal Variance

The signal variance is normalized to the measured dc power.

Synchronous Receiver

$$s^2_{syn} = \frac{< |\tilde{V}_r|^2 > - |< \tilde{V}_r >|^2}{|< \tilde{V}_r >|^2} \qquad \text{(A1.5.1)}$$

$$= e^{\sigma_w^2} g_d - 1 \qquad \text{(A1.5.2)}$$

$$s^2_{syn}dB = 10 \log_{10} s^2_{syn} \quad . \qquad \text{(A1.5.3)}$$

Using (A1.4.15) we may show that

$$s^2_{syn} = \sum_{m=1}^{\infty} \frac{\sigma_w^{2m}}{m!} I_{Cm}(\bar{k}_s) \quad . \qquad \text{(A1.5.4)}$$

Asynchronous Receiver

$$s^2_{asyn} = \frac{< |V_r|^2 > - < |V_r| >^2}{< |V_r| >^2} \qquad \text{(A1.5.5)}$$

$$s^2_{asyn} = \frac{g_d}{\left\{\frac{1}{2}(1 + g_d) - \frac{1}{8}(1 - 2g_d + e^{4\sigma_X^2})\right\}^2} - 1 \quad . \tag{A1.5.6}$$

A1.6 Average Signal Level Degradation

$$\Delta P_{dB} = 10 \log_{10} \frac{P_{dc}}{P_{dc}}\Bigg|_{\text{No fluctuations}} \quad . \tag{A1.6.1}$$

Synchronous Receiver

$$\Delta P_{dcs_{dB}} = 4.343 \, \sigma_w^2 \quad . \tag{A1.6.2}$$

Asynchronous Receiver

$$\Delta P_{dca_{dB}} = 10 \log_{10} \left\{\frac{1}{2}(1 + g_d) - \frac{1}{8}(1 - 2g_d + e^{4\sigma_X^2})\right\}^2 \quad . \tag{A1.6.3}$$

A1.7 Average Effective Aperture

The average effective aperture is

$$A_e(\bar{k}_s) = A_{e0} g_0(\bar{k}_s) g_d \quad , \tag{A1.7.1}$$

where

$$A_{e0} = |K_p|^2 \, I_{P0\ max} \tag{A1.7.2}$$

$$K_p = K_V \frac{\sqrt{\eta_0 R_1}}{|Z_1|} \quad . \tag{A1.7.3}$$

A_{e0} is the maximum effective aperture for the plane wave case.

A1.8 Average Directive Gain

The average directive gain is

$$G_d(\bar{k}_s) = G_{0\ max}\, g_0(\bar{k}_s) g_d \tag{A1.8.1}$$

$$G_{0\ max} = \frac{4\pi A_{e0}}{\lambda^2} \tag{A1.8.2}$$

$$= \frac{4\pi}{\lambda^2} |K_p|^2 \, I_{P0\ max} \quad . \tag{A1.8.3}$$

If

$$G_0(\bar{k}_s) = G_0 g_0(\bar{k}_s) \quad , \tag{A1.8.4}$$

then

$$G_d(\bar{k}_s) = G_0(\bar{k}_s) g_d \quad . \tag{A1.8.5}$$

$G_{0\ max}$ is the maximum directive gain for plane wave incidence. $G_0(\bar{k}_s)$ is the plane wave incidence power gain function. g_d is the gain degradation factor. Finally,

$$G_d(\bar{k}_s)_{dB} = G_0(\bar{k}_s)_{dB} + 10 \log_{10} g_d \quad . \tag{A1.8.6}$$

A1.9 Gain Degradation

The gain degradation is defined as

$$\Delta G(\bar{k}_s)_{dB} = G_0(\bar{k}_s)_{dB} - G_d(\bar{k}_s)_{dB} \quad . \tag{A1.9.1}$$

Therefore,

$$\Delta G(\bar{k}_s)_{dB} = -10 \log_{10} g_d \quad . \tag{A1.9.2}$$

If (A1.4.15) is used,

$$\Delta G(\bar{k}_s)_{dB} = -10 \log_{10} \left[e^{-\sigma_w^2} \sum_{m=0}^{\infty} \frac{\sigma_w^{2m}}{m!} I_{Cm}(\bar{k}_s) \right] \quad . \tag{A1.9.3}$$

APPENDIX A2

LOG AMPLITUDE AND PHASE CORRELATION

A2.1 Gaussian Spectrum

The Gaussian Spectrum is, (3.3.3),

$$\Phi_{ng}(\kappa) = \frac{\sigma_n^2 \ell_n^3}{8\pi\sqrt{\pi}} e^{-\frac{\kappa^2 \ell_n^2}{4}} .$$

From (3.5.2) - (3.5.4), in a transverse plane

$$B_{\chi,\psi}(\rho) = 2\pi^2 k^2 L \int_0^\infty f_{\chi,\psi}(\kappa)\Phi_{ng}(\kappa)J_0(\kappa\rho)\kappa\, d\kappa$$

$$= 2\pi^2 k^2 L \frac{\sigma_n^2 \ell_n^3}{8\pi\sqrt{\pi}} \int_0^\infty f_{\chi,\psi}(\kappa)\, e^{-\frac{\kappa^2 \ell_n^2}{4}} J_0(\kappa\rho)\kappa d\kappa$$

$$= \frac{\sqrt{\pi}}{4}\sigma_n^2 \ell_n^3 k^2 L \int_0^\infty \left[1 \mp \frac{\sin(\frac{\kappa^2 L}{k})}{\frac{\kappa^2 L}{k}}\right] e^{-\frac{\kappa^2 \ell_n^2}{4}} J_0(\kappa\rho)\kappa d\kappa .$$

The + sign is associated with $B_\psi(\rho)$ and the - sign with $B_\chi(\rho)$. Separating the integrals, the first integral is,

$$\int_0^\infty e^{-\frac{\kappa^2 \ell_n^2}{4}} J_0(\kappa\rho)\kappa d\kappa = \frac{2}{\ell_n^2} e^{-\frac{\rho^2}{\ell_n^2}} , \qquad \text{(A2.1.1)}$$

from [30], # 6.631.4.

The second integral is

$$\int_0^\infty \frac{\sin(\frac{\kappa^2 L}{k})}{\frac{\kappa^2 L}{k}} e^{-\frac{\kappa^2 \ell_n^2}{4}} J_0(\kappa\rho)\kappa d\kappa . \qquad \text{(A2.1.2)}$$

This is evaluated in Appendix B1.1 and is

$$= \frac{k}{2L} \sum_{m=0}^{\infty} \frac{1}{m!} \left[\frac{-\frac{\rho^2}{\ell_n^2}}{\sqrt{1 + \left(\frac{4L}{k\ell_n^2}\right)^2}} \right]^m \frac{\sin\left[m \tan^{-1}\left(\frac{4L}{k\ell_n^2}\right)\right]}{m} . \qquad \text{(A2.1.3)}$$

Combining (A2.1.1) and (A2.1.3), we have

$$\left.\begin{matrix} B_\chi(\rho) \\ B_\psi(\rho) \end{matrix}\right\} = \frac{\sqrt{\pi}}{2} \sigma_n^2 \ell_n k^2 L \left[e^{-\frac{\rho^2}{\ell_n^2}} \mp \frac{1}{W_g} \sum_{m=0}^{\infty} \frac{1}{m!} \left[\frac{-\frac{\rho^2}{\ell_n^2}}{\sqrt{1 + W_g^2}} \right]^m \frac{\sin\left[m \tan^{-1} W_g\right]}{m} \right]$$

(A2.1.4)

where

$$W_g = \frac{4L}{k\ell_n^2} \tag{A2.1.5}$$

is called the Gaussian wave parameter. We also define the wave correlation function as

$$B_w(\rho) = B_\chi(\rho) + B_\psi(\rho), \tag{A2.1.6}$$

therefore,

$$B_w(\rho) = \sqrt{\pi}\ \sigma_n^2 \ell_n k^2 L\ e^{-\frac{\rho^2}{\ell_n^2}} \quad . \tag{A2.1.7}$$

The Case of $\rho = 0$

From (A2.1.5) and (A2.1.8), the variances are

$$\sigma_\chi^2 = \frac{\sqrt{\pi}}{2}\ \sigma_n^2 \ell_n k^2 L \left[1 - \frac{\tan^{-1} W_g}{W_g}\right] \tag{A2.1.8a}$$

$$\sigma_\psi^2 = \frac{\sqrt{\pi}}{2}\ \sigma_n^2 \ell_n k^2 L \left[1 + \frac{\tan^{-1} W_g}{W_g}\right] \tag{A2.1.8b}$$

$$\sigma_w^2 = \sqrt{\pi}\ \sigma_n^2 \ell_n k^2 L \quad . \tag{A2.1.8c}$$

We note, finally, that if 'b' denotes the correlation coefficient, from (A2.1.6) and (A2.1.7),

$$\sigma_w^2 b_n(\rho) = \sigma_\chi^2 b_\chi(\rho) + \sigma_\psi^2 b_\psi(\rho) \quad . \tag{A2.1.9}$$

A2.2 Von Karman Spectrum

The Von Karman spectrum is

$$\Phi_{nV}(\kappa) = 0.033C_n^2(\kappa_L^2 + \kappa^2)^{-\frac{11}{6}} e^{-\frac{\kappa^2}{\kappa_m^2}} .$$

From (3.5.2) - (3.5.4)

$$B_{\chi,\psi}(\rho) = 2\pi^2 k^2 L \quad 0.033C_n^2 L_0^{\frac{11}{3}} \int_0^\infty \left[1 \mp \frac{\sin\left(\frac{\kappa^2 L}{k}\right)}{\left(\frac{\kappa^2 L}{k}\right)}\right]\left(1 + \frac{\kappa^2}{\kappa_L^2}\right)^{-\frac{11}{6}}$$

$$e^{-\frac{\kappa^2}{\kappa_m^2}} J_0(\kappa\rho)\kappa d\kappa .$$

Substituting $t = \frac{\kappa^2}{\kappa_L^2}$, and defining

$$Z_0 = \frac{\kappa_L^2}{\kappa_m^2} = \frac{1}{\kappa_m^2 L_0^2} \qquad \text{(A2.2.1)}$$

$$W_0 = \frac{\kappa_L^2 L}{k} = \frac{L}{kL_0^2} , \qquad \text{(A2.2.2)}$$

then

$$B_{\chi,\psi}(\rho) = 0.033\pi^2 C_n^2 L_0^{\frac{5}{3}} k^2 L \int_0^\infty \left[1 \mp \frac{\sin(W_0 t)}{W_0 t}\right] (1+t)^{-\frac{11}{6}} e^{-Z_0 t}$$

$$J_0(\kappa_L \rho \sqrt{t})\, dt \quad .$$

The integrals are evaluated separately. The first integral is

$$\int_0^\infty e^{-Z_0 t} (1+t)^{-\frac{11}{6}} J_0(\kappa_L \rho \sqrt{t})\, dt = \int_0^\infty e^{-Z_0 t}\, t^{\alpha-1} (1+t)^{\gamma-\alpha-1}$$

$$J_0(\kappa_L \rho \sqrt{t})\, dt \,, \qquad \text{(A2.2.3)}$$

where $\alpha = 1$, $\gamma = \frac{1}{6}$. This is evaluated in Appendix (B1.2.1) and is

$$= \sum_{p=0}^{\infty} \frac{(-1)^p}{(p!)^2} \left(\frac{\kappa_L \rho}{2}\right)^{2p} \Gamma(p+1)\Psi(p+1,\ p+\tfrac{1}{6},\ Z_0)$$

where Ψ is a degenerate hypergeometric function.

The second integral is

$$\int_0^\infty \frac{\sin(W_0 t)}{W_0 t} e^{-Z_0 t} (1+t)^{-\frac{11}{6}} J_0(\kappa_L \rho \sqrt{t})\, dt \quad .$$

Using $\sin(W_0 t) = Im\left\{e^{jW_0 t}\right\}$, we have

$$\frac{1}{W_0} Im\left\{\int_0^\infty e^{-(Z_0 - jW_0)t}\, t^{\alpha-1}\, (1+t)^{\gamma-\alpha-1}\, J_0(\kappa_L \rho\sqrt{t})\, dt\right\} \quad ,$$

where $\alpha = 0$, $\gamma = -\frac{5}{6}$. Let

$$Z = Z_0 - jW_0 \quad . \tag{A2.2.4}$$

Again, using (B1.2.1),

$$= \frac{1}{W_0} \sum_{p=0}^{\infty} \frac{(-1)^p}{(p!)^2} \left(\frac{\kappa_L \rho}{2}\right)^{2p} Im\left[\Gamma(p)\Psi(p,\ p+\gamma,\ Z)\right] \quad .$$

Applying Kummer's transformation [31] #13.1.29,

$$\Psi(a,b,Z) = Z^{1-b}\, \Psi(1+a-b,\ 2-b,\ Z)$$

and substituting $-\frac{5}{6}$ for γ, the integral becomes

$$\frac{1}{W_0} \sum_{p=0}^{\infty} \frac{(-1)^p}{(p!)^2} \left(\frac{\kappa_L \rho}{2}\right)^{2p} Im\left[\Gamma(p) Z^{\frac{11}{6}-p} \Psi(\tfrac{11}{6},\ \tfrac{17}{6}-p,\ Z)\right] .$$

Therefore,

$$\left.\begin{matrix} B_\chi(\rho) \\ B_\psi(\rho) \end{matrix}\right\} = 0.033\pi^2 C_n^2 L_0^{\frac{5}{3}} k^2 L \cdot \sum_{p=0}^{\infty} \frac{(-1)^p}{(p!)^2}\left(\frac{\rho}{2L_0}\right)^{2p} \cdot \left\{ \Gamma(p+1)\psi(p+1,\ p+\tfrac{1}{6}, Z_0) \right.$$

$$\left. \mp \frac{1}{W_0} Im\left[\Gamma(p) Z^{\frac{11}{6}-p} \psi(\tfrac{11}{6},\ \tfrac{17}{6}-p,\ Z)\right]\right\} , \qquad \text{(A2.2.5)}$$

where

$$Z = Z_0 - jW_0$$

$$Z_0 = \frac{1}{\kappa_m^2 L_0^2}$$

$$W_0 = \frac{L}{kL_0^2} \qquad \text{(A2.2.6a)}$$

$$W_m = \frac{W_0}{Z_0} = \frac{\kappa_m^2 L}{k} \quad . \qquad \text{(A2.2.6b)}$$

W_0 and W_m may be defined as wave parameters for the Von Karman spectrum Next, using (A2.1.6), the wave correlation function is

$$B_w(\rho) = 0.033(2\pi^2) C_n^2 L_0^{\frac{5}{3}} k^2 L \sum_{p=0}^{\infty} \frac{(-1)^p}{(p!)^2}\left(\frac{\rho}{2L}\right)^{2p} \Gamma(p+1)\psi(p+1,\ p+\tfrac{1}{6},\ Z_0).$$

For $\rho = 0$

Only the p = 0 term exists in (A2.2.5). Then, applying (B1.2.2) to the second degenerate hypergeometric function in (A2.2.5), we obtain

$$\left.\begin{matrix}\sigma_\chi^2 \\ \sigma_\psi^2\end{matrix}\right\} = 0.033\pi^2 C_n^2 L_0^{\frac{5}{3}} k^2 L \left\{ \Psi(1, \tfrac{1}{6}, Z_0) \mp \frac{1}{W_0} \, Im\left[Z^{\frac{11}{6}} \Gamma(-\tfrac{11}{6}) \Phi(\tfrac{11}{6}, \tfrac{11}{6}+1, Z) + \Gamma(0) \right] \right\} .$$

Now, since $\kappa_m L_0 \gg 1$, $Z_0 \to 0$. Hence, from [31] #13.5.10,

$$\Psi(a,b,Z_0) \to \frac{\Gamma(1-b)}{\Gamma(1+a-b)} \quad \text{as} \quad Z_0 \to 0 \qquad (0 < b < 1)$$

so that

$$\Psi(1, \tfrac{1}{6}, Z_0) \to \frac{6}{5} \quad . \tag{A2.2.7}$$

Note that $\Gamma(0)$ is pure real and, hence, drops out of the results. Performing the indicated substitutions and after some algebraic manipulations, we obtain the final solution,

$$\left.\begin{matrix}\sigma_\chi^2 \\ \sigma_\psi^2\end{matrix}\right\} = 0.033\pi^2 \, \frac{6}{5} \, C_n^2 L_0^{\frac{5}{3}} k^2 L \left\{ 1 \mp \Gamma(\tfrac{1}{6}) \, \frac{1}{W_0} \, Im\left[(-1)^{-\frac{11}{6}} \gamma(\tfrac{11}{6}, -Z_0 + jW_0) \right] \right\} \tag{A2.2.8}$$

$$\sigma_w^2 = 0.033\pi^2 \frac{12}{5} C_n^2 L_0^{\frac{5}{3}} k^2 L \quad . \tag{A2.2.9}$$

Once more, note that in general,

$$\sigma_\chi^2 b_{\chi\chi}(\rho) + \sigma_\psi^2 b_\psi(\rho) = \sigma_w^2 b_{nk}(\rho) \quad .$$

A2.3 Kolmogorov Spectrum

If the Kolmogorov spectrum (3.4.3),

$$\Phi_{nk}(\kappa) = 0.033 C_n^2 \kappa^{-\frac{11}{3}} e^{-\frac{\kappa^2}{\kappa_m^2}} ,$$

were used instead, a solution for σ_ψ^2 is not possible since the integrand is singular. However, σ_χ^2 may be obtained since $f_\chi(\kappa)$ is zero at the origin.

$$\sigma_\chi^2 = 0.033 C_n^2 (2\pi^2) k^2 L \int_0^\infty \left[1 - \frac{\sin\left(\frac{\kappa^2 L}{k}\right)}{\frac{\kappa^2 L}{k}} \right] e^{-\frac{\kappa^2}{\kappa_m^2}} \kappa^{\mu+1} \, d\kappa$$

$$\mu = -\frac{11}{3} \quad .$$

The first integral, from (B1.3.3), is

$$\frac{\Gamma(\frac{\mu}{2} + 1)}{2} (\kappa_m^2)^{\frac{\mu}{2}+1} \quad .$$

The second integral, from (B1.1.7) is

$$\frac{\Gamma(\frac{\mu}{2})(\kappa_m^2)^{\frac{\mu}{2}+1}}{2\ W_m(1+W_m^2)^{\frac{\mu}{4}}} \sin(\tfrac{\mu}{2}\tan^{-1}W_m)$$

where

$$W_m = \frac{\kappa_m^2 L}{k}$$

is the wave parameter for the Kolmogorov spectrum. Thus,

$$\int_0^\infty \left[1 - \frac{\sin(\frac{\kappa^2 L}{k})}{\frac{\kappa^2 L}{k}}\right] e^{-\frac{\kappa^2}{\kappa_m^2}} \kappa^{\mu+1}\, d\kappa$$

$$= \frac{\Gamma(\frac{\mu}{2}+1)}{2}\kappa_m^{\mu+2}\left[1 - \frac{2}{\mu(1+W_m^2)^{\frac{\mu}{4}}}\frac{\sin(\frac{\mu}{2}\tan^{-1}W_m)}{W_m}\right] \qquad \text{(A2.3.1)}$$

and

$$\sigma_\chi^2 = 0.033\pi^2\,\frac{6}{5}\,\Gamma(\tfrac{1}{6})C_n^2\kappa_m^{-\frac{5}{3}}k^2 L\left[\frac{6}{11}(1+W_m^2)^{\frac{11}{12}}\frac{\sin(\frac{11}{6}\tan^{-1}W_m)}{W_m} - 1\right].$$

(A2.3.2)

APPENDIX A3

MOMENTS OF THE RECEIVED SIGNAL

The assumptions implicit in this discussion are stated at the beginning of Section (3.8). The analysis presented in this appendix follows that of Shifrin [11].

Since it is assumed that the polarization vector of the incident wave does not vary with the position on the aperture, only the scalar components of the wave will be considered in the following.

A3.1 First Moment of the Aperture Field

As in (2.5.4),

$$\tilde{U}(\bar{P}) = A_0 \, e^{\tilde{\chi}(\bar{P})+j\tilde{\psi}(\bar{P})}$$

$$< \tilde{U}(\bar{P}) > = A_0 < e^{\tilde{\chi}(\bar{P})+j\tilde{\psi}(\bar{P})} > \quad . \tag{A3.1.1}$$

Chernov [4] has shown that, for a Gaussian turbulence spectrum, $\tilde{\chi}$ and $\tilde{\psi}$ are jointly normal. We may evaluate (A3.1.1) by the method of characteristic functions [32]. For a four-dimensional normal variable (x_1, x_2, x_3, x_4), the characteristic function is

$$g(t_1, t_2, t_3, t_4) = \langle e^{j(t_1x_1+t_2x_2+t_3x_3+t_4x_4)} \rangle$$

$$= e^{j\sum_{k=1}^{4} \langle x_k \rangle t_k - \frac{1}{2}\sum_{l=1}^{4}\sum_{k=1}^{4} \sigma_k\sigma_l b_{kl} t_k t_l}$$

(A3.1.2)

Let

$$x_1 = \tilde{\chi}(\overline{P}), \quad x_2 = \tilde{\psi}(\overline{P}).$$

Set

$$t_1 = -j. \qquad t_2 = 1.$$

Then

$$\langle \tilde{U}(\overline{P}) \rangle = A_0\, g(-j, 1, 0, 0)$$

$$= A_0\, e^{\chi_0(\overline{P})+\frac{1}{2}\left[\sigma_\chi^2(\overline{P})+2j\sigma_\chi(\overline{P})\sigma_\psi(\overline{P})b_{\chi\psi}(\overline{P},\overline{P})-\sigma_\psi^2(\overline{P})\right]}$$

where

$$\langle \tilde{\chi}(\overline{P}) \rangle = \chi_0(\overline{P})$$

$$\langle \tilde{\psi}(\overline{P}) \rangle = 0 \ . \qquad \text{(A3.1.3)}$$

The medium is homogeneous. Thus, no point on the aperture plane has statistical privilege. Hence,

$$< \tilde{\chi}(\bar{P}) > = \chi_0 \tag{A3.1.4a}$$

$$\sigma_\chi^2(\bar{P}) = \sigma_\chi^2 \tag{A3.1.4b}$$

$$\sigma_\psi^2(\bar{P}) = \sigma_\psi^2 \quad . \tag{A3.1.4c}$$

Therefore,

$$< \tilde{U}(\bar{P}) > = A_0 \, e^{\chi_0+\sigma_\chi^2 \, - \, \frac{1}{2}\left[\sigma_\chi^2+\sigma_\psi^2-2j\sigma_\chi\sigma_\psi \, b_{\chi\psi}(\bar{P},\bar{P})\right]} .$$

Let

$$U_0 = A_0 \, e^{\chi_0+\sigma_\chi^2+j\sigma_\chi\sigma_\psi b_{\chi\psi}(\bar{P},\bar{P})} \quad . \tag{A3.1.5}$$

Using (3.5.13b), we may then write

$$< \tilde{U}(\bar{P}) > = U_0 \, e^{-\frac{1}{2}\sigma_w^2} \quad . \tag{A3.1.6}$$

A3.2 Cross Moment of the Aperture Field

$$< \tilde{U}(\bar{P}_1) \, \tilde{U}(\bar{P}_2)^* > = A_0^2 \, < e^{\tilde{\chi}(\bar{P}_1)+\tilde{\chi}(\bar{P}_2)+j\left[\tilde{\psi}(\bar{P}_1)-\tilde{\psi}(\bar{P}_2)\right]} \tag{A3.2.1}$$

Again, using characteristic functions with

$$x_1 = \tilde{\chi}(\bar{P}_1),\ x_2 = \tilde{\chi}(\bar{P}_2),\ x_3 = \tilde{\psi}(\bar{P}_1).\ x_4 = \tilde{\psi}(\bar{P}_2)\ ,$$

we find that [32]

$$< \tilde{U}(\bar{P}_1)\ \tilde{U}(\bar{P}_2)^* > = A_0^2\ g(-j,\ -j,\ 1,\ -1)$$

$$= A_0\ e^{\chi_0(\bar{P}_1)+\chi_0(\bar{P}_2)\ -\ \frac{1}{2}\Delta_-}$$

where

$$\Delta_- = \sigma_{\psi_1}^2 + \sigma_{\psi_2}^2 - \sigma_{\chi_1}^2 - \sigma_{\chi_2}^2 - 2\sigma_{\chi_1}\sigma_{\chi_2}b_{\chi_1\chi_2} - 2j\sigma_{\chi_1}\sigma_{\psi_1}b_{\chi_1\psi_1} -$$

$$2j\sigma_{\chi_2}\sigma_{\psi_1}b_{\chi_2\psi_1} + 2j\sigma_{\chi_1}\sigma_{\psi_2}b_{\chi_1\psi_2} + 2j\sigma_{\chi_2}\sigma_{\psi_2}b_{\chi_2\psi_2} - 2\sigma_{\psi_1}\sigma_{\psi_2}b_{\psi_1\psi_2}\ .$$

The shorthand notation 1 and 2 for $\bar{P}_1$ and $\bar{P}_2$, respectively, has been adopted for convenience here. Fortunately, under the assumptions made in Section (3.8), this reduces to

$$\Delta_- = 2\left[\sigma_\psi^2 - \sigma_\chi^2 - \sigma_\chi^2 b_\chi(\bar{P}_1,\bar{P}_2) - \sigma_\psi^2 b_\psi(\bar{P}_1,\bar{P}_2)\right]\ .$$

Therefore,

$$< \tilde{U}(\bar{P}_1)\ \tilde{U}(\bar{P}_2)^* > = A_0\ e^{2\chi_0+\sigma_\chi^2}\ e^{-\left[\sigma_\chi^2(1-b_\chi(\bar{P}_1,\bar{P}_2)+\sigma_\psi^2(1-b_\psi(\bar{P}_1,\bar{P}_2))\right]}.$$

Using (3.5.13c), this reduces immediately to

$$< \tilde{U}(\bar{P}_1)\ \tilde{U}(\bar{P}_2)^* > = A_0\ e^{2\chi_0+2\sigma_\chi^2}\ e^{-\sigma_w^2(1-b_n(\bar{P}_1,\bar{P}_2))} \quad .$$

Finally, from (A3.1.5)

$$< \tilde{U}(\bar{P}_1)\ \tilde{U}(\bar{P}_2)^* > = |U_0|^2\ e^{-\sigma_w^2}\ e^{\sigma_w^2 b_n(\bar{P}_1,\bar{P}_2)} \quad . \qquad \text{(A3.2.2)}$$

APPENDIX A4

ASYNCHRONOUS RECEIVER CHARACTERISTICS

The fourth moment, dc power, and the variance of the signal voltage measured by an asynchronous amplitude modulation (AM) receiver will be evaluated in this appendix. The receiver will be assumed to incorporate a square law detector. It is, therefore, an envelope detector.

A4.1 The Fourth Moment of the Measured Voltage

We seek to evaluate the fourth moment of $|\tilde{V}_r|$. Using (4.1.4)

$$< |\tilde{V}_r|^4 > = |K_V|^4 \; |p \cdot p_f|^4 < \int_S \int_S A_0^2 \; e^{\chi_1 + \chi_2 + j(\psi_1 - \psi_2)} f_1 f_2^* \; e^{-j\bar{k}_s \cdot (\bar{P}_1 - \bar{P}_2)} dS_1 dS_2 \int_S \int_S A_0^2 \; e^{\chi_3 + \chi_4 + j(\psi_3 - \psi_4)} f_3 f_4^* \; e^{-j\bar{k}_s \cdot (\bar{P}_3 - \bar{P}_4)} dS_3 dS_4 > \qquad \text{(A4.1.1)}$$

where the notation χ_1, ψ_1, f_1 is used to represent $\tilde{\chi}(\bar{P}_1)$, $\tilde{\psi}(\bar{P}_1)$. $f(\bar{P}_1)$, etc. If the statistical expectation operator and the integrals are interchanged, we obtain

$$< |\tilde{V}_r|^4 > = |K_V|^4 \; |\hat{p}\cdot\hat{p}_f|^4 \; A_0^4 \int_S \int_S \int_S \int_S < e^{\chi_1+\chi_2+\chi_3+\chi_4+j(\psi_1-\psi_2+\psi_3-\psi_4)} >$$

$$f_1 f_2^* f_3 f_4^* \; e^{-j\bar{k}_s\cdot(\bar{P}_1-\bar{P}_2+\bar{P}_3-\bar{P}_4)} dS_1 dS_2 dS_3 dS_4 \; . \qquad \text{(A4.1.2)}$$

Since χ_i and ψ_i are Gaussian random variables, we use the method of characteristic functions as in Appendix A3,

$$g(t_1,t_2,t_3,t_4,t_5,t_6,t_7,t_8) = < e^{j\sum_{k=1}^{8} x_k t_k} >$$

$$= e^{j\sum_{k=1}^{8} <x_k> t_k - \frac{1}{2}\sum_{k=1}^{8}\sum_{k=1}^{8} \sigma_k \sigma_1 b_{k1} t_k t_1} \; . \qquad \text{(A4.1.3)}$$

Let

$$M = < e^{\chi_1+\chi_2+\chi_3+\chi_4+j(\psi_1-\psi_2+\psi_3-\psi_4)} > \; . \qquad \text{(A4.1.4)}$$

Assuming no statistical privilege, let

$$< \chi_k > = \chi_0 \qquad \text{(A4.1.5a)}$$

$$\sigma^2_{\chi_k} = \sigma^2_{\chi} \qquad \text{(A4.1.5b)}$$

$$< \psi_k > = 0 \qquad \text{(A4.1.5c)}$$

$$\sigma^2_{\psi_k} = \sigma^2_{\psi} \quad . \qquad \text{(A4.1.5d)}$$

We evaluate the function

$$M = g(-j,-j,-j,-j,1,-1,1,-1) \quad . \qquad \text{(A4.1.6)}$$

The first set of terms in the exponent is

$$j \sum_{k=1}^{8} < x_k > t_k = < x_1 > + < x_2 > + < x_3 > + < x_4 >$$

$$= 4 x_0 \; . \qquad \text{(A4.1.7)}$$

Let the second set of terms be written as

$$\Delta_1 = \sum_{k=1}^{8}\sum_{l=1}^{8} \sigma_k \sigma_l b_{kl} t_k t_l = -\sigma^2_{x_1} - \sigma^2_{x_2} - \sigma^2_{x_3} - \sigma^2_{x_4} + \sigma^2_{\psi_1} + \sigma^2_{\psi_2} + \sigma^2_{\psi_3} + \sigma^2_{\psi_4}$$

$$-2\Big[\sigma_{x_1}\sigma_{x_2} b_{x_1x_2} + \sigma_{x_1}\sigma_{x_3} b_{x_1x_3} + \sigma_{x_1}\sigma_{x_4} b_{x_1x_4} + \sigma_{x_2}\sigma_{x_3} b_{x_2x_3}$$

$$+ \sigma_{x_2}\sigma_{x_4} b_{x_2x_4} + \sigma_{x_3}\sigma_{x_4} b_{x_3x_4}\Big]$$

$$+2\Big[-\sigma_{\psi_1}\sigma_{\psi_2} b_{\psi_1\psi_2} + \sigma_{\psi_1}\sigma_{\psi_3} b_{\psi_1\psi_3} - \sigma_{\psi_1}\sigma_{\psi_4} b_{\psi_1\psi_4} - \sigma_{\psi_2}\sigma_{\psi_3} b_{\psi_2\psi_3}$$

$$+ \sigma_{\psi_2}\sigma_{\psi_4} b_{\psi_2\psi_4} - \sigma_{\psi_3}\sigma_{\psi_4} b_{\psi_3\psi_4}\Big]$$

$$+2j\Big[-\sigma_{x_1}\sigma_{\psi_1} b_{x_1\psi_1} + \sigma_{x_1}\sigma_{\psi_2} b_{x_1\psi_2} - \sigma_{x_1}\sigma_{\psi_3} b_{x_1\psi_3} + \sigma_{x_1}\sigma_{\psi_4} b_{x_1\psi_4}$$

$$-\sigma_{x_2}\sigma_{\psi_1} b_{x_2\psi_1} + \sigma_{x_2}\sigma_{\psi_2} b_{x_2\psi_2} - \sigma_{x_2}\sigma_{\psi_3} b_{x_2\psi_3} + \sigma_{x_2}\sigma_{\psi_4} b_{x_2\psi_4}$$

$$-\sigma_{x_3}\sigma_{\psi_1} b_{x_3\psi_1} + \sigma_{x_3}\sigma_{\psi_2} b_{x_3\psi_2} - \sigma_{x_3}\sigma_{\psi_3} b_{x_3\psi_3} + \sigma_{x_3}\sigma_{\psi_4} b_{x_3\psi_4}$$

$$-\sigma_{x_4}\sigma_{\psi_1} b_{x_4\psi_1} + \sigma_{x_4}\sigma_{\psi_2} b_{x_4\psi_2} - \sigma_{x_4}\sigma_{\psi_3} b_{x_4\psi_3} + \sigma_{x_4}\sigma_{\psi_4} b_{x_4\psi_4}\Big] . \quad \text{(A4.1.8)}$$

The assumption has been made in the above that

$$b_{\chi_k\psi_l} = b_{\chi_l\psi_k}$$

for any pair k,l. After simplifying and using (A4.1.5), this reduces to give

$$-\tfrac{1}{2}\Delta_1 = 2\sigma_\chi^2 - 2\sigma_\psi^2 + \sigma_\chi^2\left[b_{\chi_1\chi_2} + b_{\chi_1\chi_3} + b_{\chi_1\chi_4} + b_{\chi_2\chi_3} + b_{\chi_2\chi_4}\right.$$

$$\left. + b_{\chi_3\chi_4}\right] + \sigma_\psi^2\left[b_{\psi_1\psi_2} - b_{\psi_1\psi_3} + b_{\psi_1\psi_4} + b_{\psi_2\psi_3} - b_{\psi_2\psi_4}\right.$$

$$\left. + b_{\psi_3\psi_4}\right] + 2j\sigma_\chi\sigma_\psi\left[b_{\chi_1\psi_3} - b_{\chi_2\psi_4}\right] \quad . \qquad \text{(A4.1.9)}$$

Combining the two sets of terms (A4.1.7) and (A4.1.9) and using the set of relationships (3.5.13), we get

$$M = \langle e^{\chi_1+\chi_2+\chi_3+\chi_4+j(\psi_1-\psi_2+\psi_3-\psi_4)} \rangle = e^{4\chi_0+4\sigma_\chi^2}\, e^{-\sigma_w^2(1-b_{n_1n_2})}$$

$$e^{-\sigma_w^2(1-b_{n_3n_4})}\, e^{\sigma_\chi^2(b_{\chi_1\chi_3}+b_{\chi_1\chi_4}+b_{\chi_2\chi_3}+b_{\chi_2\chi_4})}$$

$$e^{\sigma_\psi^2(b_{\psi_1\psi_4}-b_{\psi_1\psi_3}+b_{\psi_2\psi_3}-b_{\psi_2\psi_4})}\, e^{2j\sigma_\chi\sigma_\psi(b_{\chi_1\psi_3}-b_{\chi_2\psi_4})} \quad . \qquad \text{(A4.1.10)}$$

Clearly, the evaluation of (A4.1.2) using (A4.1.10) is impractical, if not impossible. Simplifying assumptions need to be made to obtain meaningful results for $\langle|\tilde{V}_r|^4\rangle$.

We assume that the correlation of the refractive index is very high over the aperture of the antenna. Thus, if b_n tends to 1, then the log amplitude correlation coefficients $b_{\chi_k\chi_l}$ become approximately equal to each other, as do the phase correlation coefficients $b_{\psi_k\psi_l}$. The cross correlation coefficients $b_{\chi_1\psi_3}$ and $b_{\chi_2\psi_4}$ also approach each other. Consequently, under these assumptions

$$M \approx e^{4\chi_0+4\sigma_\chi^2} e^{4\sigma_\chi^2} . \qquad \text{(A4.1.11)}$$

Using this in (A4.1.2) and using (3.8.1) gives

$$\langle |\tilde{V}_r|^4 \rangle \approx |U_0|^4 \, |K_V|^4 \, |\mathbf{p}\cdot\mathbf{p}_f|^4 \, e^{4\sigma_\chi^2} \int_S\int_S\int_S\int_S f_1 f_2^* \, e^{-j\bar{k}_s\cdot(\bar{P}_1-\bar{P}_2)}$$

$$f_3 f_4^* \, e^{-j\bar{k}_s\cdot(\bar{P}_3-\bar{P}_4)} \, dS_1 dS_2 dS_3 dS_4$$

which may be reduced, by using the definitions in Sections (4.2) and (4.3) to give

$$\langle |\tilde{V}_r|^4 \rangle = |V_{d0}|^4 \, |g_V(\bar{k}_s)|^4 \, |\hat{\mathbf{p}}\cdot\hat{\mathbf{p}}_f|^4 \, e^{4\sigma_\chi^2} . \qquad \text{(A4.1.12)}$$

Finally, it is easily shown, using (A4.1.12) that

$$\frac{<|\tilde{V}_r|^4>}{2|Z_1|^2} R_1 = P_{RO}^2 \, g_0(\bar{k}_s)^2 \, |p \cdot p|^4 \, e^{4\sigma_X^2} \quad . \tag{A4.1.13}$$

A4.2 Signal Level

The dc power measured by an asynchronous receiver assuming a matched antenna load is

$$P_{dca} = \frac{<\tilde{V}_{asyn}>^2}{2|Z_1|^2} R_1 \tag{A4.2.1}$$

$$= \frac{<|\tilde{V}_r|>^2}{2|Z_1|^2} R_1$$

$$= <\sqrt{\frac{|\tilde{V}_r|^2}{2|Z_1|^2} R_1}>^2 \quad .$$

The square law detector precludes the measurement of $|\tilde{V}_r|$ directly. Also, the total power is (4.3.9),

$$P_R = P_{RO} \, g_0(\bar{k}_s) \, g_d \, |\hat{p} \cdot \hat{p}_f|^2$$

$$= P_0 \, g_d \quad , \tag{A4.2.2}$$

where

$$P_0 = P_{R0}\, g_0(\bar{k}_s) \quad . \tag{A4.2.3}$$

The arguments have been dropped for convenience. Then

$$\frac{P_{dca}}{P_0} = \left\langle \sqrt{\frac{|\tilde{V}_r|^2 R_1}{2|Z_1|^2}} \right\rangle^2 \quad .$$

For small fluctuations,

$$\frac{P_{dca}}{P_0} \approx 1 \quad .$$

From Taylor's theorem, for x near 1,

$$x^{\frac{1}{2}} \approx 1 + \frac{(x-1)}{2} - \frac{1}{4}\frac{(x-1)^2}{2!}$$

$$= \frac{1}{2}(1+x) - \frac{1}{8}(1-2x+x^2) \qquad x \approx 1 \quad . \tag{A4.2.4}$$

Therefore,

$$< \sqrt{\frac{|\tilde{V}_r|^2 R_1}{P_0|Z_1|^2}} > \approx \frac{1}{2}\left[1 + \frac{< |\tilde{V}_r|^2 R_1>}{P_0|Z_1|^2}\right] - \frac{1}{8}\left[1 - \frac{2 < |\tilde{V}_r|^2 R_1 >}{P_0|Z_1|^2} + \frac{< |\tilde{V}_r|^4 R_1^2 >}{P_0^2|Z_1|^4}\right] . \quad \text{(A4.2.5)}$$

Squaring both sides and using (A4.1.13), we obtain

$$P_{dca} \approx P_{R0} g_0(\bar{k}_s) \left\{\frac{1}{2}(1+g_d) - \frac{1}{8}(1-2g_d+e^{4\sigma_\chi^2})\right\}^2 |\hat{p}\cdot\hat{p}_f|^2 . \quad \text{(A4.2.6)}$$

Finally, taking the square root and simplifying this gives

$$< \tilde{V}_{asyn} > \approx |V_{d0}|\ |g_V(\bar{k}_s)| \left\{\frac{1}{2}(1+g_d) - \frac{1}{8}(1-2g_d+e^{4\sigma_\chi^2})\right\} |\hat{p}\cdot\hat{p}_f| . \quad \text{(A4.2.7)}$$

A4.3 Variance

From (4.1.8), the normalized variance measured by an asynchronous receiver may be written as

$$s^2_{asyn} = \frac{P_R - P_{dca}}{P_{dca}} = \frac{P_R}{P_{dca}} - 1 . \quad \text{(A4.3.1)}$$

Substituting from (4.3.8) and (A4.2.6), we obtain

$$s^2_{asyn} = \frac{g_d}{\left\{\frac{1}{2}(1+g_d) - \frac{1}{8}(1-2g_d+e^{4\sigma^2_\chi})\right\}^2} - 1 \,. \qquad \text{(A4.3.2)}$$

APPENDIX A5

EVALUATION OF THE CIRCULAR APERTURE

Uniform Illumination

The uniform aperture illumination function: $f(\bar{R}) = 1$.

A5.1 The Voltage Gain Function $g_V(\Theta)$

The integral I_V, from (4.2.3), becomes

$$I_V = a^2 \int_0^1 \int_0^{2\pi} e^{j\Theta R\cos(\xi-\phi')} R\,d\xi\,dR = 2\pi a^2 \int_0^1 J_0(\Theta R)\, R\,dR \ .$$

From [30] #6.561.5,

$$\int_0^1 x^{\nu+1} J_\nu(ax)\,dx = \frac{J_{\nu+1}(a)}{a} \ .$$

Therefore,

$$I_V(\theta) = A_{phys} \frac{2J_1(\theta)}{\theta} , \qquad \text{(A5.1.1)}$$

where

$$A_{phys} = \pi a^2$$

is the physical area of the aperture.

$$I_{V\ max} = A_{phys} . \qquad \text{(A5.1.2)}$$

Hence,

$$g_V(\theta) = \frac{2J_1(\theta)}{\theta} . \qquad \text{(A5.1.3)}$$

The normalized power gain pattern function is

$$g_0(\theta) = \left\{ \frac{2J_1(\theta)}{\theta} \right\}^2 . \qquad \text{(A5.1.4)}$$

A5.2 The Integral $I_C(C,\theta)$

From (4.3.10) - (4.3.13),

$$I(C,\theta,\phi) = a^4 \int_S \int_S e^{-\frac{1}{C^2}(R_1^2+R_2^2-2R_1R_2\cos(\xi_1-\xi_2)} e^{j\Theta R_1\cos(\xi_1-\phi)}$$

$$e^{-j\Theta R_2\cos(\xi_2-\phi)} R_1R_2 d\xi_1 dR_1 d\xi_2 dR_2 \quad .$$

Using the power series expansion for the exponential

$$I(C,\theta,\phi) = a^4 \sum_{p=0}^{\infty} \left(\frac{2}{C^2}\right)^p \frac{1}{p!} \int_S \int_S \cos^p(\xi_1-\xi_2)(R_1R_2)^p e^{-\frac{R_1^2+R_2^2}{C^2}}$$

$$e^{j\Theta R_1\cos(\xi_1-\phi)} e^{-j\Theta R_2\cos(\xi_2-\phi)} R_1R_2 d\xi_1 dR_1 d\xi_2 dR_2 \quad .$$

Now

$$\cos^p(\xi_1-\xi_2) = \frac{1}{2^p} \sum_{q=0}^{p} \binom{p}{q} \cos\left\{(p-2q)(\xi_1-\xi_2)\right\} .$$

Considering the ξ integrals only,

$$Q = \int_{-\pi}^{\pi}\int_{-\pi}^{\pi} \left[\cos(p-2q)\xi_1 \cos(p-2q)\xi_2 + \sin(p-2q)\xi_1 \sin(p-2q)\xi_2\right]$$

$$e^{j\theta R_1\cos(\xi_1-\phi)} e^{-j\theta R_2\cos(\xi_2-\phi)} d\xi_1 d\xi_2 \quad ,$$

but

$$\int_{-\pi}^{\pi} \sin(p-2q)\xi \; e^{\pm j\theta R\cos(\xi-\phi)} d\xi = 0$$

so that

$$Q = \int_{-\pi}^{\pi} \cos(p-2q)\xi_1 \; e^{j\theta R_1\cos(\xi_1-\phi)} d\xi_1 \int_{-\pi}^{\pi} \cos(p-2q)\xi_2$$

$$e^{-j\theta R_2\cos(\xi_2-\phi)} d\xi_2 \; .$$

From [30] #3.915.2

$$\int_0^{\pi} e^{jb\cos x} \cos nx dx = j^n \pi J_n(b) \; ,$$

therefore,

$$Q = (-1)^{p-2q} 4\pi^2 J_{p-2q}(\Theta R_1) J_{p-2q}(-\Theta R_2)$$

but

$$J_n(-x) = (-1)^n J_n(x) \quad ,$$

thus

$$Q = 4\pi^2 J_{p-2q}(\Theta R_1) J_{p-2q}(\Theta R_2)$$

and is independent of ϕ. Then

$$I(C,\Theta) = 4A_{phys}^2 \sum_{p=0}^{\infty} \left(\frac{1}{C^2}\right)^p \frac{1}{p!} \sum_{q=0}^{p} \binom{p}{q} \int_0^1 e^{-\frac{R_1^2}{C^2}} R_1^{p+1} J_{p-2q}(\Theta R_1) dR_1$$

$$\int_0^1 e^{-\frac{R_2^2}{C^2}} R_2^{p+1} J_{p-2q}(\Theta R_2) dR_2 \quad .$$

Hence,

$$\frac{I(C,\Theta)}{I_{PO}(\Theta)} = I_C(C,\Theta) = \frac{4}{g_o(\Theta)} \sum_{p=0}^{\infty} \left(\frac{1}{C^2}\right)^p \frac{1}{p!} \sum_{q=0}^{p} \binom{p}{q} \cdot$$

$$\left\{ \int_0^1 e^{-\frac{R^2}{C^2}} R^{p+1} J_{p-2q}(\Theta R) dR \right\}^2 \quad . \tag{A5.2.1}$$

Define

$$Q_p = \int_0^1 e^{-\frac{R^2}{C^2}} R^{p+1} J_{p-2q}(\Theta R) dR \quad . \tag{A5.2.2}$$

From Appendix (B2.1.2), using

$$\nu = p-2q \tag{A5.2.3}$$

$$\mu = 2t+p+1 \quad . \tag{A5.2.4}$$

Let

$$Q_p = \frac{C^{p+2}}{2} Q_C(C,\Theta) \tag{A5.2.5}$$

and

$$\delta_C = \frac{C\Theta}{2} \quad , \tag{A5.2.6}$$

where

$$Q_C(C,\Theta) = \sum_{t=0}^{\infty} \frac{(-1)^t}{t!} \frac{1}{\delta_C^{\mu+1}} \left[\frac{(\nu+\mu-1)}{2^\mu} \Theta J_\nu(\Theta) S_{\mu-1,\nu-1} \right.$$

$$\left. -\frac{1}{2^\mu} \Theta J_{\nu-1}(\Theta) S_{\mu,\nu}(\Theta) + \frac{\Gamma(\frac{\nu+\mu+1}{2})}{\Gamma(\frac{\nu-\mu+1}{2})} \right] . \qquad \text{(A5.2.6)}$$

Therefore,

$$I_C(C,\Theta) = \frac{C^4}{g_0(\Theta)} \sum_{p=0}^{\infty} \sum_{q=0}^{p} \binom{p}{q} \frac{Q_C(C,\Theta)^2}{p!} . \qquad \text{(A5.2.7)}$$

A5.3 On-Axis Incidence

For the special case of $\Theta = 0$,

$$g_V(0) = 1 \qquad \text{(A5.3.1)}$$

$$g_0(0) = 1 \quad . \qquad \text{(A5.3.2)}$$

$I_C(C,0)$ is non-zero only if $Q_C(C,0)$ is non-zero. From (A5.2.1) and (A5.2.6) with

$$p-2q = 0$$

$$Q_C(C,0) = \gamma(q+1, \frac{1}{C^2}) \quad .$$

From (A5.2.7)

$$I_C(C,0) = C^4 \sum_{2q=0}^{\infty} \frac{1}{(2q)!} \binom{2q}{q} \left\{ \gamma\left(q+1, \frac{1}{C^2}\right) \right\}^2$$

so that

$$I_C(C,0) = \sum_{p=0}^{\infty} \left\{ \frac{C^2}{p!}\, \gamma\left(p+1, \frac{1}{C^2}\right) \right\}^2 . \qquad (A5.3.3)$$

APPENDIX A6

EVALUATION OF THE CIRCULAR APERTURE

Gaussian Illumination

The Gaussian aperture illumination function: $f(\bar{R}) = e^{-\frac{R^2}{\tau^2}}$.

A6.1 The Voltage Gain Function $g_V(\Theta)$

The integral I_V, from (4.2.3) becomes

$$I_V = a^2 \int_0^1 \int_0^{2\pi} e^{-\frac{R^2}{\tau^2}} e^{j\Theta R\cos(\xi-\phi)} R d\xi dr$$

$$= 2\pi a^2 \int_0^1 e^{-\frac{R^2}{\tau^2}} J_0(\Theta R) R dR .$$

Using the results of Appendix B2.1, substituting τ for C, $n=\nu=0$ and $\delta_\tau = \frac{\tau\Theta}{2}$,

$$I_V(\Theta) = 2A_{phys}\frac{\tau^2}{2}\sum_{m=0}^{\infty}\frac{(-1)^m}{m!}\left(\frac{1}{\delta_\tau}\right)^{2m+1}\left[\frac{m}{2^{2m}}\Theta J_0(\Theta)S_{2m,-1}(\Theta)\right.$$

$$\left.+\frac{1}{2^{2m+1}}\Theta J_1(\Theta)S_{2m+1,0}(\Theta)\right]. \qquad \text{(A6.1.1b)}$$

Using (B1.3.2), when $\Theta = 0$,

$$I_{V\ max} = A_{phys}\tau^2\left[1 - e^{-\frac{1}{\tau^2}}\right], \qquad \text{(A6.1.2a)}$$

therefore,

$$g_V(\Theta) = \frac{1}{1 - e^{-\frac{1}{\tau^2}}}\sum_{m=0}^{\infty}\frac{(-1)^m}{m!}\left(\frac{1}{\delta_\tau^2}\right)^{m+1}\left[\frac{m}{2^{2m}}\Theta J_0(\Theta)S_{2m,-1}(\Theta)\right.$$

$$\left.+\frac{1}{2^{2m+1}}\Theta J_1(\Theta)S_{2m+1,0}(\Theta)\right] \qquad \text{(A6.1.3a)}$$

$$I_{PO\ max} = \left\{A_{phys}\tau^2\left[1 - e^{-\frac{1}{\tau^2}}\right]\right\}^2. \qquad \text{(A6.1.4a)}$$

The Case of Small τ

If the aperture taper constant τ is small, so that the illumination beyond the edge of the aperture is small, the integrals may be taken to infinity with small error. Then, using [30] #6.631.4

$$I_V(\Theta) = A_{phys}\tau^2 \, e^{-\delta_\tau^2} \tag{A6.1.1b}$$

$$I_{V\ max} = A_{phys}\tau^2 \tag{A6.1.2b}$$

$$g_V(\Theta) = e^{-\delta_\tau} = e^{-\frac{\tau^2\Theta^2}{4}} \quad . \tag{A6.1.3b}$$

A6.2 The Integral $I_\gamma(C,\Theta)$

From (4.3.12), let

$$I(C,\tau,\Theta,\phi) = a^4 \int_S \int_S e^{-\frac{R_1^2}{\tau^2}} e^{-\frac{R_2^2}{\tau^2}} e^{-\frac{1}{C^2}(R_1^2+R_2^2-2R_1R_2\cos(\xi_1-\xi_2))}$$

$$e^{j\Theta R_1\cos(\xi_1-\phi)} \, e^{-j\Theta R_2\cos(\xi_2-\phi)} \, R_1R_2dR_1dR_2d\xi_1d\xi_2 \quad .$$

Defining

$$\frac{1}{\tau^2} + \frac{1}{C^2} = \frac{1}{\gamma^2}$$

and performing the ξ integrals gives

$$I(C,\tau,\Theta) = 4A_{phys}^2 \sum_{p=0}^{\infty} \left(\frac{1}{C^2}\right)^p \frac{1}{p!} \sum_{q=0}^{p} \binom{p}{q} Q_{p\gamma}^2 \qquad \text{(A6.2.1)}$$

$$Q_{p\gamma} = \int_0^1 e^{-\frac{R^2}{\gamma^2}} R^{p+1} J_{p-2q}(\Theta R)\, dR \quad . \qquad \text{(A6.2.2)}$$

Again, using (B2.1.2), and the results of A5.2,

$$\nu = p-2q \qquad \text{(A6.2.3)}$$

$$\mu = 2t+p+1 \qquad \text{(A6.2.4)}$$

Let

$$Q_{p\gamma} = \frac{\gamma^{p+2}}{2} Q_C(\gamma,\Theta) \qquad \text{(A6.2.5)}$$

$$\delta_\gamma = \frac{\gamma\Theta}{2} \quad , \qquad \text{(A6.2.6)}$$

where $Q_C(\gamma,\Theta)$ is the identical to (A5.2.6) with γ substituted for C and δ_γ for δ_C.

Hence,

$$\frac{I(C,\tau,\theta)}{I_{P0}(\theta)} = I_\gamma(C,\theta) = \frac{\left(\frac{\gamma}{\tau}\right)^4}{g_0(\theta)\left[1-e^{-\frac{1}{\tau^2}}\right]^2} \sum_{p=0}^{\infty}\left(\frac{\gamma^2}{C^2}\right)^p \sum_{q=0}^{p}\binom{p}{q}\frac{Q_C(\gamma,\theta)^2}{p!} \quad . \tag{A6.2.7}$$

A6.3 On-Axis Incidence

For the special case $\theta = 0$,

$$g_V(0) = 1 \tag{A6.3.1}$$

$$g_0(0) = 1 \quad . \tag{A6.3.2}$$

$I_\gamma(C,0)$ is non-zero only if $Q_C(\gamma,\theta) \neq 0$. From (A6.2.2) we have

$$p - 2q = 0$$

$$Q_C(\gamma,0) = \gamma\left(q+1, \frac{1}{\gamma^2}\right) \quad .$$

Therefore,

$$I_{\gamma}(C,0) = \frac{1}{\left[1-e^{-\frac{1}{\tau^2}}\right]^2} \sum_{p=0}^{\infty} \left(\frac{\gamma^2}{C^2}\right)^{2p} \left\{ \frac{\gamma^2}{\tau^{2p}\, p!}\, \gamma\left(p+1, \frac{1}{\gamma^2}\right) \right\}^2 . \qquad (A6.3.3)$$

APPENDIX B1

EVALUATION OF INTEGRALS

B1.1

$$I = \int_0^\infty \frac{\sin(A\kappa^2)}{A\kappa^2} e^{-B\kappa^2} \kappa^{\mu+1} J_\nu(\rho\kappa)\, d\kappa \quad . \tag{B1.1.1}$$

Using

$$\sin(A\kappa^2) = Im\left\{ e^{jA\kappa^2} \right\} \quad .$$

Let

$$C = 4(B-jA) \quad . \tag{B1.1.2}$$

Then,

$$I = \frac{1}{A} Im\left\{ \int_0^\infty e^{-\frac{C\kappa^2}{4}} \kappa^{\mu-1} J_\nu(\rho\kappa)\, d\kappa \right\} \quad .$$

The integral can be evaluated directly using [30] #6.631.5 to give

$$\int_0^\infty \frac{\sin(A\kappa^2)}{A\kappa^2}\, e^{-B\kappa^2}\, \kappa^{\mu+1}\, J_\nu(\rho\kappa)\, d\kappa$$

$$= \frac{2^\mu \rho^\nu \Gamma(\frac{\mu+\nu}{2})}{2A\Gamma(\nu+1)}\ Im\left\{ \frac{1}{C^{\frac{\mu+\nu}{2}}} \Phi\left(\frac{\mu+\nu}{2},\ \nu+1,\ -\frac{\rho^2}{C}\right)\right\}\ , \qquad \text{(B1.1.3)}$$

where $\Phi(a,b,Z)$ is a degenerate hypergeometric function.

The Case of $\mu=\nu$

From [31] #13.6.10,

$$\Phi(a,\ a+1,\ -x) = ax^{-a}\gamma(a,x)\ .$$

Using this in (B1.1.3), we get

$$I\Big|_{\mu=\nu} = \frac{1}{2A}\, Im\left\{\left(\frac{2}{\rho}\right)^\nu \gamma(\nu,\ \frac{\rho^2}{C})\right\} \qquad \text{(B1.1.4)}$$

where $\gamma(\alpha,Z) = \sum_{k=0}^{\infty} \frac{(-1)^k Z^{k+\alpha}}{k!(k+\alpha)}$

is an incomplete gamma function. Therefore,

$$I\Big|_{\mu=\nu} = \frac{1}{2A}\left(\frac{2}{\rho}\right)^{\nu} Im\left\{\sum_{k=0}^{\infty} (-1)^k \frac{\left(\frac{\rho^2}{|C|} e^{j \tan^{-1}\left(\frac{A}{B}\right)}\right)^{k+\nu}}{k!(k+\nu)}\right\}$$

$$= \frac{1}{2A}\left(\frac{2}{\rho}\right)^{\nu} Im\left\{\sum_{k=0}^{\infty} \frac{(-1)^k \left(\frac{\rho^2}{|C|}\right)^{k+\nu}}{k!} \frac{e^{j(k+\nu)\tan^{-1}\left(\frac{A}{B}\right)}}{(k+\nu)}\right\}.$$

Hence,

$$\int_0^{\infty} \frac{\sin(A\kappa^2)}{A\kappa^2} e^{-B\kappa^2} \kappa^{\nu+1} J_{\nu}(\rho\kappa)\, d\kappa$$

$$= \frac{1}{2A}\left(\frac{2\rho}{|C|}\right)^{\nu} \sum_{k=0}^{\infty} \frac{\left(-\frac{\rho^2}{|C|}\right)^k}{k!} \frac{\sin\left[(k+\nu)\tan^{-1}\left(\frac{A}{B}\right)\right]}{(k+\nu)}, \qquad \text{(B1.1.5)}$$

where $|C| = 4\sqrt{A^2+B^2}$.

The Case of $\mu=\nu=0$

$$I\Big|_{\mu=\nu=0} = \frac{1}{2A}\sum_{k=0}^{\infty}\frac{\left(-\frac{\rho^2}{|C|}\right)^k}{k!}\,\frac{\sin\left[k\,\tan^{-1}\left(\frac{A}{B}\right)\right]}{k} \quad . \tag{B1.1.6}$$

Also, in (B1.1.4) [30] # 8.356.3 and # 8.359.1,

$$\gamma(\alpha,Z) = \Gamma(\alpha) - \Gamma(\alpha,Z)$$

$$\Gamma(0,Z) = -Ei(-Z) \quad .$$

Therefore,

$$I\Big|_{\mu=\nu=0} = \frac{1}{2A}\,Im\left\{Ei\left(\frac{-\rho^2}{C}\right)\right\} \quad , \tag{B1.1.7}$$

Where $\Gamma(\alpha,x)$ is an incomplete gamma function
$Ei(x)$ is the exponential integral.

The Case of $\nu=0$. $\rho=0$

For this case (B1.1.3) reduces to

$$\frac{2^{\mu}\Gamma(\frac{\mu}{2})}{2A}\,Im\left\{\frac{1}{C^{\frac{\mu}{2}}}\right\} \quad .$$

Thus, after some algebraic manipulations,

$$\int_0^\infty \frac{\sin(A\kappa^2)}{A\kappa^2}\, e^{-B\kappa^2}\, \kappa^{\mu+1}\, d\kappa = \frac{\Gamma(\frac{\mu}{2})}{2} \frac{B^{-(\frac{n}{2}+1)}}{\left(\frac{A}{B}\right)\left(1+\frac{A^2}{B^2}\right)^{\frac{\mu}{4}}} \sin\left(\frac{\mu}{2} \tan^{-1} \frac{A}{B}\right). \tag{B1.1.8}$$

B1.2

Consider the integral

$$I = \int_0^\infty e^{-Zt}\, t^{\alpha-1}\, (1+t)^{\gamma-\alpha-1}\, J_0(\beta\sqrt{t})\, dt .$$

Using the series expansion for $J_0(x)$, we have

$$\sum_{p=0}^{\infty} \frac{(-1)^p}{(p!)^2} \left(\frac{\beta}{2}\right)^{2p} \int_0^\infty e^{-Zt}\, t^{p+\alpha-1}\, (1+t)^{p+\gamma-(p+\alpha)-1}\, dt .$$

From [30], #9.211.4, this gives

$$I = \sum_{p=0}^{\infty} \frac{(-1)^p}{(p!)^2} \left(\frac{\beta}{2}\right)^{2p} \Gamma(p+\alpha)\Psi(p+\alpha,\, p+\gamma,\, Z) . \tag{B1.2.1}$$

where [30] #9.210.2,

$$\Psi(a,b,Z) = \frac{\Gamma(1-b)}{\Gamma(a-b+1)} \Phi(a,b,Z) + \frac{\Gamma(b-1)}{\Gamma(a)} Z^{1-b} \Phi(a-b+1, 2-b, Z) \quad \text{(B1.2.2)}$$

and $\Phi(a,b,Z)$ and $\Psi(a.b.Z)$ are degenerate hypergeometric functions.

B1.3

$$I = \int_u^\infty e^{-px^2} x^{2l+1} dx .$$

Substituting $y = x^2$. we have

$$\frac{1}{2} \int_{u^2}^\infty e^{-py} y^l dy.$$

From [30] #3.381.3, this gives

$$\int_u^\infty e^{-px^2} x^{2l+1} dx = \frac{1}{2p^{l+1}} \Gamma(l+1, pu^2) \quad . \quad \text{(B1.3.1)}$$

Similarly, using [30] #3.381.1 and #3.381.4,

$$\int_0^u e^{-px^2} x^{2l+1}\, dx = \frac{1}{2p^{l+1}}\, \gamma(l+1,\, pu^2) \qquad \text{(B1.3.2)}$$

$$\int_0^\infty e^{-px^2} x^{2l+1}\, dx = \frac{1}{2p^{l+1}}\, \Gamma(l+1) \qquad \text{(B1.3.3)}$$

$\gamma(a,x)$, $\Gamma(a,x)$ are the incomplete gamma functions of the first and second kind, respectively. $\Gamma(x)$ is the gamma function.

APPENDIX B2

EVALUATION OF INTEGRALS

B2.1.1

To evaluate

$$Q_p = \int_0^1 e^{-\frac{R^2}{C^2}} R^{2n+\nu+1} J_\nu(\Theta R)\, dR \qquad \text{(B2.1.1)}$$

$$= \sum_{m=0}^{\infty} \left(\frac{-1}{C^2}\right)^m \frac{1}{m!} \int_0^1 R^{2(m+n)+\nu+1} J_\nu(\Theta R)\, dR \quad .$$

From [30] #6.561.13,

$$\int_0^1 x^\mu J_\nu(\Theta x)dx = \frac{1}{\Theta^{\mu+1}}\left[(\nu+\mu-1)\Theta J_\nu(\Theta)S_{\mu-1,\nu-1}(\Theta) - \Theta J_{\nu-1}(\Theta)S_{\mu,\nu}(\Theta)\right.$$

$$\left. + 2^\mu \frac{\Gamma(\frac{\nu+\mu+1}{2})}{\Gamma(\frac{\nu-\mu+1}{2})}\right], \qquad \mathrm{Re}(\nu+\mu) > -1 \quad .$$

$S_{\mu,\nu}(\Theta)$ is a Lommel function.

$\Gamma(x)$ is the Gamma function.

Note that the above result is the corrected form of the expression given in [30] #6.561.13.

Here $\mu = 2m+2n+\nu+1$. Multiply and divide by $C^{2n+\nu+2}$. Then,

$$Q_p = C^{2n+\nu+2} \sum_{m=0}^{\infty} \frac{(-1)^m}{m!} \left(\frac{1}{C\Theta}\right)^{\mu+1} \left[(\nu+\mu-1)\Theta J_\nu(\Theta)\, S_{\mu-1,\nu-1}(\Theta) \right.$$

$$\left. - J_{\nu-1}(\Theta) S_{\mu,\nu}(\Theta) + 2^\mu \frac{\Gamma(\frac{\nu+\mu+1}{2})}{\Gamma(\frac{\nu-\mu+1}{2})} \right] \qquad Re(\nu+\mu) > -1 \ .$$

(B2.1.2)

B2.2 For $\Theta = 0$

From B2.1.1, Q_p can now exist only if $\nu = 0$. Therefore,

$$Q_p(0) = \int_0^1 e^{-\frac{R^2}{C^2}} R^{2n+1} \, dR.$$

From B1.3.2, this gives

$$Q_p(0) = \frac{C^{2n+2}}{2} \gamma(n+1, \frac{1}{C^2}) \ . \qquad \text{(B2.2.1)}$$

REFERENCES

[1] S. Silver, Microwave Antenna Theory and Design, 623 pages, Dover Publications, Inc., New York, 1965, p. 173.

[2] R.F. Harrington, Time Harmonic Electromagnetic Fields, 480 pages, McGraw-Hill, 1961, Chapter 3.

[3] J.A. Richmond, Unpublished Notes.

[4] L.A. Chernov, Wave Propagation in a Random Medium, 168 pages, McGraw-Hill, New York, 1960.

[5] V.I. Tatarski, Wave Propagation in a Turbulent Medium, translated from Russian by R.A. Silverman, 285 pages, McGraw-Hill, New York, 1961.

[6] V.I. Tatarski, The Effects of the Turbulent Atmosphere on Wave Propagation, translated from Russian by Israel Program for Scientific Translations, Rep. N 72-18163, 472 pages, National Technical Information Service, Springfield, Virginia.

[7] R.W. Schmeltzer, "Means, Variances, and Covariances for Laser Beam Propagation through a Random Medium", Quart. Appl. Math., Vol. 24, 1967, pp. 339-354.

[8] A. Ishimaru, Wave Propagation and Scattering in Random Media, Volume 1, Academic Press, New York, 1978.

[9] A. Ishimaru, Wave Propagation and Scattering in Random Media, Volume 2, Academic Press, New York, 1978.

[10] A. Ishimaru, "Theory and Application of Wave Propagation and Scattering in Random Media", Proc. IEEE, Vol. 65, No. 7, July 1977, pp. 1030-1061.

[11] Y.S. Shifrin, Statistical Antenna Theory, translated from Russian by P. Beckmann, 370 pages, The Golem Press, Boulder, Colorado, 1971.

[12] R.K. Crane, "Propagation Phenomena Affecting Satellite Communication Systems Operating in the Centimeter and Millimeter Wavelength Bands", Proc. IEEE, Vol. 59, No. 2, February 1971, pp. 173-188.

[13] R.K. Crane, "Fundamental Limitations Caused by RF Propagation", Proc. IEEE, Vol. 69, No. 2, February 1981, pp. 196-209.

[14] R.S. Lawrence, "A Review of the Optical Effects of the Clear Turbulent Atmopshere", Journal of the Soc. Photo-Optical Instrumentation Engineers, Vol. 75, 1976.

[15] R.S. Lawrence and J.W. Strohbehn, "A Survey of Clear Air Propagation Effects Relevant to Optical Communications", Proc. IEEE, Vol. 58, October 1970, pp. 1523-1545.

[16] J.W. Strohbehn, "Line-of-Sight Wave Propagation Through the Turbulent Atmosphere", Proc. IEEE, Vol. 56, No. 8, August 1968, pp. 1301-1318.

[17] S.F. Clifford and J.W. Strohbehn, "The Theory of Line-of-Sight Propagation Through a Turbulent Atmosphere", Trans. IEEE, Vol. AP-18, No. 20, March 1970, pp. 264-274.

[18] R.L. Fante, "Electromagnetic Beam Propagation in Turbulent Media", Proc. IEEE, Vol. 63, 1975, pp. 1669-1692.

[19] D.A. deWolf, "Propagation Regimes for Turbulent Atmospheres", Radio Science, Vol. 10, No. 1, January 1975, pp. 53-57.

[20] M.J. Beran, "Propagation of the Mutual Coherence Function Through Random Media", J. Opt. Soc. Amer., Vol. 56, 1966, pp. 1475-1480.

[21] A.N. Kolmogorov, Turbulence, Classic Papers on Statistical Theory, Editors S.K. Friedlander and L. Topper, Interscience Publishers, Inc., New York, 1961, pp. 151-161.

[22] R.W. Lee and J.C. Harp, "Weak Scattering in Random Media, with Applications to Remote Probing", Proc. IEEE, Vol. 57, No. 4, April 1969, pp. 375-406.

[23] A. Ishimaru, op. cit. [9], Appendix A.

[24] A. Ishimaru, op. cit. [9], Appendix B.

[25] A. Ishimaru, op. cit. [9], Chapter 16.

[26] V.I. Tatarski, op. cit. [6], pp. 51-54.

[27] J.W. Strohbehn, op. cit. [16].

[28] A. Ishimaru, op. cit. [9], Appendix C-12.

[29] A. Ishimaru, op. cit. [9], Chapter 17.

[30] I.S. Gradshtyn and I.M. Ryzhik, Tables of Integrals Series and Products, translated from Russian by A. Jeffrey, Academic Press, New York, 1980.

[31] M. Abramowitz and I.A. Stegun, Handbook of Mathematical Functions, Dover Publications, Inc., New York, 1970.

[32] Y.S. Shifrin, op. cit. [11], pp. 28-29.

[33] D.L. Fried, "Aperture Averaging of Scintillation", J. Opt. Soc. Amer., Vol. 57, February 1967, pp. 169-175.

[34] D.L. Fried, "Optical Resolution Through a Randomly Inhomogeneous Medium for Very Long and Very Short Exposures", J. Op. Soc. Amer., Vol. 56, No. 10, October 1966, pp. 1372-1379.

[35] D.M.J. Devasirvatham and D.B. Hodge, "Amplitude Scintillations on Earth-Space Propagation Paths at 2 and 30 GHz", Report 4299-4, March 1976, The Ohio State University ElectroScience Laboratory, Department of Electrical Engineering; prepared under Contract NAS5-22575 for NASA-Goddard Space Flight Center.

[36] D.M. Theobold and D.B. Hodge, "Gain Degradation and Amplitude Scintillation Due to Tropospheric Turbulence", Report 784299-6, February 1978, revised June 1978, The Ohio State University ElectroScience Laboratory, Department of Electrical Engineering; prepared under Contract NAS5-22575 for NASA-Goddard Space Flight Center.

[37] Y.S. Shifrin, op. cit. [11], pp. 327-328.

[38] R.B. Chadwick and K.P. Moran, "Long Term Measurements of C_n^2 in the Boundary Layer", Radio Science, Vol. 15, No. 2, 1980, pp. 355-361.

[39] E.E. Gossard, "Refractive Index Variance and its Height Distribution in Different Air Masses", Radio Science, Vol. 12, No. 1, 1977, pp. 89-105.

[40] E.E. Gossard, "A Fresh Look at the Radar Reflectivity of Clouds", Radio Science, Vol. 14, No. 6, 1979, pp. 1089-1097.

[41] D.M.J. Devasirvatham and D.B. Hodge, "Amplitude and Angle of Arrical Measurements on a 28.56 GHz Earth-Space Path", Report 712759-4, March 1981, The Ohio State University ElectroScience Laboratory, Department of Electrical Engineering; prepared under Contract NASW-3393 for The National Aeronautics and Space Administration, Headquarters.

[42] K.S. McCormick and L.A. Maynard, "Measurement of S.H.F. Tropospheric Fading Along Earth-Space Paths at Low Elevation Angles", Electronics Letters, Vol. 8, 1972, p. 274.

[43] J.P. Ruina and C.M. Angulo, "Antenna Resolution as Limited by Atmospheric Turbulence", Trans. IEEE, Vol. AP-11, No. 2, March 1963, pp. 153-161.

[44] D.L. Knepp, "Antenna Aperture Effects on Measurements of Propagation Through Turbulence", Trans. IEEE, Vol. AP-23, March 1975, pp. 688-690.

[45] W.L. Pritchard, "Satellite Communication - An Overview of the Problems and Programs", Proc. IEEE, Vol. 65, No. 3, March 1977, pp. 294-307.

[46] M. Schwartz, Information Transmission, Modulation and Noise, 672 pages, McGraw-Hill, New York, 1970.

[47] M.I. Skolnik, Introduction to Radar Systems, 648 pages, McGraw-Hill, New York, 1962.

[48] A. Papoulis, Probability, Random Variables and Stochastic Processes, 583 pages, McGraw-Hill, New York, 1965.

[49] H.L. Van Trees, Detection, Estimation and Modulation Theory, Part 1, 697 pages, John Wiley and Sons, Inc., New York, 1968.